OFFICE OF CIVILIAN RADIOACTIVE WASTE MANAGEMENT
SPECIAL INSTRUCTION SHEET

1. QA: QA

Complete Only Applicable Items

This is a placeholder page for records that cannot be scanned.

2. Record Date 08/09/2001	3. Accession Number MOL.20010815.0270
4. Author Name(s) SRETEN MASTILOVIC	5. Author Organization N/A

6. Title/Description
SYMMETRIC ROCK FALL ON WASTE PACKAGE

7. Document Number(s) CAL-EBS-ME-000009	8. Version Designator REV. 00
9. Document Type REPORT	10. Medium OPTIC/PAPER

11. Access Control Code
PUB

12. Traceability Designator
DC #26239

13. Comments
THIS IS A ONE-OF-A-KIND DOCUMENT DUE TO THE COLORED GRAPHS AND CAN BE LOCATED IN THE RPC.

OFFICE OF CIVILIAN RADIOACTIVE WASTE MANAGEMENT
CALCULATION COVER SHEET

1. QA: QA
Page: 1 Of: 35

2. Calculation Title
Symmetric Rock Fall on Waste Package

MOL.20010815.0270

3. Document Identifier (including Revision Number)
CAL-EBS-ME-000009 REV 00

4. Total Attachments	5. Attachment Numbers - Number of pages in each
3	I-16, II-38, III (electronic media attachment, see Remarks)

	Print Name	Signature	Date
6. Originator	Sreten Mastilovic		08/06/2001
7. Checker	Zekai Ceylan		8/6/01
8. Lead	Scott M. Bennett		08/09/01

9. Remarks

Attachment III is an electronic media attachment (compact disc) containing ANSYS V5.4 and LS-DYNA V950 electronic files. The file names, file dates and times, and file sizes are listed in Section 8 of this document.

Attachment III is moved from REV 00B to REV 00 of this document.

Revision History

10. Revision No.	11. Description of Revision
00	Initial issue

CONTENTS

TABLES

Page

1. PURPOSE

The objective of this calculation is to determine the structural response of the Naval SNF (spent nuclear fuel) Waste Package (WP) and the emplacement pallet (EP) subjected to the rock fall DBE (design basis event) dynamic loads. The scope of this calculation is limited to reporting the calculation results in terms of stress intensities and residual stresses in the WP, and stress intensities and maximum permanent downward displacements of the EP-lifting surface. The information provided by the sketches (Attachment I) is that of the potential design of the type of WP and EP considered in this calculation, and all obtained results are valid for those designs only. This calculation is associated with the waste package design and is performed by the Waste Package Design Section in accordance with Reference 24. AP-3.12Q, *Calculations*, is used to perform the calculation and develop the document (see Ref. 5).

2. METHOD

The finite element calculation is performed by using the commercially available ANSYS Version (V) 5.4 (Computer Software Configuration Item [CSCI] 30040 V5.4; see Ref. 8) and LS-DYNA V950 (Software Tracking Number [STN] 10300-950-00; see Ref. 4) finite element codes. ANSYS V5.4 is used for preprocessing, i.e. to create finite element representation (FER) used subsequently in LS-DYNA V950 to obtain solution. The results of this calculation are provided in terms of stress intensities, axial and tangential stresses in the outer shell (OS) of the WP, and stress intensities and lifting surface displacements in EP.

With regard to the development of this calculation, the control of electronic management of information is evaluated in accordance with AP-SV.1Q, *Control of the Electronic Management of Information* (Ref. 6). The evaluation (Ref. 26) determined that current work processes and procedures are adequate for the control of electronic management of information for this activity.

3. ASSUMPTIONS

In the course of developing this document, the following assumptions are made regarding the structural calculations.

3.1 Some of the temperature-dependent material properties (specifically: density, Poisson's ratio, and elongation) are not available for SB-575 N06022 (Alloy 22), SA-240 S31600 (316NG [nuclear grade] stainless steel [SS]), and SA-240 S31603 (316L SS) except at room temperature (RT) (20 °C). The RT density, RT Poisson's ratio, and RT elongation are assumed for these materials. The impact of using RT density, RT Poisson's ratio, and RT elongation is anticipated to be small. The rationale for this assumption is twofold: first, the said mechanical properties of the materials used (with exception of the elongation for SSs) do not change significantly at the temperature of interest in these calculation, and second, the

material properties in question do not have dominant impact on the calculation results. This assumption is used in Section 5.1.

3.2 The temperature-dependent material properties are not available for TSw2 (Topopah Spring Welded-Lithophysal Poor) rock except at RT. The corresponding RT material properties are assumed for this material. The impact of using RT material properties is anticipated to be small. The rationale for this assumption is that the mechanical properties relevant for representing the rock as an elastic solid (namely: density, modulus of elasticity, and Poisson's ratio) do not change significantly at the temperatures experienced in repository emplacement drift. This assumption is used in Section 5.1.

3.3 Some of the rate-dependent material properties are not available for materials used at any strain rate. The material properties obtained under the static loading conditions are assumed for all materials. The impact of using material properties obtained under static loading conditions is anticipated to be small. The rationale for this assumption is that the mechanical properties of subject materials do not significantly change at the peak strain rates that occur during the rock fall (maximum plastic strain rate being approximately $30\,s^{-1}$ as indicated by maximum slope $[0.12/0.004\,s]$ in Figs. II-74 and II-75). A possible exception is TSw2 rock, but since the rock is represented as the elastic solid the same justification is valid for the relevant rock properties as well. This assumption is used in Section 5.1.

3.4 The Poisson's ratio of Alloy 22 is not available in literature. The Poisson's ratio of Alloy 625 (SB-443 N06625) is assumed for Alloy 22. The impact of this assumption is anticipated to be negligible. The rationale for this assumption is that the chemical compositions of Alloy 22 and Alloy 625 are similar (see Ref. 16 [Sect. II, SB-575, Table 1] and Ref. 1 [p. 143], respectively). This assumption is used in Section 5.1.

3.5 The Poisson's ratio of 316L SS is not available in literature. The Poisson's ratio of 316 SS (SA-240 S31600) is assumed for 316L SS. The impact of this assumption is anticipated to be negligible. The rationale for this assumption is that the chemical compositions of these two stainless steels are similar (see Ref. 16, Sect. II, SA-240, Table 1). This assumption is used in Section 5.1.

3.6 The atmospheric (dry oxidation) corrosion penetration rate of Alloy 22 is not available in literature. Therefore, the aqueous corrosion penetration rate is used as an upper bound for the atmospheric corrosion penetration rate. The rationale for this notably conservative assumption is that since the atmospheric corrosion penetration rate of Alloy 22 is below the detectable level (Ref. 18, p. 70), the aqueous corrosion penetration rate provides an upper bound. In fact, an approximate calculation in Reference 18 (see p. 37 and p. 38) provides a conservative upper bound for the atmospheric corrosion penetration rate of Alloy 22, $0.0093\,\mu m/year$; this value is an order of magnitude less than the aqueous corrosion

penetration rate. This assumption is used in Section 5.1.

3.7 The uniform strain (strain corresponding to tensile strength) of 316L SS is not available in literature. Therefore, it is conservatively assumed that the uniform strain is 60% of the elongation (strain corresponding to rupture point in tensile test). The rationale for this assumption is the character of stress-strain curve for 316L SS (see Ref. 22, p. 305). This assumption is used in Section 5.1.2.

3.8 The uniform strain of Alloy 22 is not available in literature. Therefore, it is conservatively assumed that the uniform strain is 90% of the elongation. The rationale for this assumption is the character of stress-strain curve for Alloy 22 (see Ref. 14). This assumption is used in Section 5.1.2.

3.9 The uniform strain of 316 SS and 316NG SS is not available in literature. Therefore, it is conservatively assumed that the uniform strain is 90% of the elongation. The rationale for this assumption is the character of stress-strain curve for 316 SS (see Refs. 14 and 22 [p. 304]). This assumption is used in Section 5.1.2.

3.10 The change of minimum elongation with increase of temperature for the materials used in this calculation is not available in literature. Therefore, the magnitude of this change at $T = 239\ ^{o}C$ for Alloy 22, 316NG SS, and 316L SS is assumed to be +7.6%, –27%, and –36%, respectively, based on the relative change of typical elongation for said materials available in vendor catalogues (see Refs. 2 [pages 14 and 15] and 15 [p. 8], and Section 5.1.4 for details). The rationale for this conservative assumption is that the relative change of typical elongation should be bounding for the relative change of minimum elongation. This assumption is used in Section 5.1.4.

3.11 The friction coefficient for contacts occurring between the 316NG SS and 316L SS is not available in literature. It is, therefore, assumed that the dynamic (sliding) friction coefficient for this contact is 0.4. The rationale for this assumption is that this friction coefficient represents the lower bound for the steel-on-steel contacts (see Refs. 29 [Table 3.2.1, p. 3-36] and 30 [p. 441]). This assumption is used in Section 5.5.

3.12 The friction coefficients for contacts among the Alloy 22 components, or the contacts involving Alloy 22 and 316NG SS, are not available in literature. It is, therefore, assumed that the dynamic (sliding) friction coefficient for both of these contacts is 0.4. The rationale for this conservative assumption is that this friction coefficient represents the lower bound for most dry nickel-on-steel and nickel-on-nickel contacts (see Ref. 29 [Table 3.2.1, p. 3-36]); nickel being the dominant component in Alloy 22 (Ref. 16, SB-575, Table 1). This assumption is used in Section 5.5.

3.13 The friction coefficient for contacts occurring between the rock and Alloy 22 is not available in literature. It is, therefore, assumed that the dynamic (sliding) friction coefficient for this contact is 0.4. The rationale for this assumption is that this friction coefficient represents a reasonable estimate based on available information for metal-on-stone contacts (see Ref. 28 [Table 6.1, p. 306]). This assumption is used in Sections 5.5.

3.14 The variation of functional friction coefficient between the static and dynamic value as a function of relative velocity of the surfaces in contact is not available in literature for the materials used in this calculation (see Section 5.5). Therefore, the effect of relative velocity of the surfaces in contact is neglected in these calculations by assuming that the functional friction coefficient and static friction coefficient are both equal to the dynamic friction coefficient. The impact of this assumption on results presented in this document is anticipated to be negligible. The rationale for this conservative assumption is that it provides the bounding set of results by minimizing the friction coefficient within the given FE-analysis framework. This assumption is used in Sections 5.5.

4. USE OF COMPUTER SOFTWARE AND MODELS

4.1 SOFTWARE

One of the finite element analysis (FEA) computer codes used for this calculation is ANSYS V5.4, which is obtained from Software Configuration Management in accordance with appropriate procedures, and is identified by Computer Software Configuration Item number (CSCI) 30040 5.4 (see Ref. 8). ANSYS V5.4 is a commercially available FEA code and is appropriate for structural calculations of WPs as performed in this calculation. The calculations using ANSYS V5.4 software were executed on the Hewlett-Packard (HP) 9000 series UNIX workstation identified with the YMP (Yucca Mountain Project) property tag number 117162, located in Las Vegas, Nevada. ANSYS evaluation performed for this calculation is fully within the range of the validation performed for ANSYS V5.4 code. Access to the code is granted by the Software Configuration Secretariat in accordance with the appropriate procedures.

The input files (identified by .inp file extensions) and output files (identified by .out file extensions) for ANSYS V5.4 are provided in Attachment III.

The second FEA computer code, used for this calculation, is the Livermore Software Technology Corporation LS-DYNA V950, which is obtained from Software Configuration Management in accordance with appropriate procedures, and is identified by Software Tracking Number (STN) 10300-950-00 (see Ref. 4). LS-DYNA V950 is a commercially available FEA code and is appropriate for structural calculations of WPs as performed in this calculation. The calculations were executed on HP 9000 series UNIX workstations identified with the YMP property tag numbers 117161 and 117162, located in Las Vegas, Nevada. LS-DYNA evaluation performed for this calculation is fully within the range of the validation performed for LS-DYNA V950 code. Access to the code is granted by the Software Configuration Secretariat in accordance with the appropriate procedures.

The input files (identified by .k and .inc file extensions) and output files (d3hsp) for LS-DYNA V950 are provided in Attachment III.

4.2 MODELS

None used.

5. CALCULATION

5.1 MATERIAL PROPERTIES

Material properties used in these calculations are listed in this section. Some of the temperature-dependent and rate-dependent material properties are not available for Alloy 22, 316 SS, 316NG SS, 316L SS, and TSw2 rock. Therefore, RT density, RT Poisson's ratio, and RT elongation obtained under the static loading conditions are used for for Alloy 22, 316 SS, 316NG SS, and 316L SS (see Assumptions 3.1 and 3.3). The RT material properties obtained under the static loading conditions are used for TSw2 rock (Assumptions 3.2 and 3.3).

SB-575 N06022 (Alloy 22) (OS, OS lids, upper and lower trunnion collar sleeves, EP plates #2 through #9, and EP tubes):

- Density = 8690 kg/m^3 (0.314 lb/in^3) (at RT) (Ref. 16, Sect. II, SB-575, Sect. 7.1)
- Yield strength = 229 *MPa* (33.2 *ksi*) (at 450 ^oF = 232 ^oC) (Ref. 16, Sect. II, Table Y-1)
  Yield strength = 222 *MPa* (32.2 *ksi*) (at 500 ^oF = 260 ^oC) (Ref. 16, Sect. II, Table Y-1)
- Tensile strength = 657 *MPa* (95.3 *ksi*) (at 400 ^oF = 204 ^oC) (Ref. 16, Sect. II, Table U)
  Tensile strength = 641 *MPa* (92.9 *ksi*) (at 500 ^oF = 260 ^oC) (Ref. 16, Sect. II, Table U)
- Elongation = 0.45 (at RT) (Ref. 16, Sect. II, SB-575, Table 3)
- Poisson's ratio = 0.278 (at RT) (Ref. 1, p. 143; see Assumption 3.4)
- Modulus of elasticity = 206 *GPa* (at RT) (Ref. 2, p. 14)
  Modulus of elasticity = 190 *GPa* (at 316 ^oC) (Ref. 2, p. 14)
- Corrosion penetration rate = 0.16 $\mu m/year$ (at RT) (Ref. 18, p. 69; see Assumption 3.6)

SA-240 S31600 (316NG SS, which is 316 SS with tightened control on carbon and nitrogen content and has the same material properties as 316 SS [see Ref. 9, p. 931, and Ref. 16, Sect. II, SA-240, Table 1]) (Inner shell, inner shell lids, inner shell lifting feature, and EP SS tubes):

- Density = 7980 kg/m^3 (at RT) (Ref. 10, Table X1.1, p. 7)
- Yield strength = 148 *MPa* (21.4 *ksi*) (at 400 ^oF = 204 ^oC) (Ref. 16, Sect. II, Table Y-1)
  Yield strength = 138 *MPa* (20.0 *ksi*) (at 500 ^oF = 260 ^oC) (Ref. 16, Sect. II, Table Y-1)

- Tensile strength = 496 *MPa* (71.9 *ksi*) (at 400 ^{o}F = 204 ^{o}C) (Ref. 16, Sect. II, Table U)
  Tensile strength = 495 *MPa* (71.8 *ksi*) (at 500 ^{o}F = 260 ^{o}C) (Ref. 16, Sect. II, Table U)

- Elongation = 0.40 (at RT) (Ref. 16, Sect. II, SA-240, Table 2)

- Poisson's ratio = 0.298 (at RT) (Ref. 1, Figure 15, p. 755)

- Modulus of elasticity = 183 *GPa* ($26.5 \cdot 10^{6}$ *psi*) (at 400 ^{o}F = 204 ^{o}C) (Ref. 16, Sect. II, Table TM-1)
  Modulus of elasticity = 178 *GPa* ($25.8 \cdot 10^{6}$ *psi*) (at 500 ^{o}F = 260 ^{o}C) (Ref. 16, Sect. II, Table TM-1)

SA-240 S31603 (316L SS) (Naval canister [Ref. 3, Enclosure 3, p. 4]):

- Density = 7980 kg/m^3 (at RT) (Ref. 10, Table X1.1, p. 7)
- Yield strength = 121 *MPa* (17.5 *ksi*) (at 400 ^{o}F = 204 ^{o}C) (Ref. 16, Sect. II, Table Y-1)
  Yield strength = 113 *MPa* (16.4 *ksi*) (at 500 ^{o}F = 260 ^{o}C) (Ref. 16, Sect. II, Table Y-1)

- Tensile strength = 429 *MPa* (62.2 *ksi*) (at 400 ^{o}F = 204 ^{o}C) (Ref. 16, Sect. II, Table U)
  Tensile strength = 426 *MPa* (61.8 *ksi*) (at 500 ^{o}F = 260 ^{o}C) (Ref. 16, Sect. II, Table U)

- Elongation = 0.40 (at RT) (Ref. 16, Sect. II, SA-240, Table 2)

- Poisson's ratio = 0.298 (at RT) (Ref. 1, Figure 15, p. 755) (see Assumption 3.5)

- Modulus of elasticity = 183 *GPa* ($26.5 \cdot 10^{6}$ *psi*) (at 400 ^{o}F = 204 ^{o}C) (Ref. 16, Sect. II, Table TM-1)
  Modulus of elasticity = 178 *GPa* ($25.8 \cdot 10^{6}$ *psi*) (at 500 ^{o}F = 260 ^{o}C) (Ref. 16, Sect. II, Table TM-1)

TSw2 Rock:

- Density = 2370 kg/m^3 (at RT) (Ref. 11, p. 3)

- Poisson's ratio = 0.21 (at RT) (Ref. 21, Table 4)

- Modulus of elasticity = 33.0 *GPa* (at RT) (Ref. 21, Table 3)

5.1.1 Calculations for Available Elevated-Temperature Material Properties

The maximum WP OS temperature experienced in repository emplacement drift is $T_{max} = 239\ ^{o}C$ (Ref. 19, Table 6-7). The material properties at this temperature are obtained by linear interpolation of corresponding material properties presented in Section 5.1, by using the formula:

$$p = p(T) = p_l + \left(\frac{T - T_l}{T_u - T_l}\right) \cdot (p_u - p_l)$$

Subscripts u and l denote the bounding values of generic material property p at the corresponding bounding temperatures.

In the case of Alloy 22, available material properties at $239^{o}C$ are:

Yield strength $= 229 + [(239 - 232) \cdot (222 - 229)]/(260 - 232) = 227\ MPa$
Tensile strength $= 657 + [(239 - 204) \cdot (641 - 657)]/(260 - 204) = 647\ MPa$
Modulus of elasticity $= 206 + [(239 - 20) \cdot (190 - 206)]/(316 - 20) = 194\ GPa$

Similarly, for 316 SS and 316NG SS:

Yield strength $= 148 + [(239 - 204) \cdot (138 - 148)]/(260 - 204) = 142\ MPa$
Tensile strength $= 496 + [(239 - 204) \cdot (495 - 496)]/(260 - 204) = 495\ MPa$
Modulus of elasticity $= 183 + [(239 - 204) \cdot (178 - 183)]/(260 - 204) = 180\ GPa$

Finally, for 316L SS:

Yield strength $= 121 + [(239 - 204) \cdot (113 - 121)]/(260 - 204) = 116\ MPa$
Tensile strength $= 429 + [(239 - 204) \cdot (426 - 429)]/(260 - 204) = 427\ MPa$
Modulus of elasticity $= 183 + [(239 - 204) \cdot (178 - 183)]/(260 - 204) = 180\ GPa$

5.1.2 Calculations for True Measures of Ductility

The material properties in Section 5.1 refer to engineering stress and strain definitions: $s = P/A_0$ and $e = L/L_0 - 1$ (see Ref. 7, Chapter 9). Where P stands for the force applied during a static tensile test, L is the length of the deformed specimen, and L_0 and A_0 are the original length and cross-sectional area of the specimen, respectively. The engineering stress-strain curve does not give a true indication of the deformation characteristics of a material during plastic deformation since it is based entirely on the original dimensions of the specimen. In addition, ductile metal that is pulled in

tension becomes unstable and necks down during the course of the test. Hence, LS-DYNA V950 FEA code requires input in terms of true stress and strain definitions: $\sigma = P/A$ and $\varepsilon = \ln(L/L_0)$ (see Ref. 7, Chapter 9).

The relationships between the true stress and strain definitions and the engineering stress and strain definitions, $\sigma = s \cdot (1+e)$ and $\varepsilon = \ln(1+e)$, can be readily derived based on constancy of volume ($A_0 \cdot L_0 = A \cdot L$) and strain homogeneity during plastic deformation (see Ref. 7, Chapter 9). These expressions are applicable only in the hardening region of the stress-strain curve that is limited by the onset of necking.

The following parameters are used in the subsequent calculations:

$s_y \approx \sigma_y$ = yield strength
s_u = engineering tensile strength
σ_u = true tensile strength
$e_y \approx \varepsilon_y$ = strain corresponding to yield strength
e_u = engineering strain corresponding to tensile strength (engineering uniform strain)
ε_u = true strain corresponding to tensile strength (true uniform strain)

In absence of data on the uniform strain in available literature, it needs to be estimated based on the character of stress-strain curves and elongation (strain corresponding to rupture of the tensile specimen).

The stress-strain curves for Alloy 22, 316 SS and 316NG SS do not manifest three-stage deformation character (see Assumptions 3.8 and 3.9). Therefore, the elongation reduced by 10% (to take into account the specimen-failure part of the stress-strain curve) is assumed for uniform strain.

In the case of Alloy 22 ($e_u = 0.9 \cdot elongation = 0.405$), the true measures of ductility are

$$\varepsilon_u = \ln(1+e_u) = \ln(1+0.405) = 0.34$$
$$\sigma_u = s_u \cdot (1+e_u) = 647 \cdot (1+0.405) = 909\ MPa$$

Therefore, the true tensile strength of Alloy 22 at temperature of $239\,^{o}C$ is 909 *MPa*.

For 316 SS and 316NG SS, $e_u = 0.9 \cdot elongation = 0.36$, therefore:

$$\varepsilon_u = \ln(1+e_u) = \ln(1+0.36) = 0.31$$
$$\sigma_u = s_u \cdot (1+e_u) = 495 \cdot (1+0.36) = 673\ MPa$$

Hence, the true tensile strength of 316 SS and 316NG SS at temperature of $239\,^{o}C$ is 673 *MPa*.

Unlike the previous two cases, the stress-strain curve for 316L SS exhibits pronounced three-stage (elastic-hardening-softening) deformation character. The uniform strain is, therefore, estimated to be 60% of elongation based on the available stress-strain curves (see Assumption 3.7).

$$e_u = 0.6 \cdot elongation = 0.6 \cdot 0.40 = 0.24$$
$$\varepsilon_u = \ln(1 + e_u) = \ln(1 + 0.24) = 0.22$$
$$\sigma_u = s_u \cdot (1 + e_u) = 427 \cdot (1 + 0.24) = 530\ MPa$$

Thus the true tensile strength of 316L SS at temperature of $239\,^{o}C$ is estimated to be 530 *MPa*.

5.1.3 Calculations for Tangent Moduli

As previously discussed, the results of this simulation are required to include elastic and plastic deformations for Alloy 22, 316 SS, 316NG SS, and 316L SS. When the materials are driven into the plastic range, the slope of stress-strain curve continuously changes. A ductile failure is preceded by a protracted regime of hardening and substantial accumulation of inelastic strains. Thus, a simplification for stress-strain curve is needed to incorporate plasticity into the FEA. A standard approximation commonly used in engineering is to use a straight line that connects the yield point and the tensile strength point of the material. The parameters used in the subsequent calculations in addition to those defined in Section 5.1.2 are modulus of elasticity (E) and tangent (hardening) modulus (E_1). The tangent modulus represents the slope of the stress-strain curve in the plastic region.

In the case of Alloy 22 the tangent modulus is:

$E_1 = (\sigma_u - \sigma_y)/(\varepsilon_u - \sigma_y/E) = (0.909 - 0.227)/(0.34 - 0.227/194) = 2.01\ GPa$ (see Sections 5.1, 5.1.1, and 5.1.2)

Similarly, for 316 SS and 316NG SS:

$E_1 = (\sigma_u - \sigma_y)/(\varepsilon_u - \sigma_y/E) = (0.673 - 0.142)/(0.31 - 0.142/180) = 1.72\ GPa$ (see Sections 5.1, 5.1.1, and 5.1.2)

Finally, for 316L SS:

$E_1 = (\sigma_u - \sigma_y)/(\varepsilon_u - \sigma_y/E) = (0.530 - 0.116)/(0.22 - 0.116/180) = 1.89\ GPa$ (see Section 5.1, 5.1.1, and 5.1.2)

5.1.4 Effect of Change of Elongation on Material Properties

The change of minimum elongation with increase of temperature for the materials used in this calculation is not available in literature. Therefore, for Alloy 22, 316NG SS, and 316L SS the magnitude of this change at temperature of $239\,^{o}C$ is estimated based on the change of typical elongation for said materials (Assumption 3.10). In the case of Alloy 22 Reference 2 (pages 14 and 15) indicates an increase of typical elongation with respect to RT value for 6.5% at $T = 204\ ^{o}C$, and for 10% at $T = 316\ ^{o}C$. Hence, by using linear interpolation, the increase of elongation corresponding to an increase of temperature from RT to $T = 239\ ^{o}C$ is 7.6%. On the other hand, Reference 15 (p. 8) suggests for 316 SS (and consequently 316NG SS; see Section 5.1) elongation decrease with respect to RT value for 25% at $T = 204\ ^{o}C$, and for 30% at $T = 316\ ^{o}C$. Hence, the decrease of elongation corresponding to an increase of temperature from RT to $T = 239\ ^{o}C$ is 27%. Finally, Reference 15 (p. 8) suggests for 316L SS elongation decrease with respect to RT value for 34% at $T = 204\ ^{o}C$, and for 40% at $T = 316\ ^{o}C$. Hence, the decrease of elongation corresponding to an increase of temperature from RT to $T = 239\ ^{o}C$ is 36%. Consequently, the true measures of ductility and tangent moduli, calculated in Sections 5.1.2 and 5.1.3, have to be changed to accommodate the variability of elongation due to change of temperature.

In the case of Alloy 22, $e_u = (1 + 0.076)\cdot(0.9 \cdot elongation) = 0.44$, the true uniform strain is

$$\varepsilon_u = \ln(1 + e_u) = \ln(1 + 0.44) = 0.36$$

while the true tensile strength is

$$\sigma_u = s_u \cdot (1 + e_u) = 647 \cdot (1 + 0.44) = 932\ MPa$$

Consequently, the tangent modulus becomes

$$E_1 = (\sigma_u - \sigma_y)/(\varepsilon_u - \sigma_y/E) = (0.932 - 0.227)/(0.36 - 0.227/194) = 1.96\,GPa$$

For 316NG SS, $e_u = (1 - 0.27)\cdot(0.9 \cdot elongation) = 0.26$, the true uniform strain is

$$\varepsilon_u = \ln(1 + e_u) = \ln(1 + 0.26) = 0.23$$

while the true tensile strength is

$$\sigma_u = s_u \cdot (1 + e_u) = 495 \cdot (1 + 0.26) = 624\ MPa$$

Consequently, the tangent modulus is

$$E_1 = (\sigma_u - \sigma_y)/(\varepsilon_u - \sigma_y/E) = (0.624 - 0.142)/(0.23 - 0.142/180) = 2.10\,GPa$$

Finally, for 316L SS, $e_u = (1 - 0.36)\cdot(0.6 \cdot elongation) = 0.15$, the true uniform strain is

$$\varepsilon_u = \ln(1 + e_u) = \ln(1 + 0.15) = 0.14$$

while the true tensile strength is

$$\sigma_u = s_u \cdot (1 + e_u) = 427 \cdot (1 + 0.15) = 491\,MPa$$

Consequently, the tangent modulus is

$$E_1 = (\sigma_u - \sigma_y)/(\varepsilon_u - \sigma_y/E) = (0.491 - 0.116)/(0.14 - 0.116/180) = 2.69\,GPa$$

5.2 ROCK VELOCITY AND MAXIMUM ANGLE OF INCLINATION

5.2.1 Calculations for Impact Velocity

To reduce the computer execution time while preserving all features of the problem relevant to the structural calculation, the rock is set in a position just before impact and given an appropriate initial velocity. The initial velocity is defined by the peak ground velocity (PGV) due to seismic activity ($V_{pg} = 0.939\,m/s$ for 10^{-5} annual exceedence probability [Ref. 23]) and the maximum distance between the WP and the emplacement drift ceiling (H_{max}).

The distance between the WP and the emplacement drift ceiling is calculated below by using the following parameters (see Attachment I for geometrical details):

$D = 5.5\,m$ = emplacement drift diameter (Ref. 12, Section 1.2.4.9, p. 14)
$a = 0.806\,m$ = distance from drift invert to bottom of EP (Ref. 13, Fig. 5)
$r = 1.869/2 = 0.9345\,m$ = OS outer radius (p. I-1)
$hg = 0.092\,m$ = rectangular tube height (p. I-13)
$wd = 0.0381\,m$ = half width of rectangular tube (p. I-13)
$th_1 = 0.00952\,m$ = thickness of EP plate #1 (p. I-16)
$th_6 = 0.0222\,mm$ = thickness of EP plate #6 (p. I-16)
$\alpha = 30^\circ$ = angle between EP plate #6 and horizontal plane (p. I-6)

The distance between the lowest point of the upper surface of the EP plate #6 and the bottom plane of the EP is

$$h = hg - wd \cdot Tan(\alpha) + th_1 + \frac{th_6}{Cos(\alpha)} = 0.092 - 0.0381 \cdot Tan(30^o) + 0.00952 + \frac{0.0222}{Cos(30^o)} = 0.105\,m$$

The distance between the WP and the emplacement drift ceiling is

$$H_{max} = D - a - [r/Cos(\alpha) + r + h] = 5.5 - 0.806 - [0.9345/Cos(30^\circ) + 0.9345 + 0.105] = 2.58\,m$$

From the equation of motion governing the fall of a body in the gravitational-acceleration field ($g = 9.81\ m/s^2$ is the acceleration due to gravity):

$$\ddot{y} = \pm g$$

and the initial conditions ($t = 0$):

$$\dot{y}(0) = V_{pg} \text{ and } y(0) = 0$$

the position of the body can be obtained in the form

$$y = \pm g \cdot t^2/2 + V_{pg} \cdot t \qquad (1)$$

The corresponding velocity

$$\dot{y} = \pm g \cdot t + V_{pg} \qquad (2)$$

is readily obtained by differentiation with respect to time of the Eq. (1). The positive sign corresponds to the case when gravity acceleration acts in the positive direction of the coordinate axis, and vice versa. These two expressions represent the solution of the problem of the fall of a body in the gravitational-acceleration field.

In order to derive the maximum impact velocity, it is necessary to postulate the most conservative sequence of events amenable to the closed-form solution. Due to the high-frequency nature of the seismic event (causing the rock fall) the number of scenarios is virtually unlimited. Nonetheless, the most conservative set of boundary conditions is the following:

i) The initial distance between the loose rock and the WP is equal to the initial distance between the WP and the emplacement drift ceiling ($H_{\max}$).
ii) The initial velocity of both the loose rock and the WP/EP assembly is the maximum possible velocity, i.e. the PGV (V_{pg}), in the direction of gravity (downward).
iii) The final velocity of the WP/EP assembly, just before the impact, is the PGV, in the direction opposite to gravity (upward).

The first two conditions can be achieved if the ground during the earthquake originally moves upward with the PGV, and then reverses the motion with the reversal acceleration equal to the acceleration due to gravity. At the moment when the ground, moving downward, reaches the PGV, the rock gets loose. This sequence of events also ensures that the contacts between the EP and EP support, and the WP and EP are maintained incessantly; events including contact separations are beyond the scope of present calculation. The velocity of the WP/EP assembly is, under these circumstances, controlled by the ground motion and the most conservative scenario is that they are moving downward with the PGV ($V = V_{pg} = Const.$). On the other hand, the loose rock is accelerating due to gravity. Thus, the rock is catching up with the WP/EP assembly, and finally they get into contact. It is supposed that just before the impact the ground momentarily reaches the PGV in the direction opposite to the gravity. This simplified approach maximizes the duration of the rock fall and consequently maximizes the velocity of the rock and the impact velocity.

Consequently, the distance traveled by the rock before the impact

$$S_{rock} = g \cdot t_f^2/2 + V_{pg} \cdot t_f \tag{3}$$

is obtained by substituting the impact time ($t \equiv t_f$) into the Eq. (1). Since the WP/EP assembly is moving with constant velocity ($V = V_{pg} = Const.$), the distance it travels before the impact is simply $S_{wp} = V_{pg} \cdot t_f$.

The final time by which the rock catches up with the WP

$$t_f = \sqrt{\frac{2 \cdot H_{\max}}{g}} \tag{4}$$

can be derived straightforwardly from the condition $S_{rock} = H_{\max} + S_{wp}$.

In the preceding calculation it is conservatively assumed that the reversal of ground velocity from V_{pg} to $-V_{pg}$ is instantaneous. The more realistic approach takes into account the finite reversal acceleration (a_{rev}) and the time necessary for the reversal (t_{rev}).

The expression for the distance traveled by rock before the impact (Eq. [3]) is still valid, but the distance is smaller since the impact time is reduced. The impact time can be expressed from the standpoint of the WP/EP assembly motion in the following manner:

$$t_f = \frac{S_{rock} - H_{\max}}{V_{pg}} + t_{rev} = \frac{S_{rock} - H_{\max}}{V_{pg}} + \frac{V_{pg} - (-V_{pg})}{a_{rev}}$$

The first term in the preceding sum is the time during which the WP/EP assembly is traveling downward with the constant velocity (PGV). The second term is the time necessary for the WP/EP-assembly velocity reversal from V_{pg} to $-V_{pg}$ at constant reversal acceleration ($a_{rev} = Const.$). Notice that the constant reversal acceleration ensures that the location of the WP/EP assembly at the end of reversal is the same as at the beginning.

From the preceding equation an alternative expression for the distance traveled by the rock before the impact can be readily derived:

$$S_{rock} = H_{\max} + V_{pg} \cdot t_f - \frac{2 \cdot V_{pg}^2}{a_{rev}} \tag{5}$$

Finally, the time of impact

$$t_f = \sqrt{\frac{2 \cdot H_{\max}}{g} \cdot \left(1 - \frac{2 \cdot V_{pg}^2}{H_{\max} \cdot a_{rev}}\right)} \tag{6}$$

follows from the equality of the Eqs. (3) and (5). Notice that as a_{rev} tends to infinity the Eq. (6) reduces to Eq. (4). Since the maximum possible ground acceleration during the seismic event is, by definition, the peak ground acceleration (PGA) it would be appropriate to use it in place of the reversal acceleration. In absence of the PGA, consistent with the PGV used in this calculation, Eq. (6) will be evaluated for illustrative purpose only, while the Eq. (4) will be used throughout this calculation. In the case of PGA being $1 \cdot g = 9.81 m/s^2$ and $1.25 \cdot g = 12.3 m/s^2$, the use of the Eq. (4) conservatively overestimates the collision time by 3.5% and 2.8%, respectively. This example illustrates that the Eq. (4) is good approximation of the Eq. (6) under the given circumstances.

Finally, the corresponding rock velocity is

$$V_f = g \cdot t_f + V_{pg} = V_{pg} + \sqrt{2 \cdot g \cdot H_{\max}}$$

When the initial rock velocity is zero the previous equation reduces to the familiar expression for the

free-fall velocity. The maximum velocity of the rock relative to the WP is obtained in the case when the WP, just prior to the impact, moves in the direction opposite to rock with velocity $V_{wp} = -V_{pg}$:

$$V = V_f - V_{wp} = 2 \cdot V_{pg} + \sqrt{2 \cdot g \cdot H_{\max}}$$

Therefore, for previously calculated $H_{\max} = 2.58\,m$ and $V_{pg} = 0.939\,m/s$ (Ref. 23), the impact velocity is:

$$V = 2 \cdot V_{pg} + \sqrt{2 \cdot g \cdot H_{\max}} = 2 \cdot 0.939 + \sqrt{2 \cdot 9.81 \cdot 2.58} = 9.0\,m/s$$

5.2.2 Calculations for Maximum Angle of Rock Inclination

The rock length (L_R) and the maximum distance between the emplacement drift ceiling and the WP define the maximum angle of rock inclination with respect to horizontal plane at the moment of impact:

$$\alpha = \arcsin(H_{\max}/L_R)$$

The maximum distance between the emplacement drift ceiling and the WP is calculated in Section 5.2.1. The rock dimensions are available in Reference 17 (Table IX-2, and pages IX-4 through IX-15) for selected rock sizes. The 6-MT (metric tons) and 10-MT rock lengths are obtained by linear interpolation of the lengths of nearest available rock dimensions; i.e. 5.3 *m* (5 *MT*) and 7.8 *m* (8 *MT*), and 7.8 *m* (8 *MT*) and 13.6 m (15 *MT*), respectively. The rock dimensions and corresponding maximum angles of rock inclination with respect to horizontal plane are given in Table 1. The calculated angles are presented with two significant digits rounded to the smaller number.

Table 1. Maximum Angle of Rock Inclination

Mass (MT)	Height (m)	Length (m)	Angle (degrees)
6	1.3	6.1	25
10	1.3	9.4	16

As for the 1-MT rock, the rock height and length, 1.6 *m* and 2.4 *m*, respectively (Ref. 17, Table IX-2), are such that any rock inclination is possible, i.e. the maximum distance between the WP and emplacement drift ceiling exerts no limit to the maximum angle of inclination. Consequently, the calculation for 1-MT rock fall is performed with angle of rock inclination of 57^o, for which the center of gravity of the rock is located right above the initial contact region (see Attachment III, 1_mt/57-degrees/rock.out, lines #2941 and #2995). This configuration, which is arrived at iteratively, maximizes the impact stresses in the WP OS.

5.3 MASS AND GEOMETRIC DIMENSIONS OF NAVAL SNF CANISTER

This calculation is performed by using the bounding mass and geometric dimensions of the Naval SNF canister obtained from Reference 3 (Enclosure 3, p. 2):

Mass $= 44452\ kg\ (49\ tons)$
Outside diameter $= 1.689\ m\ (66.5\ in)$
Length $= 5.385\ m\ (212\ in)$

5.3.1 Calculation for Density of Naval SNF Canister

The internal structure of the WP is simplified in the FER by reducing the structure of the Naval SNF canister to a solid cylinder of circular cross section and uniform density. This uniform density is calculated as a ratio of its mass and volume.

$$\text{Volume} = 5.385 \cdot \left(1.689^2 \cdot \pi\right)/4 = 12.065\ m^3$$
$$\text{Density} = 44452/12.065 = 3684\ kg/m^3$$

5.4 REDUCTION OF THICKNESS DUE TO CORROSION

Corrosion penetration rate for Alloy 22 is assumed to be $0.16\,\mu m/year$ (see Section 5.1 and Assumption 3.6). Furthermore, it is recommended in Reference 25 (p. 3-147) that the general corrosion rate should be corrected for the maximum bias due to silica scale deposit formation by adding a constant value of $0.063\,\mu m/year$ to each estimated value of the general corrosion rate. Therefore, the expected cumulative decrease of thickness of the WP OS and the EP plates over 10,000 years of post-closure emplacement would be $10000\cdot(0.16+0.063)\cdot 10^{-3}=2.23\,mm$. However, the effect of thermal aging can increase the corrosion penetration rate in Alloy 22-components of the WP by an enhancement factor of 2.5 (see Ref. 18, p. 102). This value represents an upper bound determined for the fully aged material. This enhancement factor is not applicable to the EP components since, due to lower temperature, they are not susceptible to aging-related corrosion rate enhancement. The second effect that may accelerate degradation of Alloy 22-components of both EP and WP is microbial-influenced corrosion. Corresponding enhancement factor is estimated in Reference 18 (p. 103) to be approximately 2.

Having in mind these estimates of the depth of corroded layer and the corrosion-acceleration effects, the simulation of rock fall on the corroded WP/EP assembly is performed with thickness of the WP OS conservatively reduced for $(2\cdot 2.5)\cdot 2.23=11.2\,mm$, and the thickness of EP plates reduced for $2\cdot 2.23=4.5\,mm$.

5.5 FINITE ELEMENT REPRESENTATION

The first step in this calculation is to estimate the effect of axial location of the initial impact region on the stress magnitudes in the OS (see Fig. 1). The objective of these preliminary calculations is to determine the most conservative simulation setup.

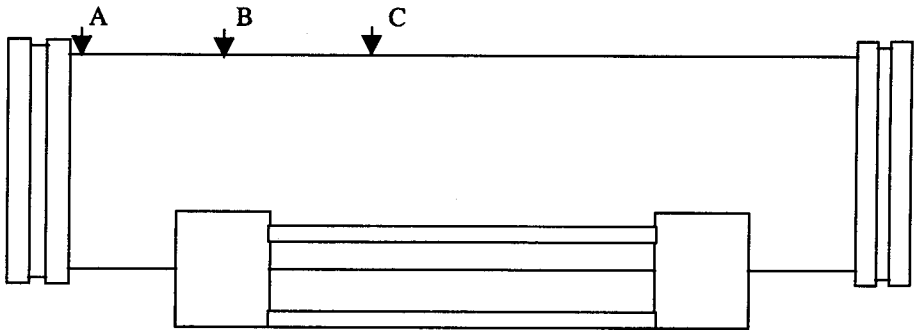

Figure 1. Initial contact locations

The results of corresponding calculations (see Table 2) suggest that the most conservative results are obtained when the axial location of the initial impact zone is close to the trunnion collar sleeve (Case A in Fig. 1). Consequently, the remaining calculations are performed for the Case A, that is the most conservative simulation setup achievable under given geometrical constraints.

Three three-dimensional half-symmetry FERs of the WP mounted on the EP and the rock are developed in ANSYS V5.4 for the three different rock sizes (1 MT, 6 MT, and 10 MT). FERs are developed by using the dimensions provided in Attachment I and Sections 5.2 through 5.4. The internal structure of the WP is simplified by reducing the structure of the Naval SNF canister to a solid cylinder of circular cross section and uniform density. The total mass and geometric dimensions of the Naval SNF canister define the density (see Sections 5.3 and 5.3.1). The benefit of using this approach is to reduce the computer execution time while preserving all features of the problem relevant to the structural calculation.

The FER of the WP is developed in such a way that the loose-fit gap between the outer and inner shell is maximized to $4\,mm$ (Ref. 20, p. 15). As a result, having in mind the importance of preserving the nominal dimensions of the OS, the thickness of the inner shell is reduced from $50\,mm$ to $46\,mm$. Consequently, the inner shell is free to move within the OS, as well as the Naval canister within the inner shell. Having in mind that there are gaps between inner shell and OS, and the inner shell and the Naval canister, the dominant mode of deformation of the shells is bending; the thinning of the shell (reduction of thickness) in the impact region is considered negligible. It is, therefore, considered appropriate to represent the inner shell and the OS with quadrilateral shell elements.

These three FERs are then used in LS-DYNA V950 to perform a transient dynamic analysis of rock fall. The rock shapes are based on the rock geometry and dimensions obtained from the Subsurface Facility Department (Ref. 17, Table IX-2, and pages IX-4 through IX-15). For all rock sizes the calculations are performed for both horizontal and inclined initial rock configurations. For the smallest rock (1 MT) the angle of rock inclination with respect to the WP, 57°, is such that the center of gravity of the rock is approximately above the initial contact region (see Section 5.2.2). This configuration is conservative, since almost entire kinetic energy of the rock is transferred to deformation energy within a relatively small impact area. On the other hand, in the case of 6-MT and 10-MT rocks, the maximum distance between the emplacement drift ceiling and the WP limits the maximum angle of inclination (Section 5.2.2). In order to simplify the calculations and obtain a bounding set of results, the rock velocity, calculated in Section 5.2.1, is adopted for all rocks regardless of their angle of inclination.

Contact elements are used to represent contacts between: rock and OS, rock and trunnion collar sleeve, OS and inner shell, OS and EP, and inner shell and Naval canister. In absence of more appropriate data the dynamic friction coefficients for all contacts are assumed to be 0.4 (see Assumptions 3.11 through 3.13). Moreover, the functional friction coefficient used by LS-DYNA V950 FE code is defined in terms of static and dynamic friction coefficients, and relative velocity of the surfaces in contact. The effect of the relative velocity of the surfaces in contact is introduced by the way of a fitting parameter - exponential decay coefficient. The variation of friction coefficient between the static and dynamic value as a function of relative velocity of the surfaces in contact is not available in literature for the materials used in this calculation. Therefore, it is not possible to objectively evaluate the exponential decay coefficient. Hence, the effect of relative velocity of the surfaces in contact is neglected in these calculations by assuming that the functional friction coefficient and the static friction coefficient are equal to the dynamic friction coefficient. This approach provides the bounding set of results by minimizing the friction coefficient within the given FEA framework (Assumption 3.14).

The specified rock-fall-simulation termination times are such to allow the rock to bounce off the WP after the impact, and for the steady-state stresses to establish.

For the simulation of the rock fall on corroded WP/EP assembly, the thickness of the Alloy 22 components is appropriately reduced based on the calculation of the depth of corroded layer presented in Section 5.4. Having in mind that Alloy 22 has much superior corrosion-resistance properties than 316 SS, the EP SS tubes are removed from the FER in this simulation.

The mesh of the FER was appropriately generated and refined in the contact region according to standard engineering practice (see Fig. II-1). Thus, the accuracy and representativeness of the results of this calculation were deemed acceptable (see Table 3).

6. RESULTS

This document may be affected by technical product input information that requires confirmation. Any changes to the document that may occur as a result of completing the confirmation activities will be reflected in subsequent revisions. The status of the technical product input information quality may be confirmed by review of the Document Input Reference System database.

LS-DYNA stress results include high-frequency response. In the case of stress histories used for determination of residual stresses, these results are filtered using a Butterworth low-pass filter with cut-off frequency of 20 Hz. The purpose of the filtering is to obtain steady-state residual stresses by removing the high-frequency response. Since the stress results after the filtering produced steady-state values anticipated by visual inspection of unfiltered (raw) stress histories (see, for example, Figures II-5, II-9 and II-13), this type of filtering was deemed acceptable. Consequently, all axial and tangential stress histories across the OS thickness, presented in Attachment II, are filtered in described manner.

The stress-field plots obtained from LS-DYNA V950 (Figs. II-72 and II-73) are reported in terms of maximum shear stress. Since the maximum stress intensities are desired, and the stress-intensity time histories are presented throughout the document, the stress-field results needed to be translated appropriately. The maximum shear stress is defined as one-half the difference between maximum and minimum principal stress. Stress intensity is defined as the difference between maximum and minimum principal stress. Therefore, the results presented in Figures II-72 and II-73 need to be multiplied by two, to obtain the corresponding stress intensities.

The maximum stresses are found by careful examination of each time step recorded by LS-DYNA V950, which outputs the element with the highest magnitude of certain stress component, at each recorded step, for each defined part.

The first set of results, presented in Table 2, refers to the three possible simulation configurations illustrated in Figure 1. All three calculations are performed for the case of 6-MT rock fall, with the angle of initial rock inclination being 25^{o}. All presented stress magnitudes, recorded in the OS, are the maximum values of the corresponding stress quantity; the qualifier "maximum" is suppressed for brevity in the Tables 2 and 3. The residual stresses are recorded on the outer surface of the OS.

The results in Table 2 indicate that the Case A (see Figure 1) is characterized by the maximum residual stresses in the OS, while the Case C is characterized by the maximum stress intensity. On the other hand, the Case B results in the maximum first principal stress. Therefore, the Case C is the most interesting from the point of view of potential immediate crack nucleation and propagation due to impact, while the Case A seems to be more critical from the standpoint of stress corrosion cracking (SSC). Nonetheless, while the difference in the maximum stress intensity is relatively small ($\approx 5.0\%$), the difference in the residual stresses is more pronounced ($\approx 25\% - 30\%$). Additionally

the simulation of the rock impacting close to the OS lid weld seems more interesting in itself. The remaining calculations are, therefore, performed for the Case A.

Table 2. Stress Components in OS for Three Different Initial Impact Locations

	Stress Intensity (MPa)	Residual Stress Intensity on Outer Surface (MPa)	First Principal Stress (MPa)	Residual First Principal Stress on Outer Surface (MPa)
Case A	579 (Fig. II-2)	370 (Fig. II-3)	507 (Fig. II-4)	155 (Fig. II-5)
Case B	578 (Fig. II-6)	310 (Fig. II-7)	523 (Fig. II-8)	121 (Fig. II-9)
Case C	609 (Fig. II-10)	280 (Fig. II-11)	461 (Fig. II-12)	104 (Fig. II-13)

Furthermore, the calculation results for 25-degrees 6-MT rock fall are presented in Table 3 for two different FER mesh densities. The purpose of this inquiry is to verify the objectivity of the mesh, i.e. that the calculation results are not mesh-sensitive. Having that purpose in mind the canister mesh of the second FE representation is refined more in the impact region compared to the first one. Specifically, the area of the OS element size in the initial-impact region (characterized by the highest stresses) in the second FER mesh is reduced by 37% compared to the original mesh (number of axial and tangential divisions are increased from 28 to 36 and from 26 to 32, respectively; see corresponding wpp1.inp files [lines #723 through #740] in Attachment III [6_mt/25-degrees/Case_A: /Intact and /Refined_Mesh]).

Table 3. Stress Intensity and First Principal Stresses for Two Different FER Meshes

	Stress Intensity (MPa)	Residual Stress Intensity on Outer Surface (MPa)	First Principal Stress (MPa)	Residual First Principal Stress on Outer Surface (MPa)
Original Mesh	579 (Fig. II-2)	370 (Fig. II-3)	507 (Fig. II-4)	155 (Fig. II-5)
Refined Mesh	567 (Fig. II-14)	369 (Fig. II-15)	479 (Fig. II-16)	155 (Fig. II-17)
Difference (%)	-2.1	-0.3	-5.8	0

The calculation results presented in Table 3 indicate that the reduction of the element-size area by almost one-half in the contact region results in very mild sensitivity of the stress intensities and the first principal stresses. The original FER mesh is, therefore, deemed acceptable, and all remaining calculations are performed with the coarser mesh.

The further calculation results, presented in Tables 4 and 5, refer to the three different evaluated rock sizes (1 *MT*, 6 *MT*, and 10 *MT*), and both horizontal and inclined initial rock configurations. The stress measures presented in Table 4 are the stress intensity and the first principal stress.

Table 4. Stress Intensity and First Principal Stress in OS for Three Different Rock Sizes

Rock Mass (MT)	Angle of Initial Rock Inclination (degree)	Maximum Stress Intensity (MPa)	Maximum Residual Stress Intensity on Outer Surface (MPa)	Maximum First Principal Stress (MPa)	Maximum Residual First Principal Stress on Outer Surface (MPa)
1	0	322 (Fig. II-18)	223 (Fig. II-19)	317 (Fig. II-20)	88 (Fig. II-21)
	57	502 (Fig. II-26)	330 (Fig. II-27)	501 (Fig. II-28)	103 (Fig. II-29)
6	0	409 (Fig. II-34)	308 (Fig. II-35)	390 (Fig. II-36)	180 (Fig. II-37)
	25	579 (Fig. II-2)	370 (Fig. II-3)	507 (Fig. II-4)	155 (Fig. II-5)
10	0	416 (Fig. II-45)	305 (Fig. II-46)	402 (Fig. II-47)	195 (Fig. II-48)
	16	499 (Fig. II-53)	325 (Fig. II-54)	486 (Fig. II-55)	210 (Fig. II-56)

The maximum stress intensities and first principal stresses in all cases are below 70% of the true tensile strength for Alloy 22 ($0.7 \cdot 909\ MPa = 636\ MPa$) at the given temperature. It should be noted that the stresses are smaller for the 10-MT inclined impact than for the 6-MT inclined impact. The possible explanation is that the center of gravity of 6-MT rock is much closer to the impact region than in the case of the 10-MT rock.

Table 5 presents the stress components in the global coordinate system, namely the axial and tangential stress. It seems appropriate to explain some of the presented stress measures. Numbers in columns 3 though 6 represent corresponding stress quantities at three different positions across the shell thickness; specifically at the outer, middle (reference), and inner surface. The maximum axial and tangential residual stresses, respectively presented in columns 3 and 5, refer to the element with maximum corresponding residual stress component at the outer (upper) surface. One should keep in mind though that the nature of the load application is such that the maximum (tensile) stress is almost always at the inner surface of the shell. Lastly, the stresses in columns 4 and 6 refer to the element with maximum axial and tangential residual stress component at the middle (reference) surface that also exhibits the tensile stresses at the outer surface. It should be noticed that results presented in these two columns are obtained by careful examination of many, but naturally not each and every location. Therefore, it is not certain that the given location is the most favorable to SCC.

It seems necessary to reemphasize that in the case of inclined rock fall the simulations are terminated after the first impact. It should be also noticed that in the case of 6-MT and 10-MT horizontal rock fall the unavoidable initial impact of the rock tail with the trunnion collar sleeve reduces the maximum stresses in the OS that occur at the place of impact where maximum stresses occur.

Table 5. Stress Components in OS for Three Different Rock Sizes

Rock Mass (MT)	Angle of Initial Rock Inclination (degree)	Maximum Residual Axial Stress (MPa)	Residual Axial Stress (MPa)	Maximum Residual Tangential Stress (MPa)	Residual Tangential Stress (MPa)
1	0	88 / -44 / 76 (Fig. II-22)	12 / 17 / 22 (Fig. II-23)	37 / 62 / 22 (Fig. II-24)	37 / 63 / 22 (Fig. II-25)
	57	92 / -50 / 37 (Fig. II-30)	37 / 46 / 74 (Fig. II-31)	87 / 22 / -51 (Fig. II-32)	80 / 106 / -73 (Fig. II-33)
6	0	105 / -20 / -125 (Fig. II-38)	18 / 22 / 2 (Fig. II-39)	155 / 30 / -47 (Fig. II-40)	83 / 110 / 45 (Fig. II-41)
	25	98 / 98 / 80 (Fig. II-42)	98 / 98 / 80 (Fig. II-42)	137 / 20 / -95 (Fig. II-43)	42 / 108 / 77 (Fig. II-44)
10	0	120 / -60 / 87 (Fig. II-49)	12 / 16 / 22 (Fig. II-50)	162 / 32 / -58 (Fig. II-51)	82 / 110 / 52 (Fig. II-52)
	16	202 / -45 / -210 (Fig. II-57)	94 / 115 / 85 (Fig. II-58)	130 / 13 / -90 (Fig. II-59)	47 / 113 / 64 (Fig. II-60)

NOTE: Stresses are given in the following order: outer / middle / inner shell surface.

The calculation results in Tables 6 and 7 are presented for the comparison of the OS stresses in the corroded vs. intact WP/EP assembly (see Section 5.4). Both calculations are performed for 6-MT rock, with 25^{o} angle of initial rock inclination.

The results, presented in Table 6, indicate higher maximum stresses in the corroded OS, as expected. The stress intensity and the first principal stress in the corroded OS are above 70% but below 90% of the true tensile strength for Alloy 22 ($636\,MPa$ and $818\,MPa$, respectively) at the given temperature.

Table 6. Stress Intensity and First Principal Stress in Corroded vs. Intact OS

	Maximum Stress Intensity (MPa)	Maximum Residual Stress Intensity on Outer Surface (MPa)	Maximum First Principal Stress (MPa)	Maximum Residual First Principal Stress on Outer Surface (MPa)
Intact OS	579 (Fig. II-2)	370 (Fig. II-3)	507 (Fig. II-4)	155 (Fig. II-5)
Corroded OS	810 (Fig. II-61)	363 (Fig. II-62)	714 (Fig. II-63)	217 (Fig. II-64)

Table 7 presents the axial and tangential stress components in the global coordinate system, in the same manner used previously in Table 5.

Table 7. Stress Components in Corroded vs. Intact OS

	Maximum Residual Axial Stress (MPa)	Residual Axial Stress (MPa)	Maximum Residual Tangential Stress (MPa)	Residual Tangential Stress (MPa)
Intact OS	98 / 98 / 80 (Fig. II-42)	98 / 98 / 80 (Fig. II-42)	137 / 20 / -95 (Fig. II-43)	42 / 108 / 77 (Fig. II-44)
Corroded OS	128 / 109 / 52 (Fig. II-65)	128 / 109 / 52 (Fig. II-65)	150 / 0 / -117 (Fig. II-66)	95 / 112 / 99 (Fig. II-67)

NOTE: Stresses are given in the following order: outer / middle / inner shell surface.

Notice that the residual axial and tangential stresses are, for both intact and corroded shell, recorded at the same location for the sake of comparison.

The calculation results in Table 8 are obtained from the same pair of simulations (6-MT rock, 25^o angle of initial rock inclination) that are previously presented in Tables 6 and 7. The difference is that in the Table 8 the emphasis is on the EP rather than the WP.

Table 8. Stress Intensity and Vertical Displacement of Lifting Surface: Corroded vs. Intact EP

	Maximum Stress Intensity (MPa)	Average Vertical Displacement of Lifting Surface (EP plate #9) (mm)
Intact EP	327 (Fig. II-68)	0.00 (Fig. II-69)
Corroded EP	394 (Fig. II-70)	-0.20 (Fig. II-71)

Having in mind retrieval concerns, the presented results are limited to the maximum stress intensity and the maximum displacement of the lifting surface (EP plate #9) in negative direction of vertical axis. The results indicate that the permanent vertical displacement of the lifting surface, following 6-MT rock fall, is negligible for both intact and corroded EPs. The stress intensities in both cases are below 70% of the true tensile strength for Alloy 22 ($636\,MPa$) at the given temperature. The difference between the maximum stress intensities, in the two cases, is approximately 20%.

7. REFERENCES

1. ASM (American Society for Metals) 1980. *Properties and Selection: Stainless Steels, Tool Materials and Special-Purpose Metals.* Volume 3 of *Metals Handbook.* 9th Edition. Benjamin, D., ed. Metals Park, Ohio: American Society for Metals. TIC: 209801.

2. Haynes International 1997. *Hastelloy C-22 Alloy.* Kokomo, Indiana: Haynes International. TIC: 238121.

3. Naples, E.M. 1999. Thermal, Shielding, and Structural Information on the Naval Spent Nuclear Fuel (SNF) Canister. Letter from E.M. Naples (Department of the Navy) to D.C. Haught (DOE/YMSCO), August 6, 1999, with enclosures. ACC: MOL.19991001.0133.

4. CRWMS M&O 2000. *Software Code: LS-DYNA.* V950. HP 9000. 10300-950-00.

5. AP-3.12Q, Rev. 0, ICN 4. *Calculations.* Washington, D.C.: U.S. Department of Energy, Office of Civilian Radioactive Waste Management. ACC: MOL.20010404.0008.

6. AP-SV.1Q, Rev. 0, ICN 2. *Control of the Electronic Management of Information.* Washington, D.C.: U.S. Department of Energy, Office of Civilian Radioactive Waste Management. ACC: MOL.20000831.0065.

7. Dieter, G.E. 1976. *Mechanical Metallurgy.* 2nd Edition. Materials Science and Engineering Series. New York, New York: McGraw-Hill Book Company. TIC: 247879.

8. CRWMS M&O 1998. *ANSYS.* V5.4. HP-UX 10.20. 30040 5.4.

9. ASM International 1987. *Corrosion.* Volume 13 of *Metals Handbook.* 9th Edition. Metals Park, Ohio: ASM International. TIC: 209807.

10. ASTM G 1-90 (Reapproved 1999). 1990. *Standard Practice for Preparing, Cleaning, and Evaluating Corrosion Test Specimens.* West Conshohocken, Pennsylvania: American Society for Testing and Materials. TIC: 238771.

11. MO9808RIB00041.000. Reference Information Base Data Item: Rock Geomechanical Properties. Submittal date: 08/05/1998.

12. CRWMS M&O 2000. *Emplacement Drift System Description Document.* SDD-EDS-SE-000001 REV 01. Las Vegas, Nevada: CRWMS M&O. ACC: MOL.20000803.0348.

13. CRWMS M&O 2000. *Invert Configuration and Drip Shield Interface.* TDR-EDS-ST-000001 REV 00. Las Vegas, Nevada: CRWMS M&O. ACC: MOL.20000505.0232.

14. CRWMS M&O 2000. *Stress-Strain-Curve Character for Alloy 22 and 316 Stainless Steel.* Input Transmittal 00384.T. Las Vegas, Nevada: CRWMS M&O. ACC: MOL.20001013.0053.

15. Allegheny Ludlum 1999. "Technical Data Blue Sheet, Stainless Steels, Chromium-Nickel-Molybdenum, Types 316 (S31600), 316L (S31603), 317 (S31700), 317L (S31703)." Pittsburgh, Pennsylvania: Allegheny Ludlum Corporation. Accessed July 31, 2000. TIC: 248631. http://www.alleghenytechnologies.com/ludlum/pages/products/t316_317.pdf

16. ASME (American Society of Mechanical Engineers) 1998. *1998 ASME Boiler and Pressure Vessel Code.* 1998 Edition with 1999 and 2000 Addenda. New York, New York: American Society of Mechanical Engineers. TIC: 247429.

17. CRWMS M&O 2000. *Drift Degradation Analysis.* ANL-EBS-MD-000027 REV 01. Las Vegas, Nevada: CRWMS M&O. ACC: MOL.20001206.0006.

18. CRWMS M&O 2000. *General Corrosion and Localized Corrosion of Waste Package Outer Barrier.* ANL-EBS-MD-000003 REV 00. Las Vegas, Nevada: CRWMS M&O. ACC: MOL.20000202.0172.

19. CRWMS M&O 2000. *Drift Scale Thermal Analysis.* CAL-WIS-TH-000002 REV 00. Las Vegas, Nevada: CRWMS M&O. ACC: MOL.20000420.0401.

20. CRWMS M&O 2000. *Waste Package Operations Fabrication Process Report.* TDR-EBS-ND-000003 REV 00. Las Vegas, Nevada: CRWMS M&O. ACC: MOL.20000217.0244.

21. MO0003RIB00079.000. Rock Mechanical Properties. Submittal date: 03/30/2000.

22. Boyer, H.E., ed. 2000. *Atlas of Stress-Strain Curves.* Metals Park, Ohio: ASM International. TIC: 248901.

23. MO0008SEPPGVRL.020. Preliminary Seismic Design Peak Ground Velocity for the Repository Level (Point B) for 10-5 Annual Exceedence Probability. Submittal date: 08/24/2000.

24. BSC (Bechtel SAIC Company) 2001. *Technical Work Plan for: Waste Package Design Description for SR.* TWP-EBS-MD-000003 REV 01. Las Vegas, Nevada: Bechtel SAIC Company. ACC: MOL.20010629.0074.

25. CRWMS M&O 2000. *Waste Package Degradation Process Model Report.* TDR-WIS-MD-000002 REV 00 ICN 02. Las Vegas, Nevada: CRWMS M&O. ACC: MOL.20001228.0229.

26. CRWMS M&O 2000. Process Control Evaluation for Supplement V: "CAL-EBS-ME-000009 REV 00". Las Vegas, Nevada: CRWMS M&O. ACC: MOL.20000922.0080.

27. Guida, R.A. 1997. Size and Weight Limits for Canisters Used for Disposal of Naval Spent Nuclear Fuel. Letter from R.A. Guida (Department of the Navy) to Dr. R. Dyer (DOE), October 29, 1997. ACC: MOL.19980121.0011.

28. Beer, F.P. and Johnston, E.R., Jr. 1977. *Vector Mechanics for Engineers, Statics.* 3rd Edition. New York, New York: McGraw-Hill Book Company. TIC: 247391.

29. Avallone, E.A. and Baumeister, T., III, eds. 1987. *Marks' Standard Handbook for Mechanical Engineers.* 9th Edition. New York, New York: McGraw-Hill. TIC: 206891.

30. Meriam, J.L. and Kraige, L.G. 1987. *Statics.* Volume 1 of *Engineering Mechanics.* 2nd Edition. Pages 441, 443. New York, New York: John Wiley & Sons. TIC: 241293.

8. ATTACHMENTS

Attachment I (16 pages): Design sketches (*Naval SNF Long Waste Package Configuration for Site Recommendation* [SK-0194 REV 01], two sheets [this attachment uses Reference 27]; *Naval SNF Long Waste Package Weld Configuration* [SK-0195 REV 00], one sheet; *Emplacement Pallet Long* [SK-0232 REV 00], thirteen sheets)

Attachment II (38 pages): Figures obtained from LS-DYNA V950

Attachments III (Compact Disc): ANSYS V5.4 and LS-DYNA V950 electronic files

Table 9. Attachment III: File Directories, Names, Dates, Times, and Sizes

Directory	Name	Date	Time	Size
1_mt/0-degrees	d3hsp	07/20/01	10:08 a.m.	6,959 KB
	r1mt.k	07/20/01	10:08 a.m.	8 KB
	r1mte2.inc	07/20/01	10:08 a.m.	111 KB
	r1mtn2.inc	07/20/01	10:08 a.m.	97 KB
	r1mts2.inc	07/20/01	10:08 a.m.	18 KB
	r1mts22.inc	07/20/01	10:08 a.m.	2 KB
	rmte1.inc	07/20/01	10:08 a.m.	1,032 KB
	rmtn1.inc	07/20/01	10:08 a.m.	1,158 KB
	rmts1.inc	07/20/01	10:08 a.m.	9 KB
	rmts12.inc	07/20/01	10:08 a.m.	10 KB
	rmts13.inc	07/20/01	10:08 a.m.	1 KB
	rock.inp	07/20/01	10:08 a.m.	7 KB
	rock.out	07/20/01	10:08 a.m.	92 KB
	wpp1.inp	07/20/01	10:08 a.m.	22 KB
	wpp1.out	07/20/01	10:08 a.m.	190 KB
1_mt/57-degrees	d3hsp	07/20/01	03:14 p.m.	7,396 KB
	r1mt.k	07/20/01	10:09 a.m.	8 KB
	r1mte2.inc	07/20/01	10:09 a.m.	234 KB
	r1mtn2.inc	07/20/01	10:09 a.m.	195 KB
	r1mts2.inc	07/20/01	10:09 a.m.	35 KB
	r1mts22.inc	07/20/01	10:09 a.m.	3 KB
	rmte1.inc	07/20/01	10:09 a.m.	1,032 KB
	rmtn1.inc	07/20/01	10:09 a.m.	1,158 KB
	rmts1.inc	07/20/01	10:09 a.m.	9 KB
	rmts12.inc	07/20/01	10:09 a.m.	10 KB
	rmts13.inc	07/20/01	10:09 a.m.	1 KB
	rock.inp	07/20/01	10:09 a.m.	7 KB
	rock.out	07/20/01	10:09 a.m.	150 KB
	wpp1.inp	07/20/01	10:09 a.m.	22 KB
	wpp1.out	07/20/01	10:09 a.m.	190 KB

10_mt/0-degrees	d3hsp	07/20/01	10:07 a.m.	10,296 KB
	r10mt.k	07/20/01	10:06 a.m.	8 KB
	r10mte2.inc	07/20/01	10:06 a.m.	1,082 KB
	r10mtn2.inc	07/20/01	10:06 a.m.	845 KB
	r10mts2.inc	07/20/01	10:06 a.m.	150 KB
	r10mts22.inc	07/20/01	10:06 a.m.	8 KB
	rmte1.inc	07/20/01	10:06 a.m.	1,032 KB
	rmtn1.inc	07/20/01	10:06 a.m.	1,158 KB
	rmts1.inc	07/20/01	10:06 a.m.	9 KB
	rmts12.inc	07/20/01	10:06 a.m.	10 KB
	rmts13.inc	07/20/01	10:06 a.m.	1 KB
	rock.inp	07/20/01	10:06 a.m.	7 KB
	rock.out	07/20/01	10:06 a.m.	475 KB
	wpp1.inp	07/20/01	10:06 a.m.	22 KB
	wpp1.out	07/20/01	10:06 a.m.	190 KB
10_mt/16-degrees	d3hsp	07/23/01	08:14 a.m.	10,299 KB
	r10mt.k	07/23/01	08:14 a.m.	8 KB
	r10mte2.inc	07/23/01	08:14 a.m.	1,082 KB
	r10mtn2.inc	07/23/01	08:14 a.m.	845 KB
	r10mts2.inc	07/23/01	08:14 a.m.	150 KB
	r10mts22.inc	07/23/01	08:14 a.m.	8 KB
	rmte1.inc	07/23/01	08:14 a.m.	1,032 KB
	rmtn1.inc	07/23/01	08:14 a.m.	1,158 KB
	rmts1.inc	07/23/01	08:14 a.m.	9 KB
	rmts12.inc	07/23/01	08:14 a.m.	10 KB
	rmts13.inc	07/23/01	08:14 a.m.	1 KB
	rock.inp	07/23/01	08:14 a.m.	7 KB
	rock.out	07/23/01	08:14 a.m.	475 KB
	wpp1.inp	07/23/01	08:14 a.m.	22 KB
	wpp1.out	07/23/01	08:14 a.m.	190 KB
6_mt/0-degrees	d3hsp	07/23/01	08:13 a.m.	7,687 KB
	r6mt.k	07/23/01	08:13 a.m.	8 KB
	r6mte2.inc	07/23/01	08:13 a.m.	321 KB
	r6mtn2.inc	07/23/01	08:13 a.m.	264 KB
	r6mts2.inc	07/23/01	08:13 a.m.	47 KB
	r6mts22.inc	07/23/01	08:13 a.m.	4 KB
	rmte1.inc	07/23/01	08:13 a.m.	1,032 KB
	rmtn1.inc	07/23/01	08:13 a.m.	1,158 KB
	rmts1.inc	07/23/01	08:13 a.m.	9 KB
	rmts12.inc	07/23/01	08:13 a.m.	10 KB
	rmts13.inc	07/23/01	08:13 a.m.	1 KB
	rock.inp	07/23/01	08:13 a.m.	7 KB
	rock.out	07/23/01	08:13 a.m.	99 KB
	wpp1.inp	07/23/01	08:13 a.m.	22 KB
	wpp1.out	07/23/01	08:13 a.m.	190 KB

6_mt/25-degrees/Case_A/Intact	d3hsp	07/20/01	10:03 a.m.	7,687 KB
	r6mt.k	07/20/01	10:03 a.m.	8 KB
	r6mte2.inc	07/20/01	10:03 a.m.	321 KB
	r6mtn2.inc	07/20/01	10:03 a.m.	264 KB
	r6mts2.inc	07/20/01	10:03 a.m.	47 KB
	r6mts22.inc	07/20/01	10:03 a.m.	4 KB
	rmte1.inc	07/20/01	10:03 a.m.	1,032 KB
	rmtn1.inc	07/20/01	10:03 a.m.	1,158 KB
	rmts1.inc	07/20/01	10:03 a.m.	9 KB
	rmts12.inc	07/20/01	10:03 a.m.	10 KB
	rmts13.inc	07/20/01	10:03 a.m.	1 KB
	rock.inp	07/20/01	10:03 a.m.	7 KB
	rock.out	07/20/01	10:03 a.m.	99 KB
	wpp1.inp	07/20/01	10:03 a.m.	22 KB
	wpp1.out	07/20/01	10:03 a.m.	190 KB
6_mt/25-degrees/Case_A/Corroded	d3hsp	07/23/01	01:21 p.m.	7,074 KB
	r6mt.k	07/23/01	01:21 p.m.	8 KB
	r6mte2.inc	07/23/01	01:21 p.m.	321 KB
	r6mtn2.inc	07/23/01	01:21 p.m.	264 KB
	r6mts2.inc	07/23/01	01:21 p.m.	47 KB
	r6mts22.inc	07/23/01	01:21 p.m.	4 KB
	rmte1.inc	07/23/01	01:21 p.m.	900 KB
	rmtn1.inc	07/23/01	01:21 p.m.	1,158 KB
	rmts1.inc	07/23/01	01:21 p.m.	9 KB
	rmts12.inc	07/23/01	01:21 p.m.	10 KB
	rmts13.inc	07/23/01	01:21 p.m.	1 KB
	rock.inp	07/23/01	01:21 p.m.	7 KB
	rock.out	07/23/01	01:21 p.m.	99 KB
	wpp1.inp	07/23/01	01:20 p.m.	22 KB
	wpp1.out	07/23/01	01:20 p.m.	190 KB
6_mt/25-degrees/Case_B	d3hsp	07/23/01	03:14 p.m.	7,696 KB
	r6mt.k	07/20/01	10:08 a.m.	8 KB
	r6mte2.inc	07/20/01	10:08 a.m.	321 KB
	r6mtn2.inc	07/20/01	10:08 a.m.	264 KB
	r6mts2.inc	07/20/01	10:08 a.m.	47 KB
	r6mts22.inc	07/20/01	10:08 a.m.	4 KB
	rmte1.inc	07/20/01	10:08 a.m.	1,013 KB
	rmtn1.inc	07/20/01	10:08 a.m.	1,136 KB
	rmts1.inc	07/20/01	10:08 a.m.	9 KB
	rmts12.inc	07/20/01	10:08 a.m.	10 KB
	rmts13.inc	07/20/01	10:08 a.m.	1 KB
	rock.inp	07/20/01	10:08 a.m.	7 KB
	rock.out	07/20/01	10:08 a.m.	99 KB
	wpp1.inp	07/20/01	10:08 a.m.	22 KB
	wpp1.out	07/20/01	10:08 a.m.	184 KB

6_mt/25-degrees/Case_C	d3hsp	07/23/01	10:05 p.m.	7,562 KB
	r6mt.k	07/20/01	10:05 a.m.	8 KB
	r6mte2.inc	07/20/01	10:05 a.m.	321 KB
	r6mtn2.inc	07/20/01	10:05 a.m.	264 KB
	r6mts2.inc	07/20/01	10:05 a.m.	47 KB
	r6mts22.inc	07/20/01	10:05 a.m.	4 KB
	rmte1.inc	07/20/01	10:05 a.m.	1,010 KB
	rmtn1.inc	07/20/01	10:04 a.m.	1,133 KB
	rmts1.inc	07/20/01	10:04 a.m.	9 KB
	rmts12.inc	07/20/01	10:04 a.m.	10 KB
	rmts13.inc	07/20/01	10:04 a.m.	1 KB
	rock.inp	07/20/01	10:04 a.m.	7 KB
	rock.out	07/20/01	10:04 a.m.	99 KB
	wpp1.inp	07/20/01	10:04 a.m.	22 KB
	wpp1.out	07/20/01	10:04 a.m.	184 KB
6_mt/25-degrees/Case_A/Refined_Mesh	d3hsp	07/23/01	10:11 p.m.	8,745 KB
	r6mt.k	07/20/01	10:11 a.m.	8 KB
	r6mte2.inc	07/20/01	10:11 a.m.	321 KB
	r6mtn2.inc	07/20/01	10:11 a.m.	264 KB
	r6mts2.inc	07/20/01	10:11 a.m.	47 KB
	r6mts2.inc	07/20/01	10:11 a.m.	4 KB
	rmte1.inc	07/20/01	10:11 a.m.	1,213 KB
	rmtn1.inc	07/20/01	10:11 a.m.	1,367 KB
	rmts1.inc	07/20/01	10:11 a.m.	9 KB
	rmts12.inc	07/20/01	10:11 a.m.	10 KB
	rmts13.inc	07/20/01	10:11 a.m.	1 KB
	rock.inp	07/20/01	10:11 a.m.	7 KB
	rock.out	07/20/01	10:11 a.m.	99 KB
	wpp1.inp	07/20/01	10:11 a.m.	22 KB
	wpp1.out	07/20/01	10:11 a.m.	203 KB

NOTE: The file sizes may vary with operating system.

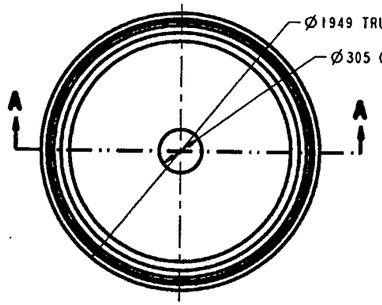

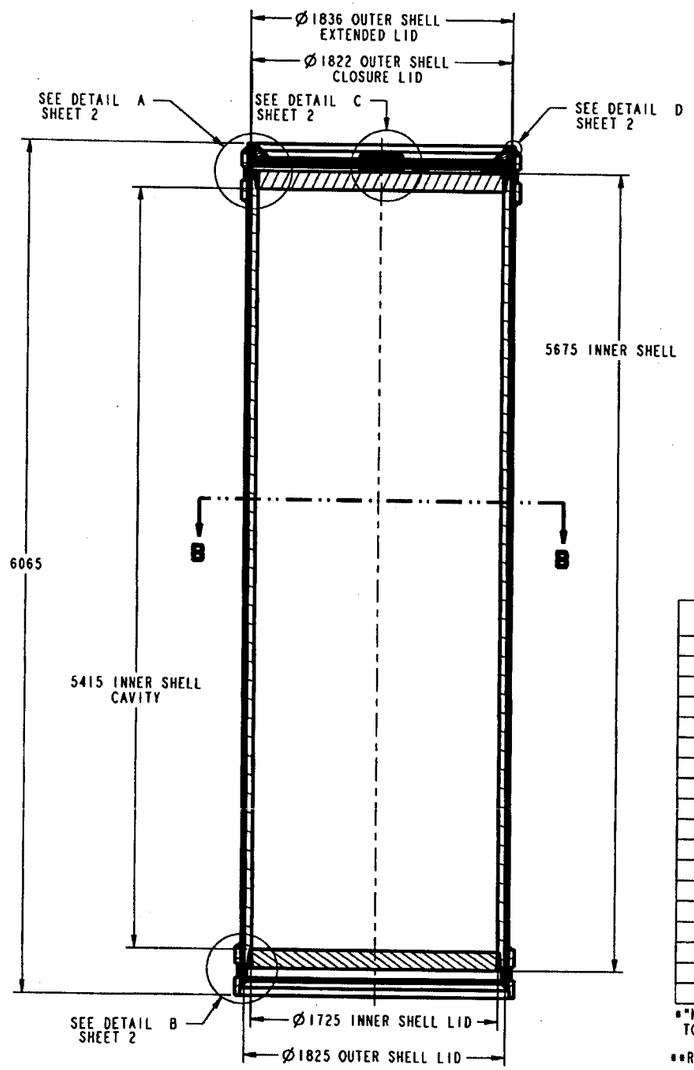

SECTION A-A

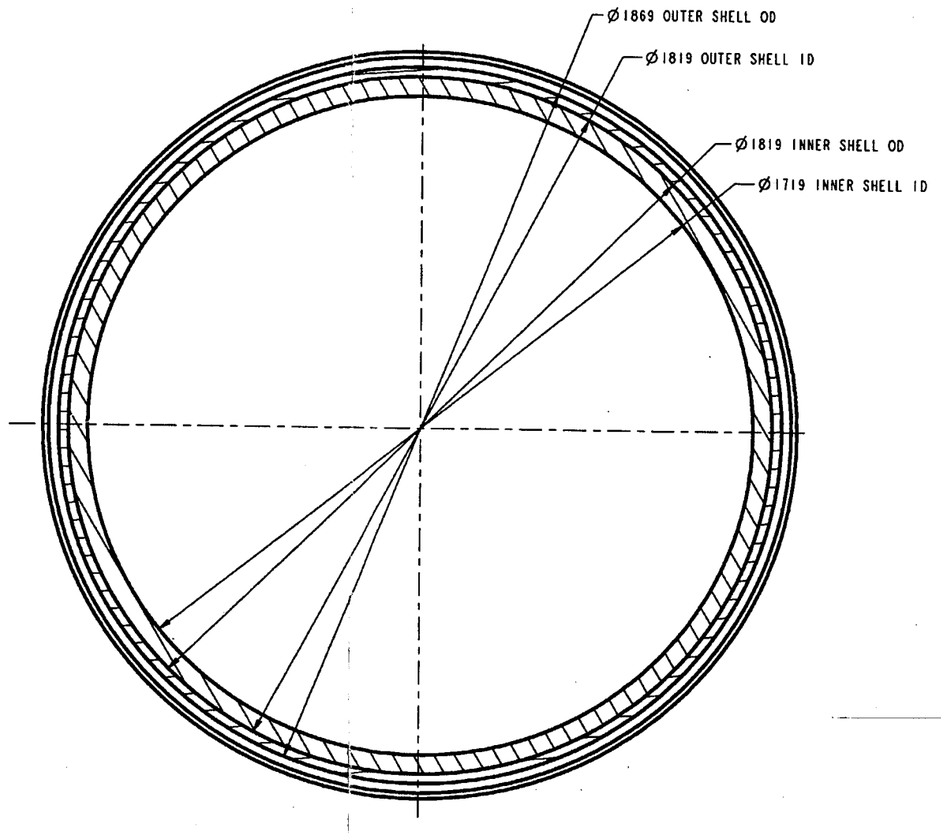

SECTION B-B

COMPONENT NAME	MATERIAL	THICKNESS	MASS (KG)	QTY ROD
INNER SHELL	SA-240 S31600	50	12372	1
INNER SHELL LID	SA-240 S31600	130	2390	2
INNER LID LIFTING FEATURE	SA-240 S31600	27	12	1
OUTER SHELL	SB-575 N06022	25	7430	1
EXTENDED OUTER SHELL LID	SB-575 N06022	25	158	1
EXTENDED OUTER SHELL LID BASE	SB-575 N06022	25	528	1
EXTENDED LID REINFORCEMENT RING	SB-575 N06022	50	118	1
OUTER LID LIFTING FEATURE	SB-575 N06022	27	13	2
OUTER SHELL FLAT CLOSURE LID	SB-575 N06022	10	227	1
OUTER SHELL FLAT BOTTOM LID	SB-575 N06022	25	564	1
UPPER TRUNNION COLLAR SLEEVE	SB-575 N06022	40	604	1
LOWER TRUNNION COLLAR SLEEVE	SB-575 N06022	40	592	1
INNER SHELL SUPPORT RING	SB-575 N06022	20	49	1
TOTAL ALLOY 22 WELDS	SFA-5.14 N06022	-	298	**
TOTAL 316 WELDS	SFA-5.9 S31680	-	243	**
WASTE PACKAGE ASSEMBLY	-	-	28005	1
NAVAL SNF	-	-	44452*	1
WASTE PACKAGE WITH SNF	-	-	72457	1

*"MAXIMUM EXPECTED PARAMETERS FOR NAVAL REACTORS CANISTERS" 10/29/97 FROM: RICHARD GUIDA TO: RUSSELL DYER. MOL.19980121.0011

**REFER TO SK-0195 REV 00 "NAVAL SNF LONG WASTE PACKAGE WELD CONFIGURATION"

UNITS: mm

DO NOT SCALE FROM SKETCH

"FOR INFORMATION ONLY"

NAVAL SNF LONG WASTE PACKAGE CONFIGURATION FOR SITE RECOMMENDATION

SKETCH NUMBER:	SK-0194 REV 01	SHEET 1 OF 2
SKETCHED BY:	GENE CONNELL 01/26/00	SNB 01/26/00 JAC 1/26/00
DATE:	01/11/00	
FILE:	/home/pro_library/checkout/sketches/naval/naval snf long/SK-0194.dwg	

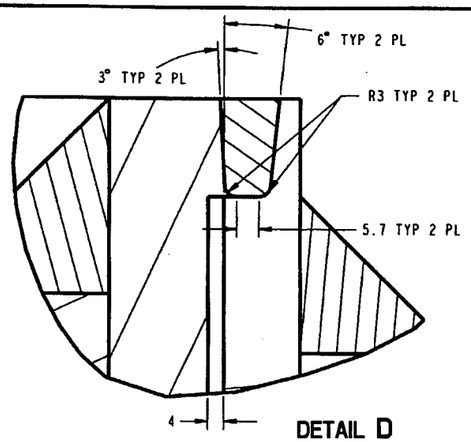

DETAIL D

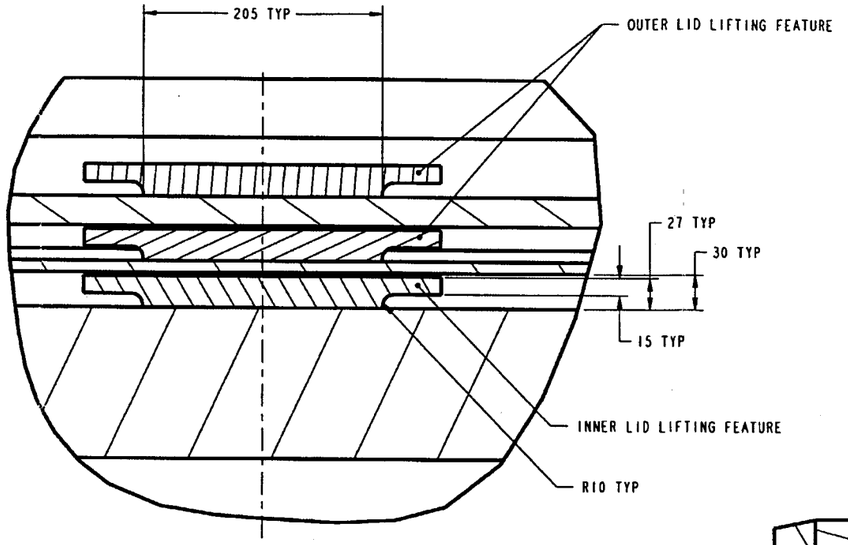

DETAIL C

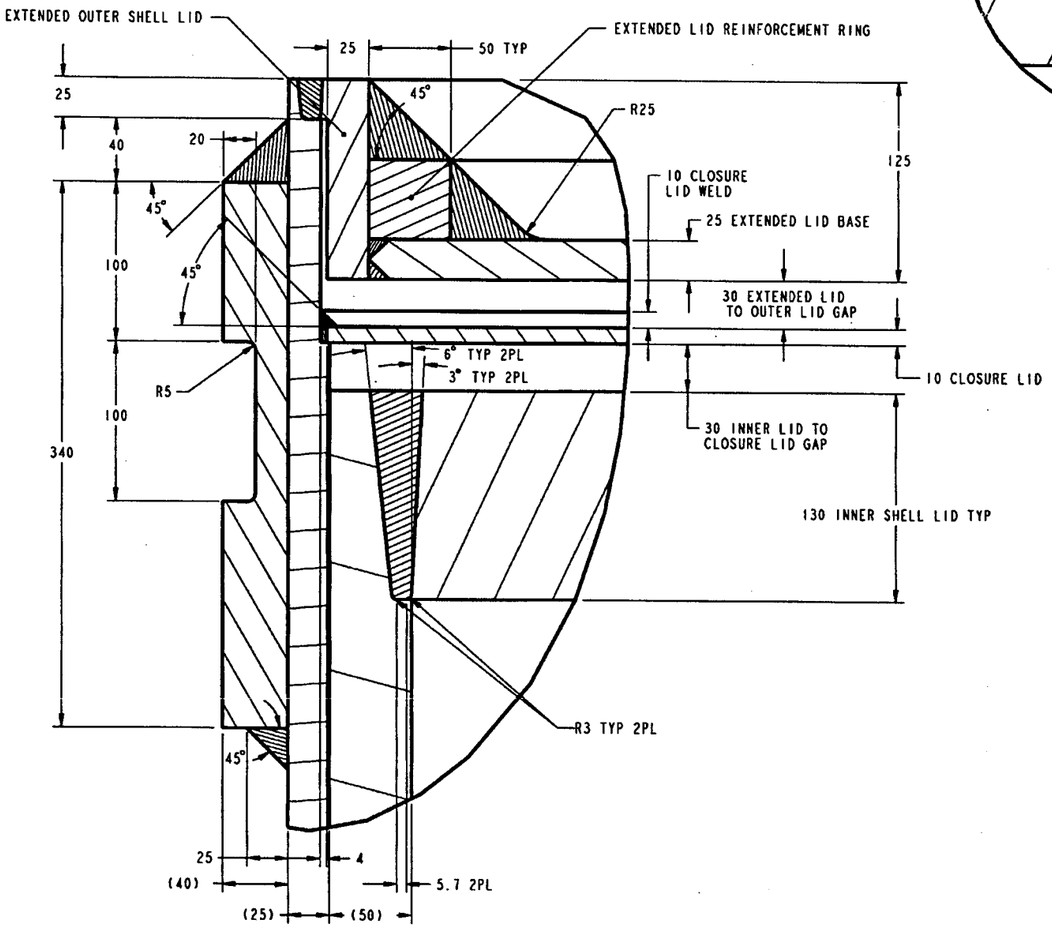

DETAIL A

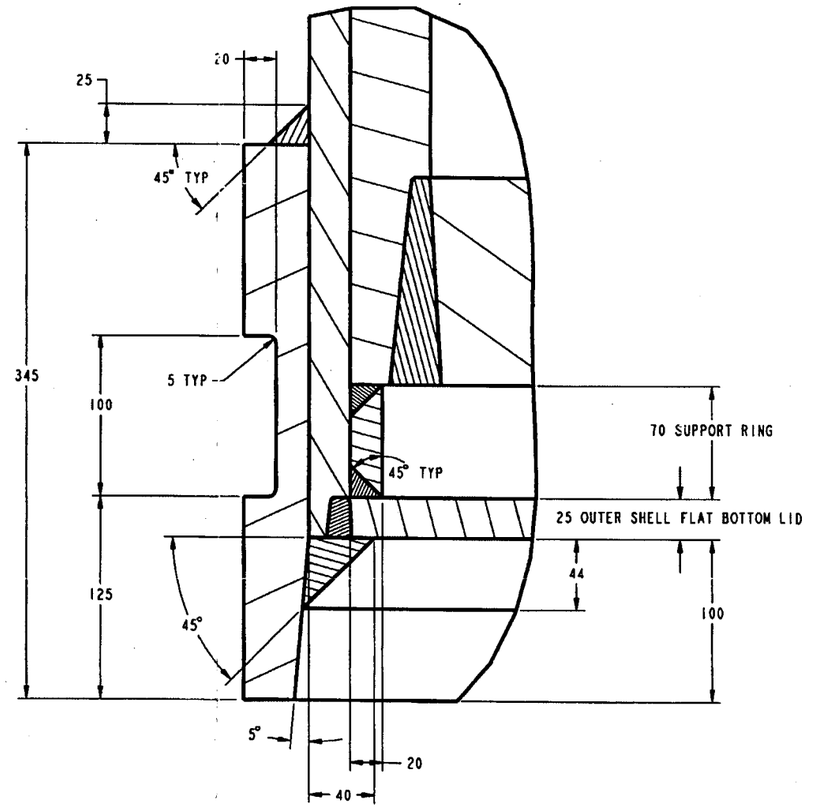

DETAIL B

01 SMB 01/27/00

SK-0194 REV 00 | SHEET 2 OF 2

ALL SHEETS ARE THE SAME REVISION STATUS

SHEET NUMBER	SHEET	REVISION
SK-0195	1 OF 1	00

REVISION HISTORY

ZONE	REV	DESCRIPTION	DATE	APPROVED

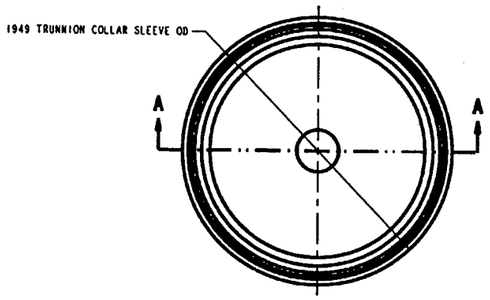

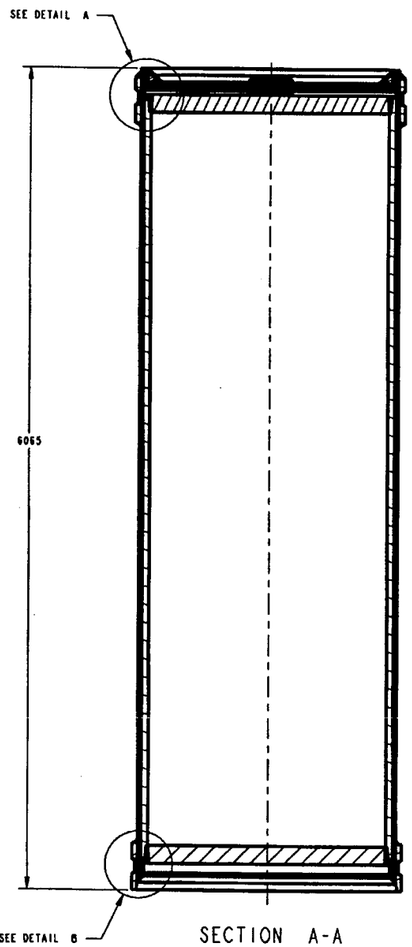

SECTION A-A
SCALE 0.055

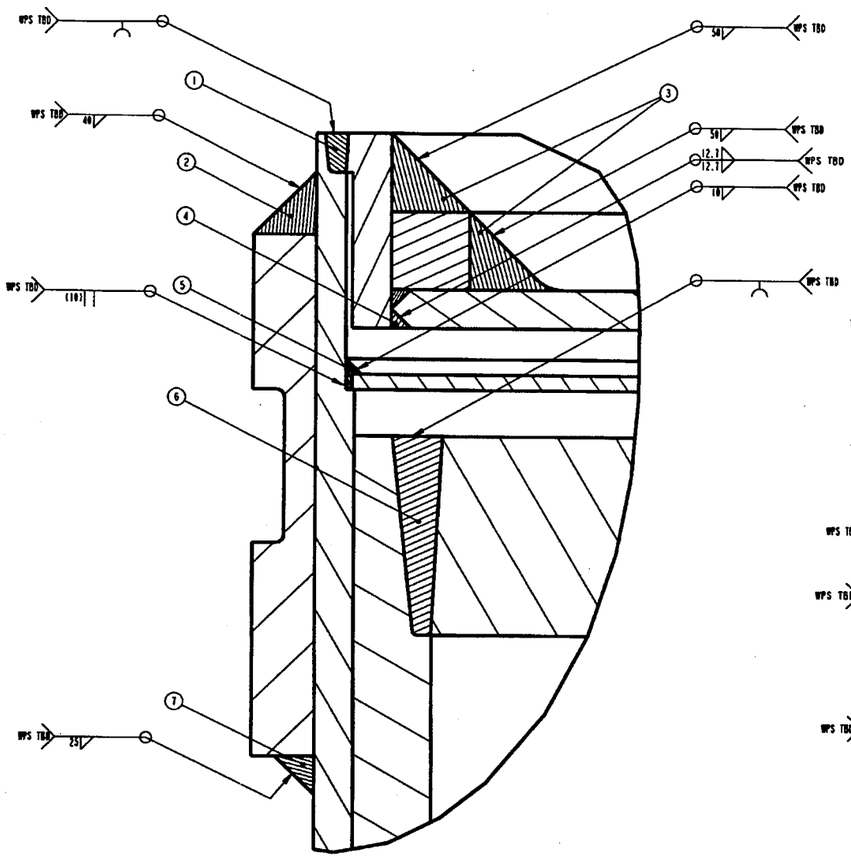

DETAIL A
SCALE 0.625

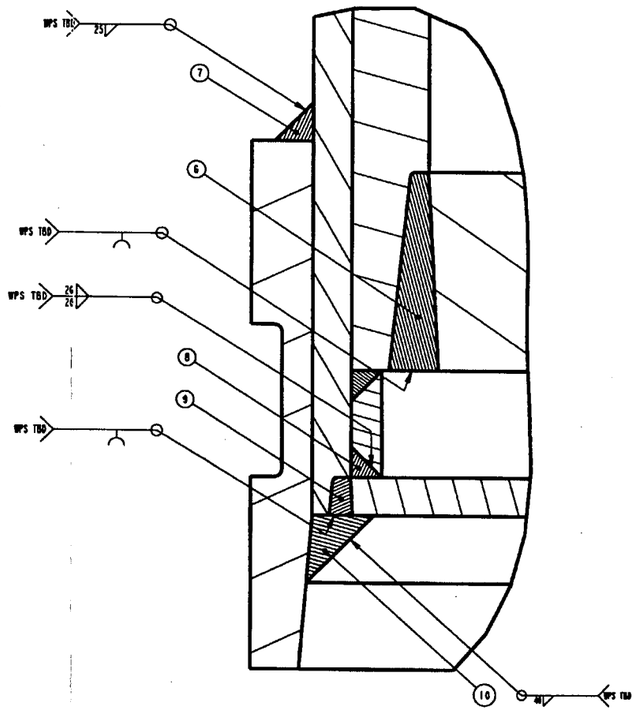

DETAIL B
SCALE 0.625

WELDS	MATERIAL	MASS (KG)	QTY REQ
WELD 1	SFA-5.14 NO6022	16	1
WELD 2	SFA-5.14 NO6022	41	1
WELD 3	SFA-5.14 NO6022	116	1
WELD 4	SFA-5.14 NO6022	3.8	2
WELD 5	SFA-5.14 NO6022	4.5	1
WELD 6	SFA-5.9 S31680	123	2
WELD 7	SFA-5.14 NO6022	16	2
WELD 8	SFA-5.14 NO6022	9.9	2
WELD 9	SFA-5.14 NO6022	16	1
WELD 10	SFA-5.14 NO6022	44	1
TOTAL ALLOY 22 WELDS	SFA-5.14 NO6022	298	-
TOTAL 316 WELDS	SFA-5.9 S31680	246	-

"FOR INFORMATION ONLY"

THIRD ANGLE PROJECTION

DIMENSIONS ARE IN MILLIMETERS AND DEGREES UNLESS OTHERWISE NOTED

DO NOT SCALE FROM SKETCH

APPROVALS	INITIAL/DATE
SKETCHED BY BRYAN HARKINS	BH 28 March 00
STRUCTURAL LEAD SCOTT BENNETT	SMB 03/29/00
MANUFACTURING MGR JERRY COGAR	JC 04/10/00
DESIGN GROUP MGR THOMAS DOERING	TD 5/9/00

WASTE PACKAGE DEPARTMENT

M&O Civilian Radioactive Waste Management System MANAGEMENT & OPERATING CONTRACTOR

TITLE

NAVAL SNF LONG WASTE PACKAGE WELD CONFIGURATION

SKETCH NUMBER	REVISION
SK-0195	00
SCALE .055	SHEET 1 OF 1

REVISION HISTORY			
REV	DESCRIPTION	DATE	APPROVED
00	ISSUED APPROVED		

ALL SHEETS ARE THE SAME REVISION STATUS

SHEET NUMBER SN-0232 | SHEET 1 OF 13 | REVISION 00

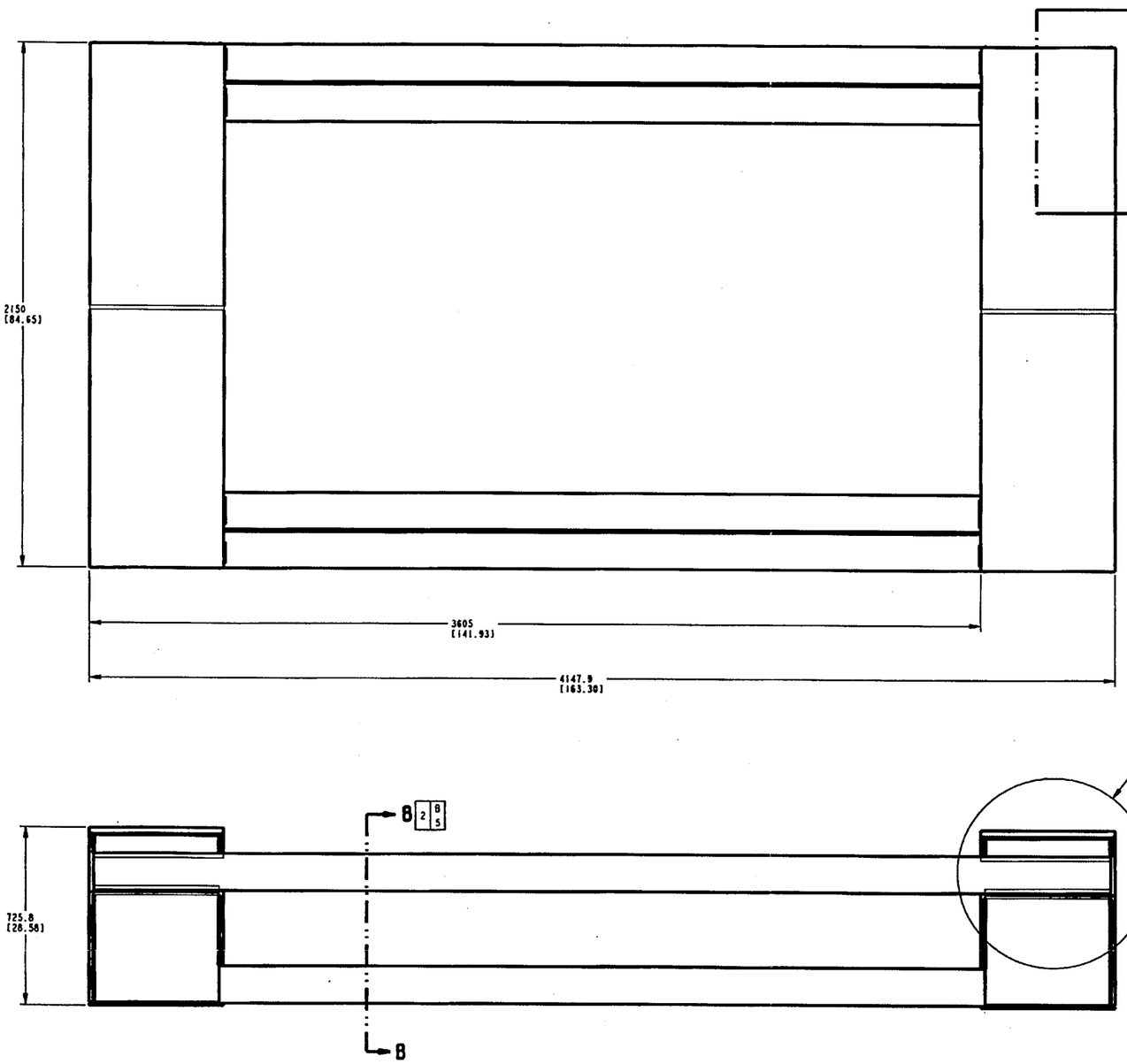

NOTES:

1. ALL DIMENSIONS SHOWN IN BRACKETS ARE IN INCHES.
2. ⚠ WELDS 20, 21 AND 22 ARE SQUARE BUTT WELDS.
3. FOR COMPONENT LIST, SEE SHEET 13
4. FOR WELD LIST, SEE SHEET 13

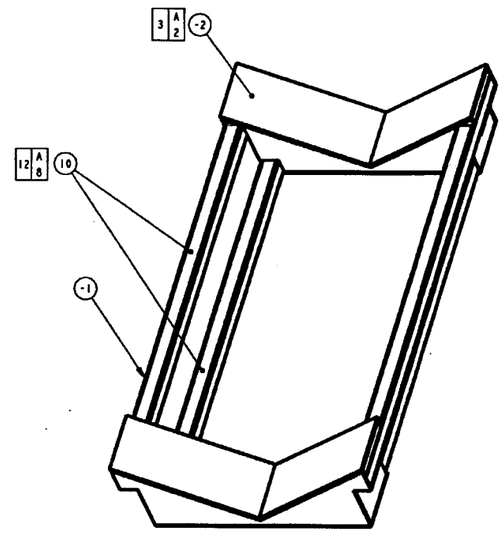

"FOR INFORMATION ONLY"	APPROVALS	INITIAL/DATE	WASTE PACKAGE PROJECT
THIRD ANGLE PROJECTION	SKETCHED BY EUGENE CONNELL	EGC 05/07/01	Bechtel SAIC Company, LLC
	CHECKED BY BRYAN HARKINS	BH 05/07/01	TITLE: EMPLACEMENT PALLET LONG
DIMENSIONS ARE IN MILLIMETERS AND DEGREES UNLESS OTHERWISE NOTED	STRUCTURAL LEAD SCOTT BENNETT	SAB 05/07/01	SKETCH NUMBER: SK-0232
	MANUFACTURING MGR JERRY COGAR	5/7/01	REVISION: 00
DO NOT SCALE FROM SKETCH	DESIGN GROUP MGR MICHAEL ANDERSON	5/7/01	SCALE: 0.109 SHEET 1 OF 13

SEE DETAIL A
5 A 6

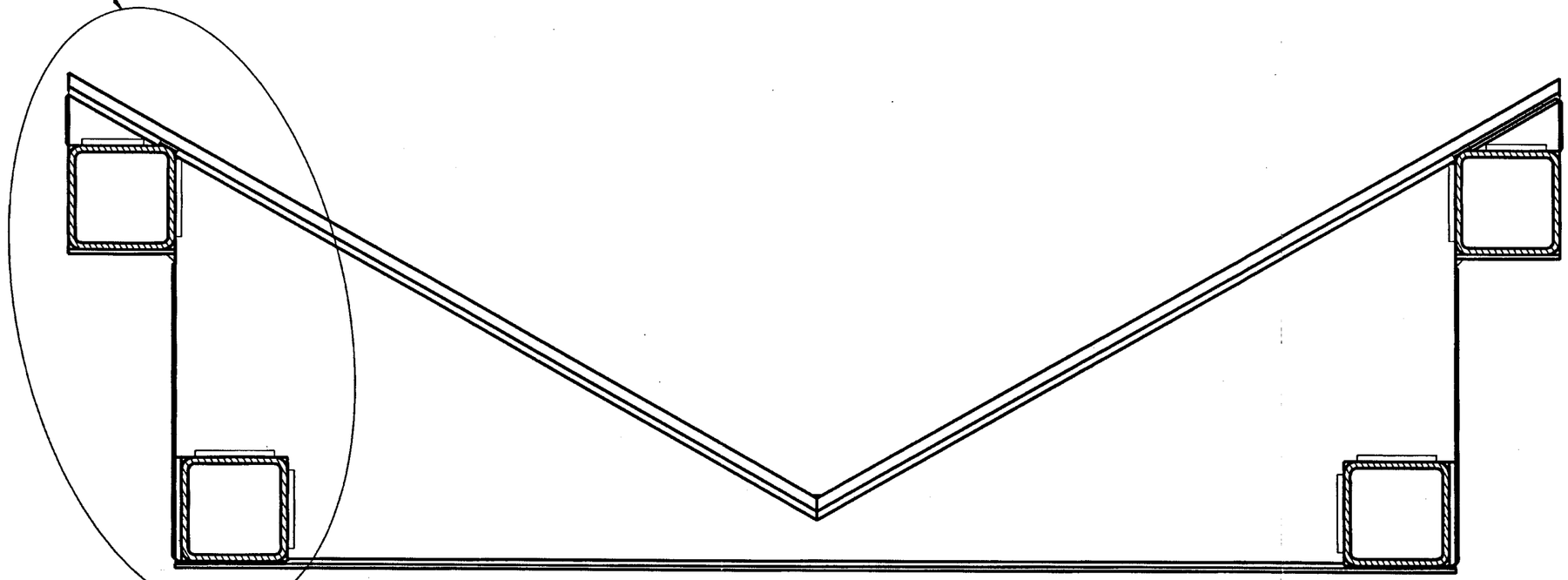

1 B 7 SECTION B-B
SCALE 0.312

WASTE PACKAGE PROJECT	
Bechtel SAIC Company, LLC	
SKETCH NUMBER SK-0232	REVISION 00
SCALE 0.109	SHEET 2 OF 13

SKETCH NUMBER SK-0232 | SHEET 2 OF 13 | REVISION 00

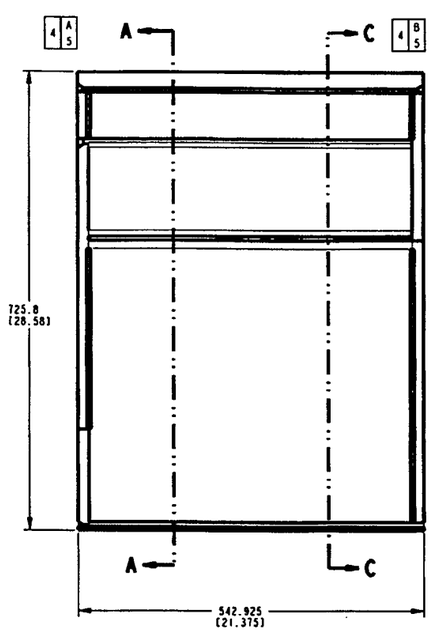

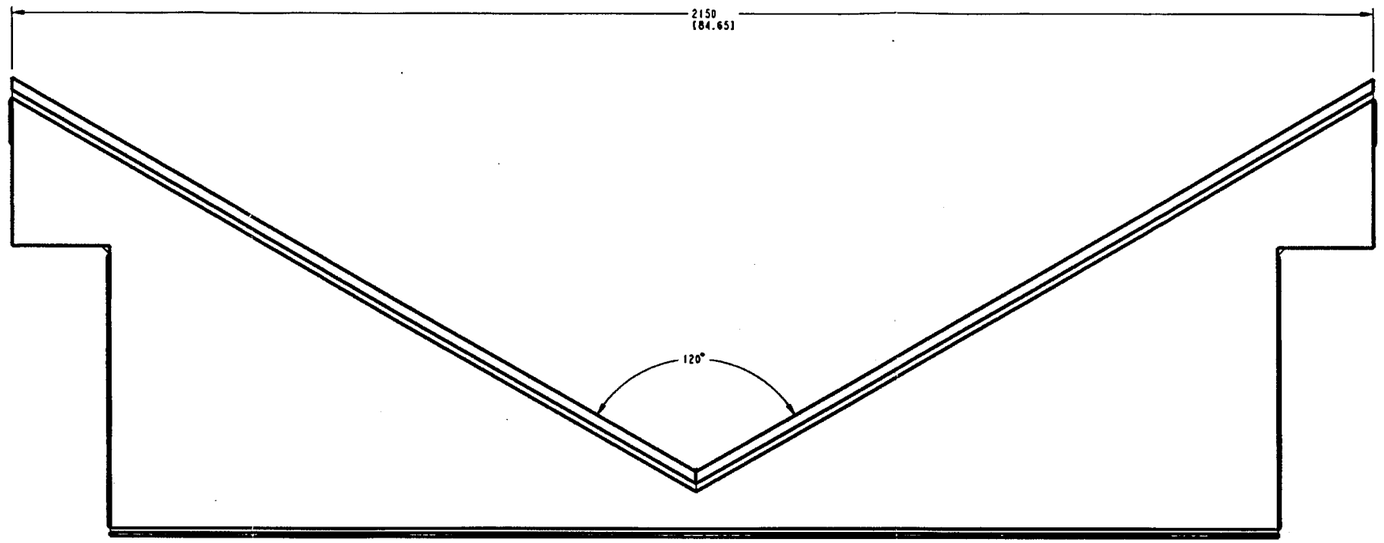

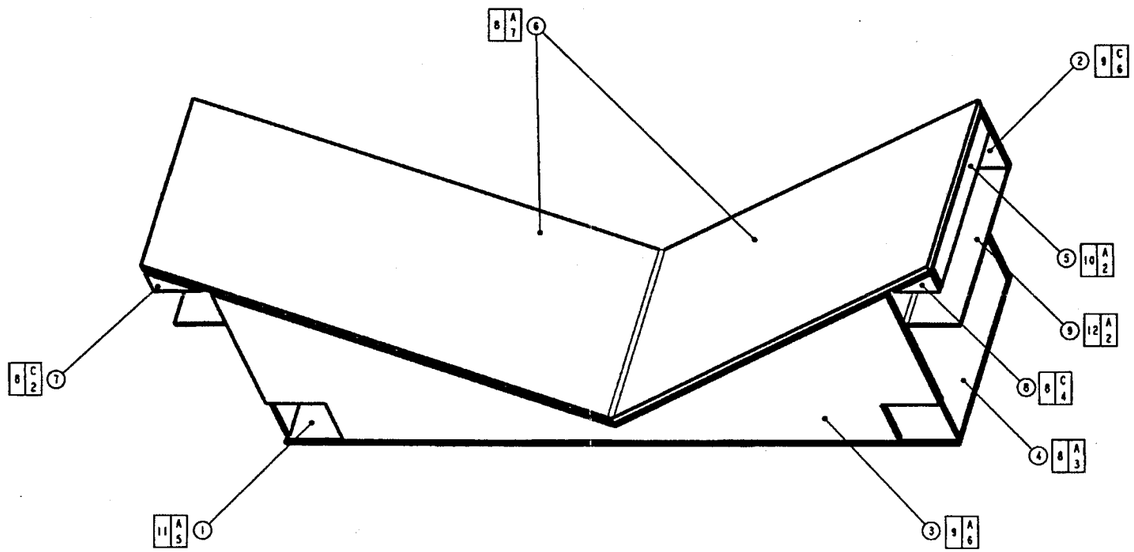

ASSEMBLY -2
SUB-PALLET ASSEMBLY
SCALE 0.250

WASTE PACKAGE PROJECT	Bechtel SAIC Company, LLC
SKETCH NUMBER	SK-0232
REVISION	00
SCALE 0.109	SHEET 3 OF 13

SEE DETAIL B
6 A 7

SEE DETAIL C
7 C 1

12 12 A 5

11 10 A 6

SEE DETAIL D
6 A 3

3 D 7 SECTION C-C
SCALE 0.250

461.4 [18.17] TYP

620.9 TYP [24.45]

3 D 8 SECTION A-A
SCALE 0.250

WASTE PACKAGE PROJECT			
Bechtel SAIC Company, LLC			
SKETCH NUMBER	SK-0232	REVISION	00
SCALE	0.109	SHEET	4 OF 13

2 D 8 DETAIL A
SCALE 0.625

1 D 4 SECTION F-F
SCALE 0.625

WASTE PACKAGE PROJECT	
Bechtel SAIC Company, LLC	
SKETCH NUMBER SK-0232	REVISION 00
SCALE 0.109	SHEET 5 OF 13

DETAIL B
SCALE 0.625

DETAIL D
SCALE 0.625

WASTE PACKAGE PROJECT	
Bechtel SAIC Company, LLC	
SKETCH NUMBER SK-0232	REVISION 00
SCALE 0.109	SHEET 6 OF 13

B 1 B 4 DETAIL N
SCALE 0.250

4 D 5 DETAIL C
SCALE 0.375

7 C 3 SECTION E-E
SCALE 0.375

7 C 3 SECTION D-D
SCALE 0.650

WASTE PACKAGE PROJECT	
Bechtel SAIC Company, LLC	
SKETCH NUMBER SK-0232	REVISION 00
SCALE 0.109	SHEET 7 OF 13

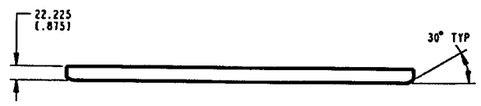

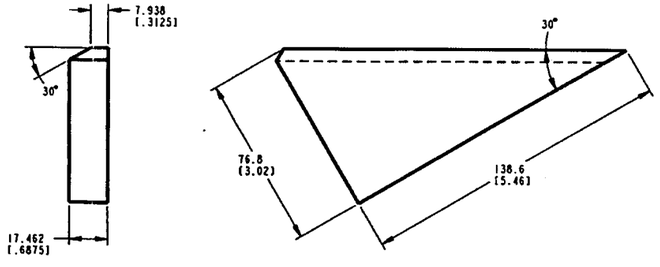

3 A 3 ITEM 8
PLATE 8
SCALE 0.875

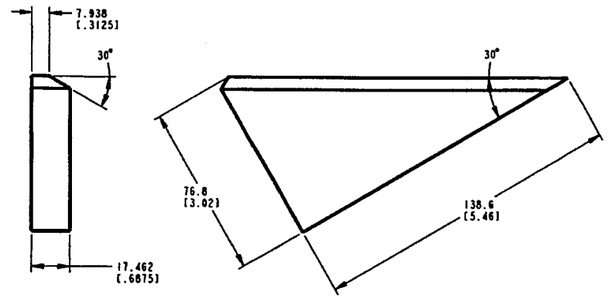

3 A 7 ITEM 7
PLATE 7
SCALE 0.875

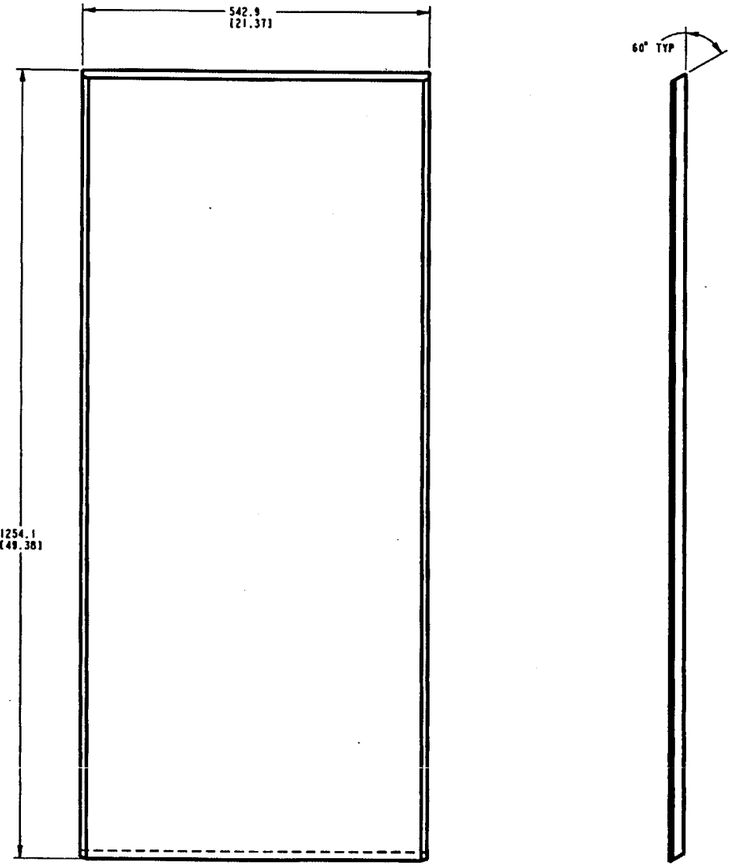

3 B 5 ITEM 6
PLATE 6
SCALE 0.250

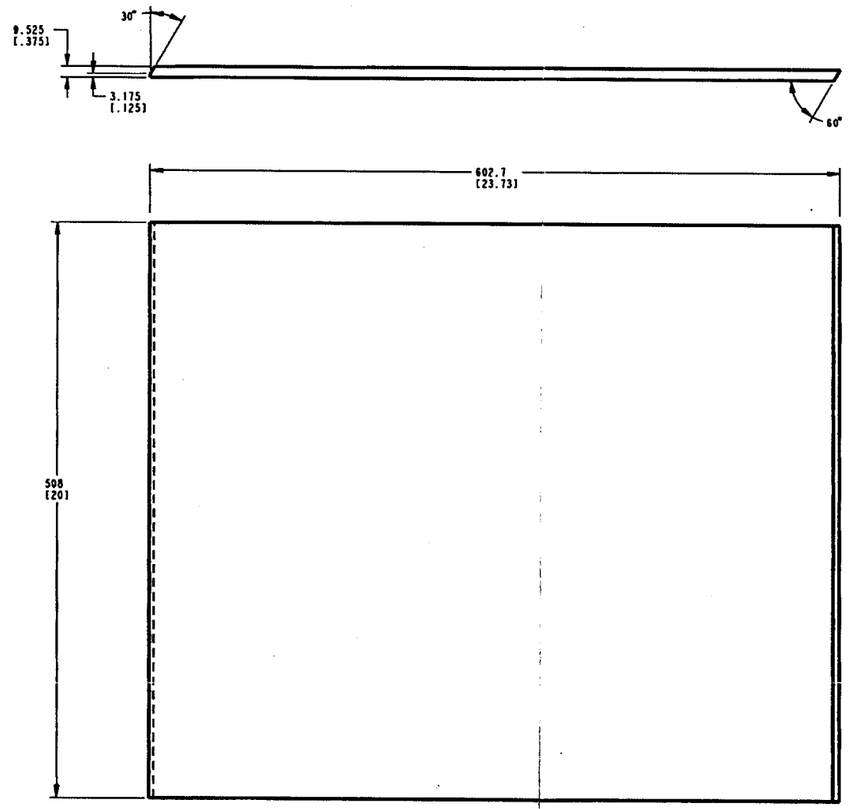

3 A 3 ITEM 4
PLATE 4
SCALE 0.250

WASTE PACKAGE PROJECT	
Bechtel SAIC Company, LLC	
SKETCH NUMBER: SK-0232	REVISION: 00
SCALE: 0.189	SHEET: 8 OF 13

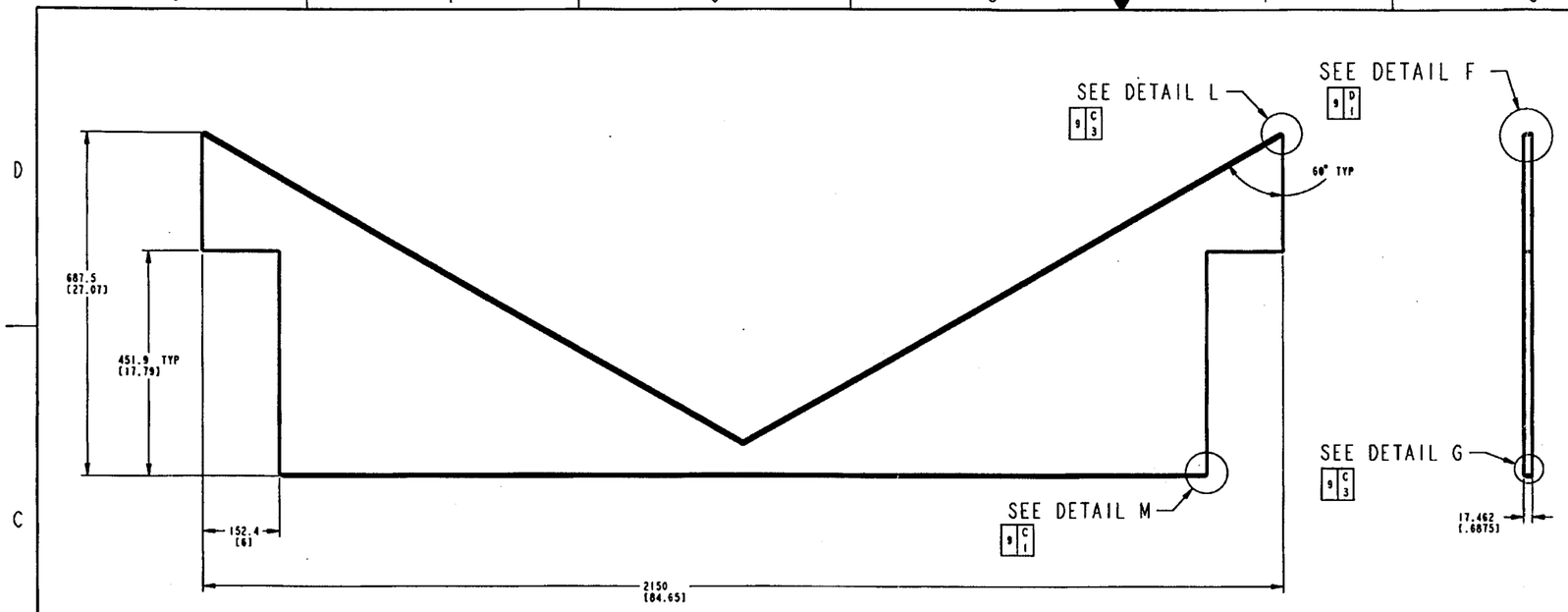

3 B 3 ITEM 2
PLATE 2
SCALE 0.200

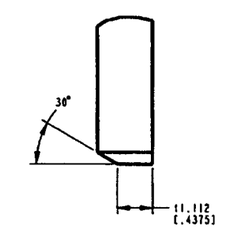

9 C 4 DETAIL G
SCALE 1.250

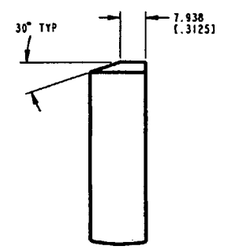

9 D 4 DETAIL F
SCALE 1.250

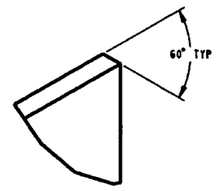

9 D 5 DETAIL L
SCALE 1.250

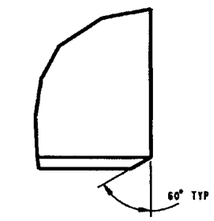

9 C 5 DETAIL M
SCALE 1.250

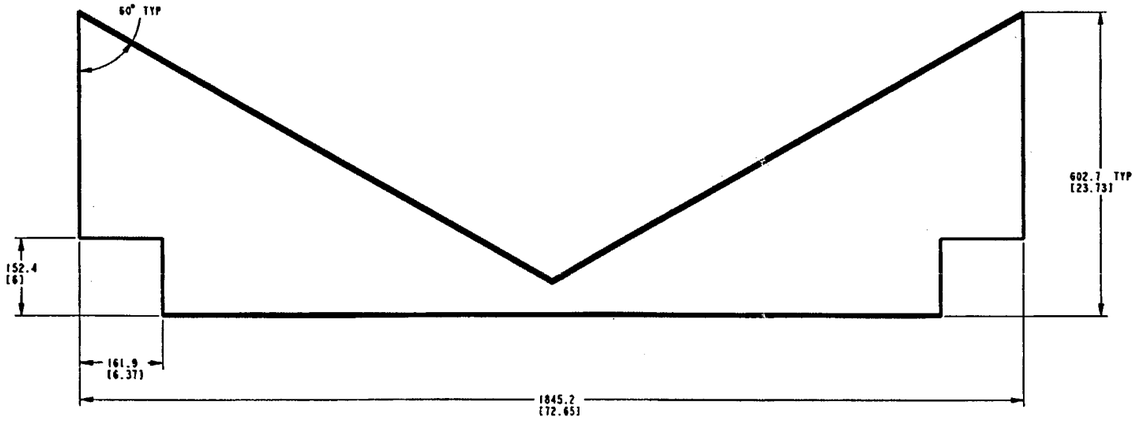

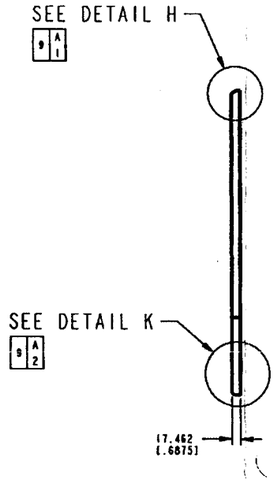

3 A 4 ITEM 3
PLATE 3
SCALE 0.200

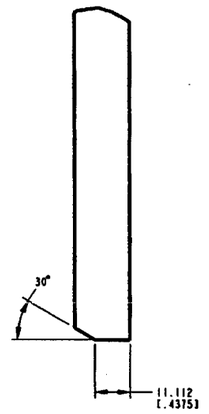

9 A 4 DETAIL K
SCALE 1.250

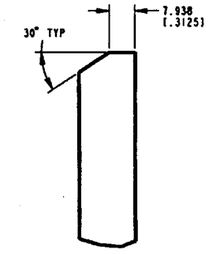

9 B 4 DETAIL H
SCALE 1.250

WASTE PACKAGE PROJECT	
Bechtel SAIC Company, LLC	
SKETCH NUMBER	REVISION
SK-0232	00
SCALE 0.100	SHEET 9 OF 13

4 C 4 ITEM 11
TUBE 2
SCALE 1.191

3 B 3 ITEM 5
PLATE 5
SCALE 0.812

WASTE PACKAGE PROJECT	
Bechtel SAIC Company, LLC	
SKETCH NUMBER SK-0232	REVISION 00
SCALE 0.109	SHEET 10 OF 13

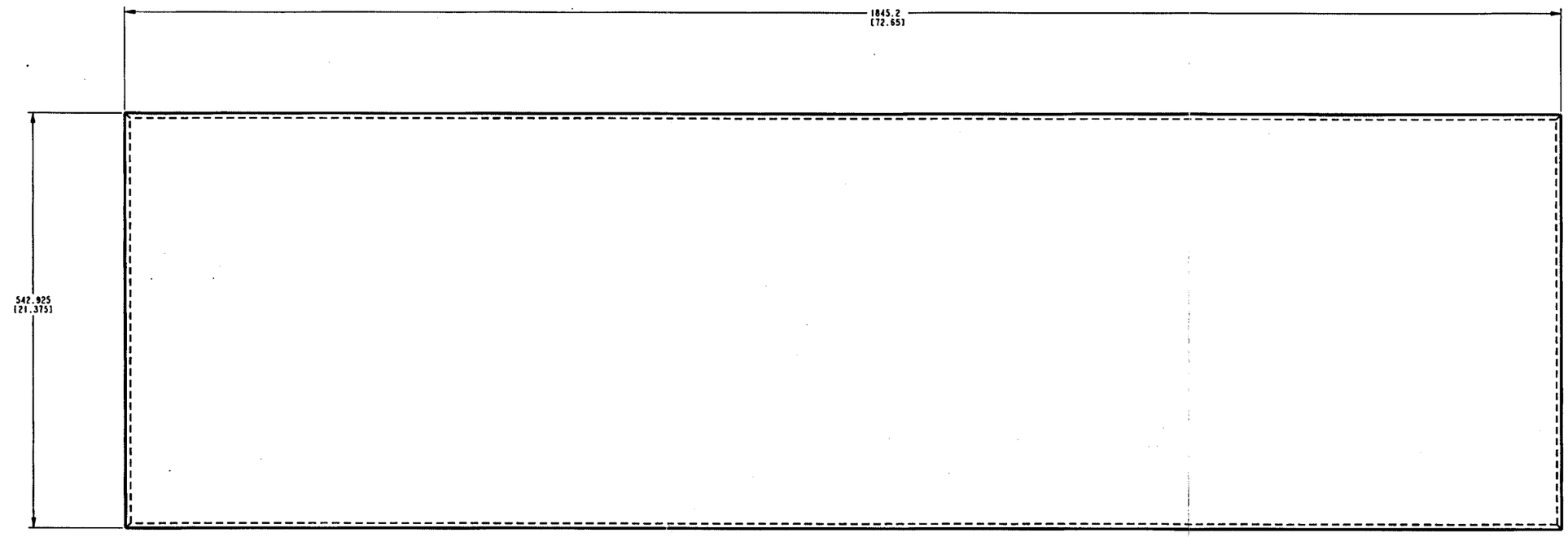

3 A 7 ITEM 1
PLATE 1
SCALE 0.375

WASTE PACKAGE PROJECT	
Bechtel SAIC Company, LLC	
SKETCH NUMBER SK-0232	REVISION 00
SCALE 0.109	SHEET 11 OF 13

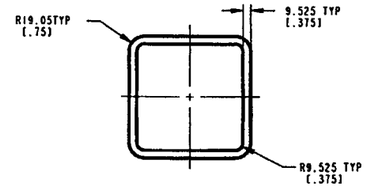

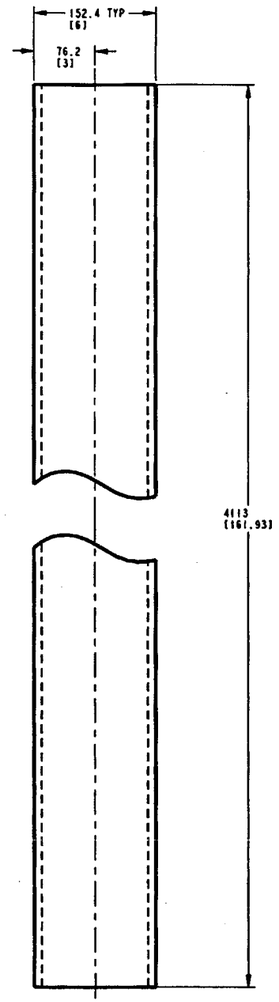

1 C 3 ITEM 10
TUBE 1
SCALE 0.312

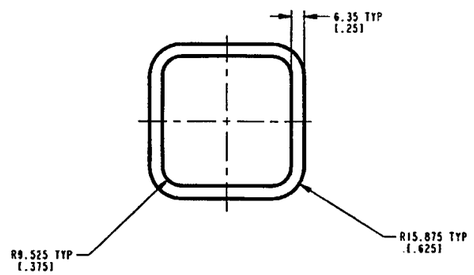

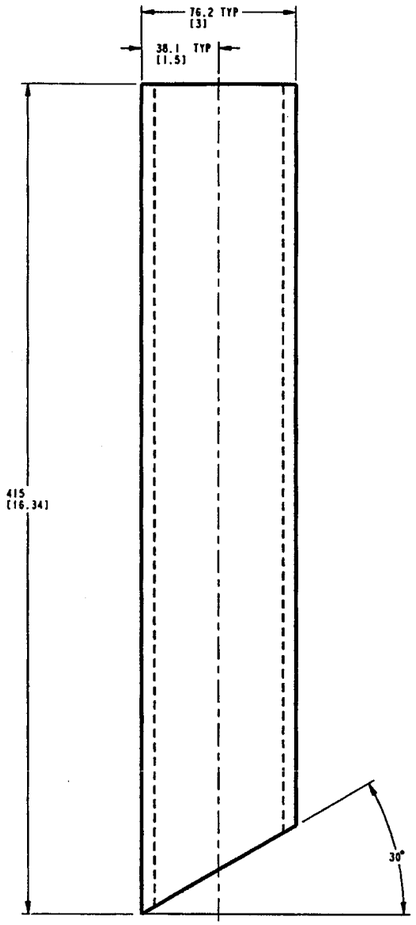

4 D 3 ITEM 12
TUBE 3
SCALE 0.794

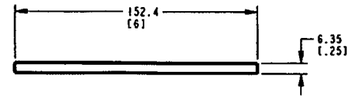

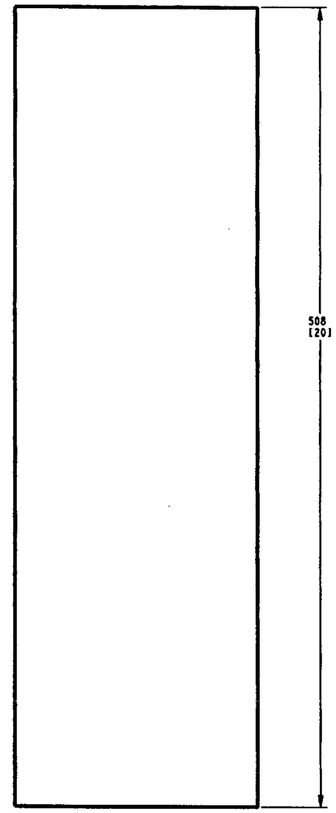

3 A 3 ITEM 9
PLATE 9
SCALE 0.625

WASTE PACKAGE DEPARTMENT	
Bechtel SAIC Company, LLC	
SKETCH NUMBER SK-0232	REVISION 00
SCALE 0.109	SHEET 12 OF 13

COMPONENT LIST							
ITEM NUMBER	ASSEMBLY	SUBASSEMBLY	COMPONENT NAME	MATERIAL	THICKNESS	MASS (KG)	QTY (EA)
-1	EMPLACEMENT PALLET LONG	-	-	-	-	1971	1
10	-	-	TUBE 1	SA-240 S31600	9.525	171	4
-2	-	SUB-PALLET ASSEMBLY	-	-	-	640	2
1	-	-	PLATE 1	SB-575 N06022	9.525	82	2
2	-	-	PLATE 2	SB-575 N06022	17.462	102	2
3	-	-	PLATE 3	SB-575 N06022	17.462	86	2
4	-	-	PLATE 4	SB-575 N06022	9.525	25	4
5	-	-	PLATE 5	SB-575 N06022	22.225	7.1	4
6	-	-	PLATE 6	SB-575 N06022	22.225	130	4
7	-	-	PLATE 7	SB-575 N06022	17.462	0.80	2
8	-	-	PLATE 8	SB-575 N06022	17.462	0.80	2
9	-	-	PLATE 9	SB-575 N06022	6.35	4.3	4
11	-	-	TUBE 2	SB-575 N06022	6.35	3.9	4
12	-	-	TUBE 3	SB-575 N06022	6.35	5.5	8
-	-	-	TOTAL ALLOY 22 WELDS	SFA-5.14 N06022	-	21	-

WELD LIST				
WELD NUMBER	WELD	MATERIAL	MASS (KG)	QTY (EA)
1	FILLET	SFA-5.14 N06022	0.36	4
2	GROOVE	SFA-5.14 N06022	0.17	8
3	GROOVE	SFA-5.14 N06022	0.20	8
4	FILLET	SFA-5.14 N06022	0.19	2
5	FILLET	SFA-5.14 N06022	0.23	4
6	GROOVE	SFA-5.14 N06022	0.07	4
7	GROOVE	SFA-5.14 N06022	0.57	4
8	GROOVE	SFA-5.14 N06022	0.48	4
9	FILLET	SFA-5.14 N06022	0.08	8
10	FILLET	SFA-5.14 N06022	0.09	8
11	GROOVE	SFA-5.14 N06022	0.37	2
12	GROOVE	SFA-5.14 N06022	0.31	2
13	GROOVE	SFA-5.14 N06022	0.11	4
14	GROOVE	SFA-5.14 N06022	0.34	12
15	FILLET	SFA-5.14 N06022	0.05	12
16	GROOVE	SFA-5.14 N06022	0.35	4
17	FILLET	SFA-5.14 N06022	0.03	4
18	FILLET	SFA-5.14 N06022	0.20	4
19	GROOVE	SFA-5.14 N06022	0.08	4
20	SQUARE	SFA-5.14 N06022	0.01	8
21	SQUARE	SFA-5.14 N06022	0.04	4
22	SQUARE	SFA-5.14 N06022	0.06	4
TOTAL ALLOY 22 WELDS	-	-	21	-

SKETCH NUMBER	SK-0232
SHEET	13 OF 13
REVISION	00

WASTE PACKAGE DEPARTMENT
Bechtel SAIC Company, LLC
SKETCH NUMBER SK-0232 | REVISION 00
SCALE 0.109 | SHEET 13 OF 13

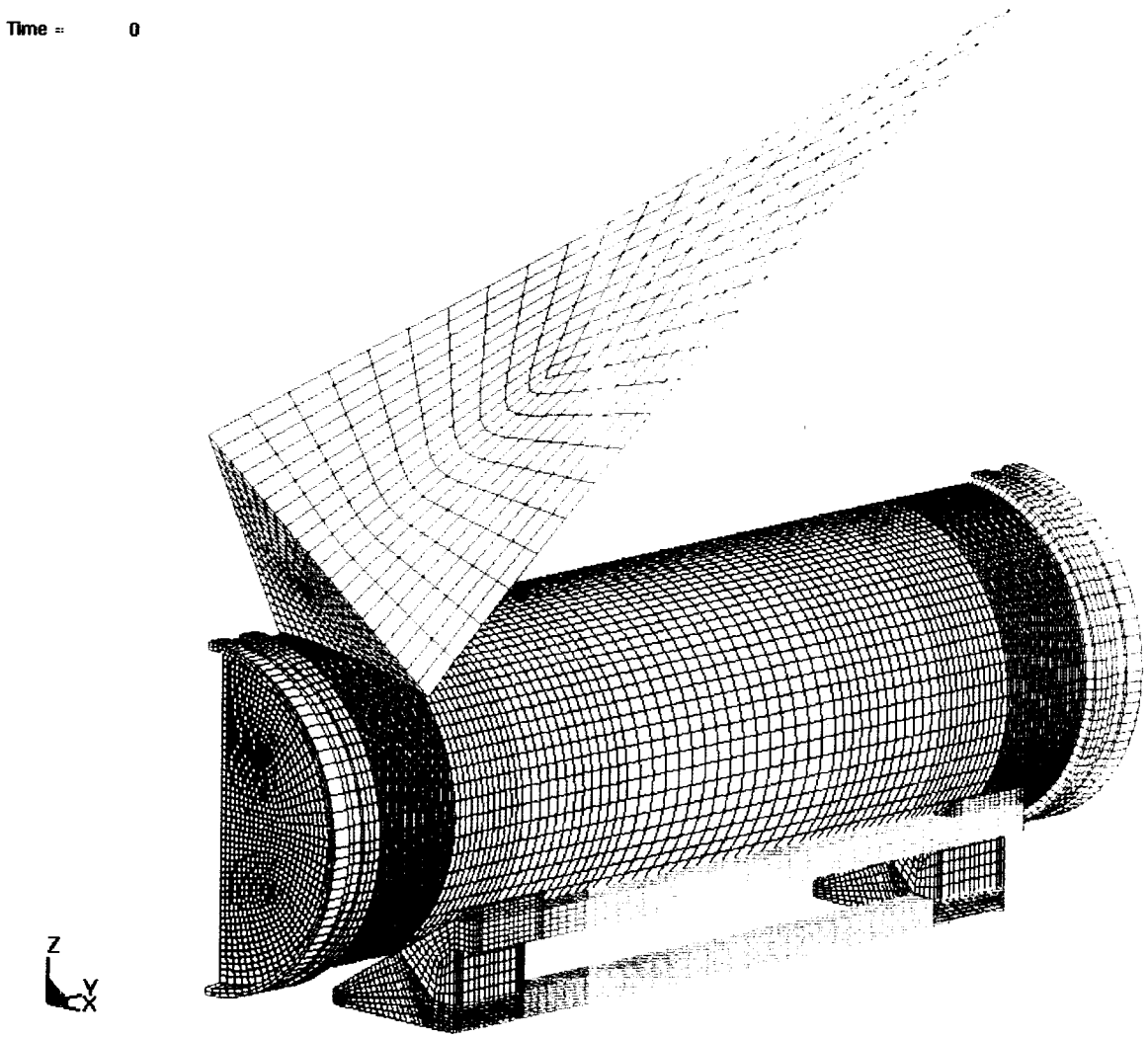

Figure II-1. Finite Element Representation of Emplacement Pallet, Waste Package and Rock (Case A)

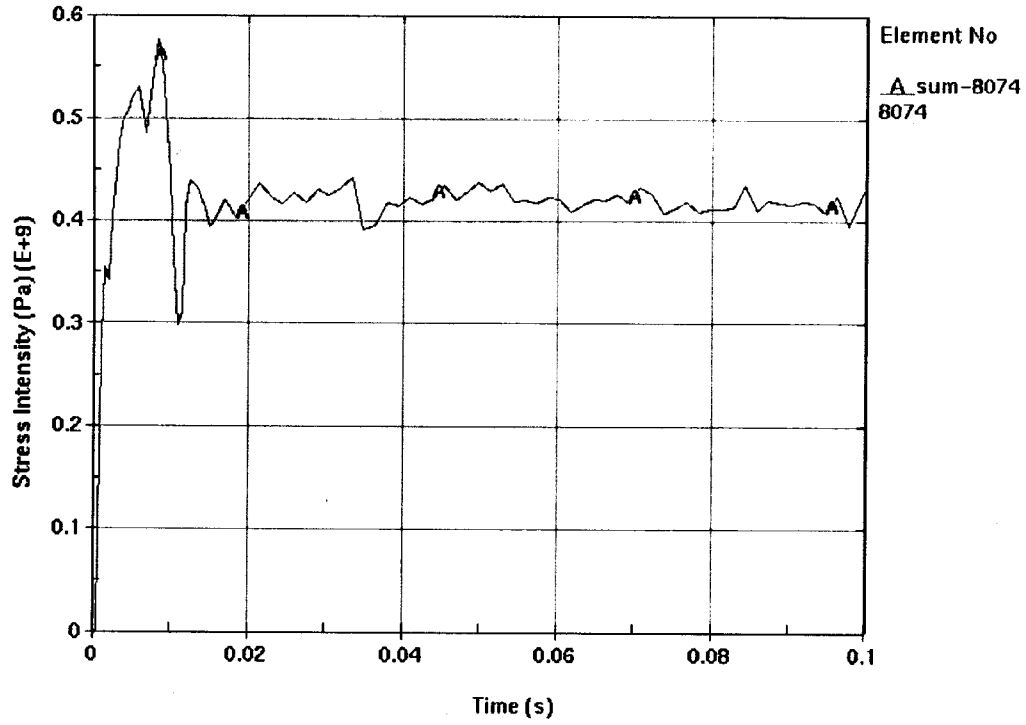

Figure II-2. Stress Intensity Plot for Element No. 8074 of Outer Shell (Case A)

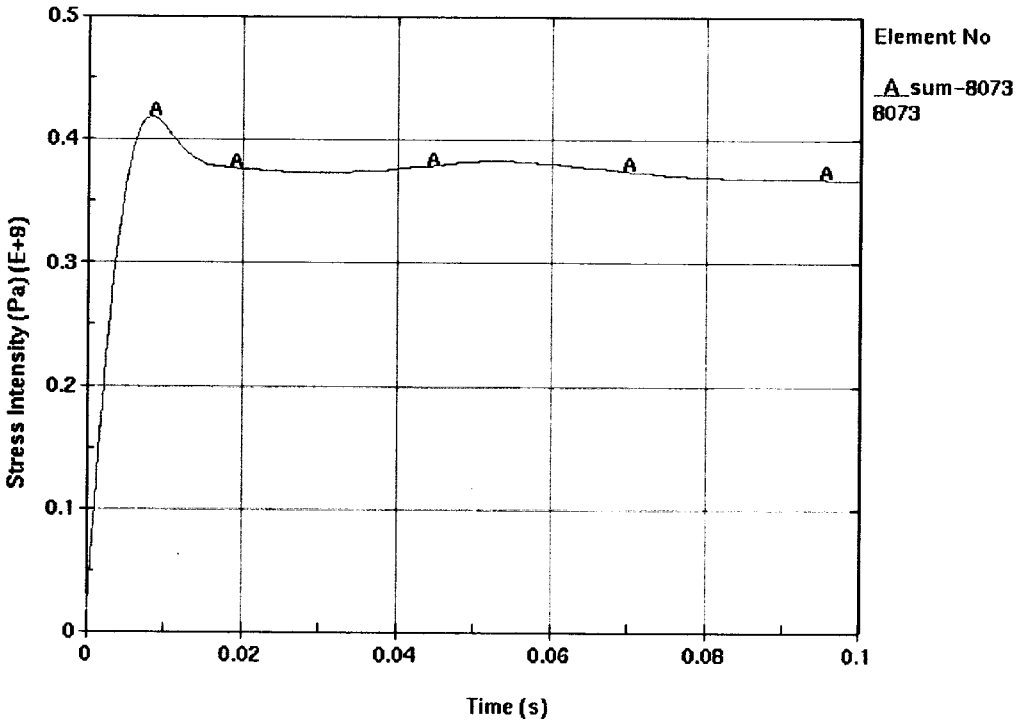

Figure II-3. Stress Intensity Plot for Element No. 8073 of Outer Shell Outer Surface (Case A)

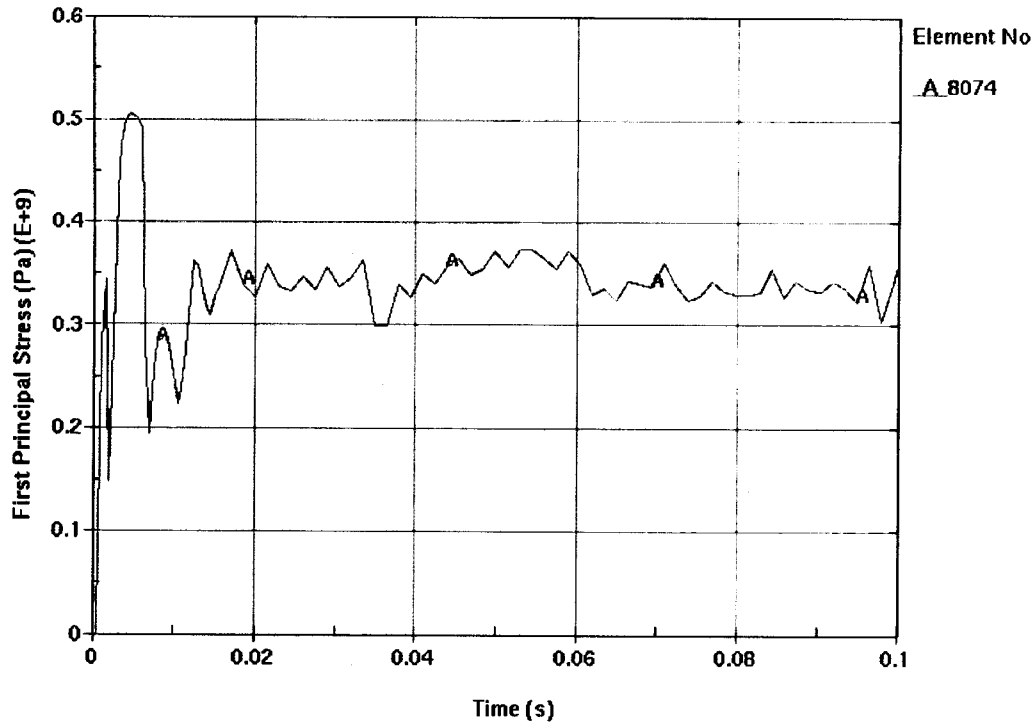

Figure II-4. First Principal Stress Plot for Element No. 8074 of Outer Shell (Case A)

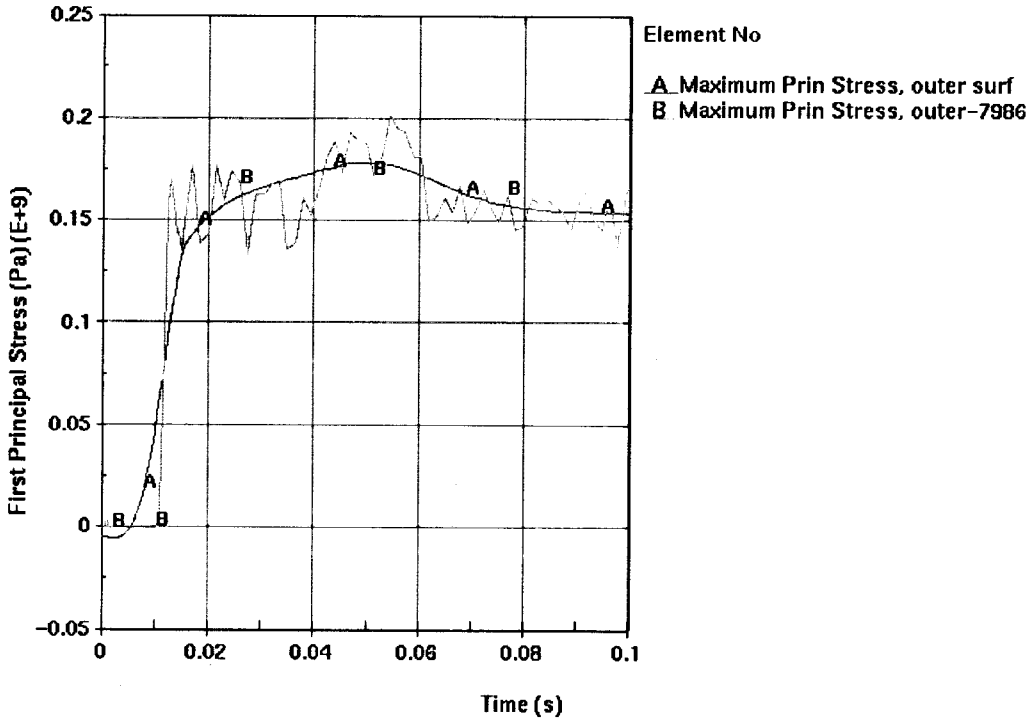

Figure II-5. Raw and Filtered First Principal Stress Plot Plot for Element No. 7986 of Outer Shell Outer Surface (Case A)

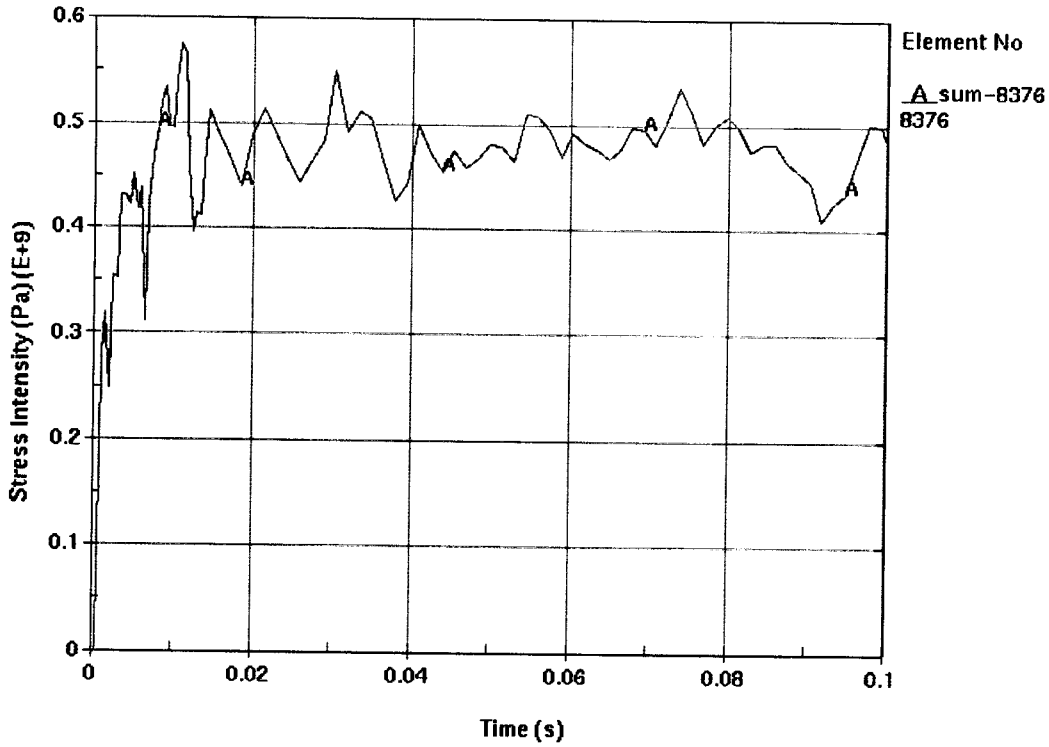

Figure II-6. Stress Intensity Plot for Element No. 8376 of Outer Shell (Case B)

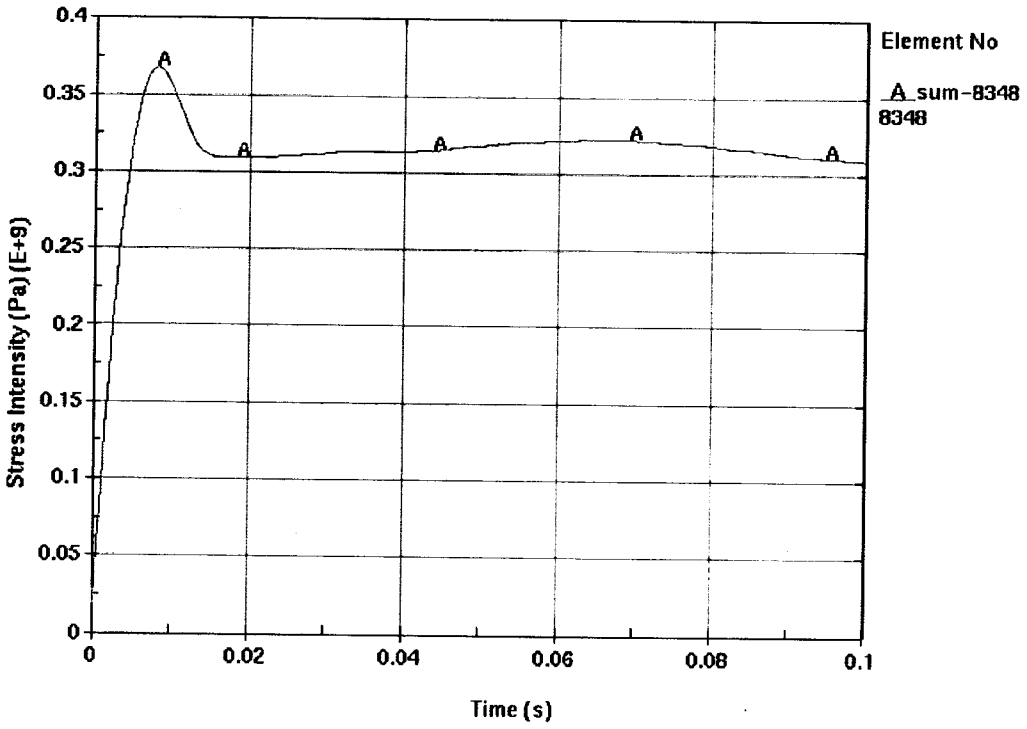

Figure II-7. Stress Intensity Plot for Element No. 8348 of Outer Shell Outer Surface (Case B)

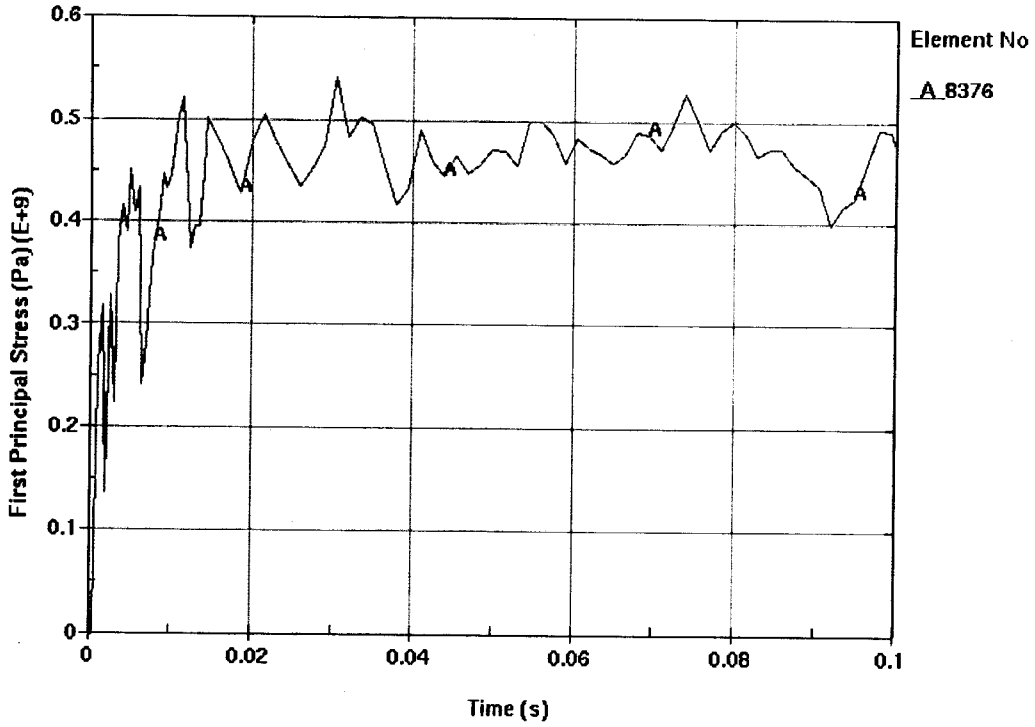

Figure II-8. First Principal Stress Plot for Element No. 8376 of Outer Shell (Case B)

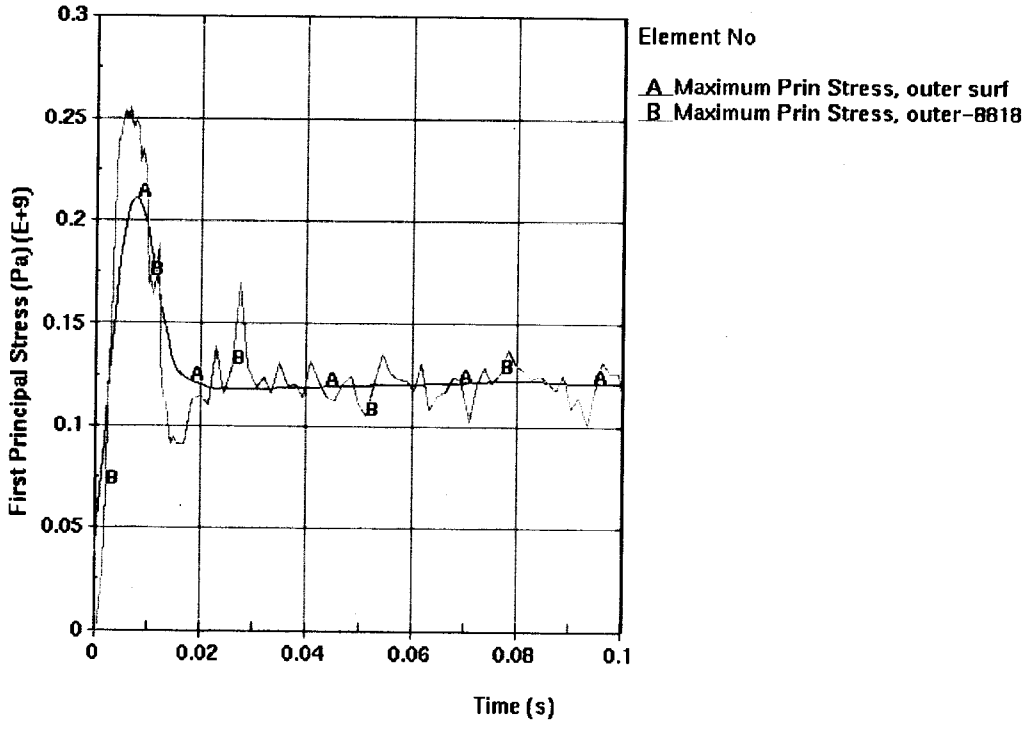

Figure II-9. Raw and Filtered First Principal Stress Plot Plot for Element No. 8818 of Outer Shell Outer Surface (Case B)

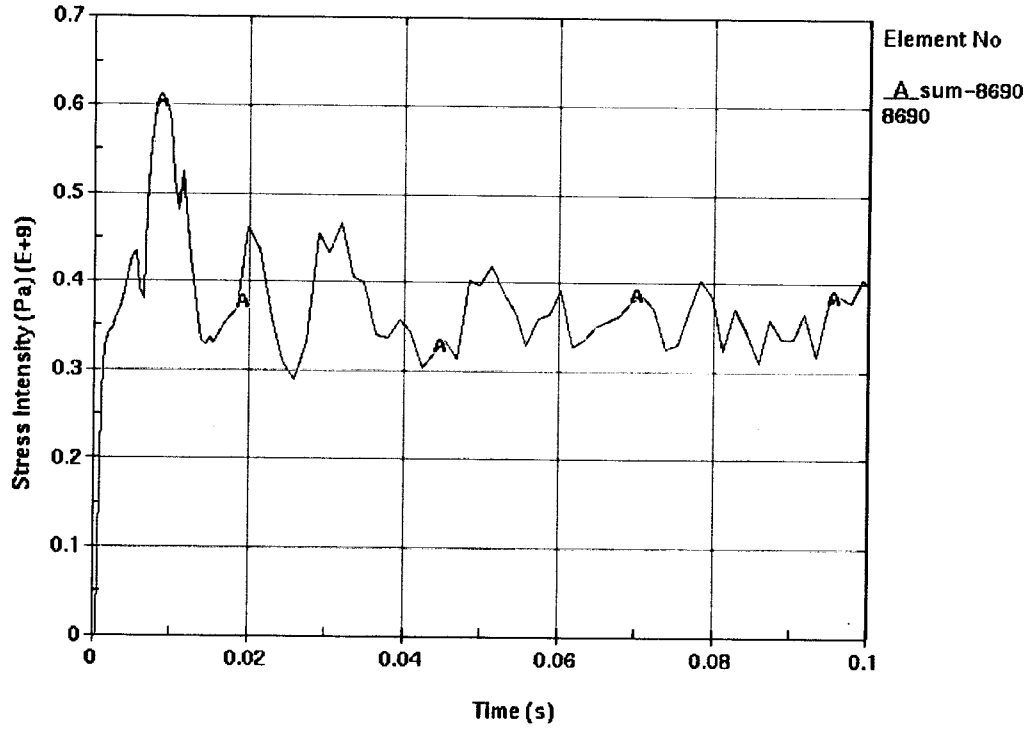

Figure II-10. Stress Intensity Plot for Element No. 8690 of Outer Shell (Case C)

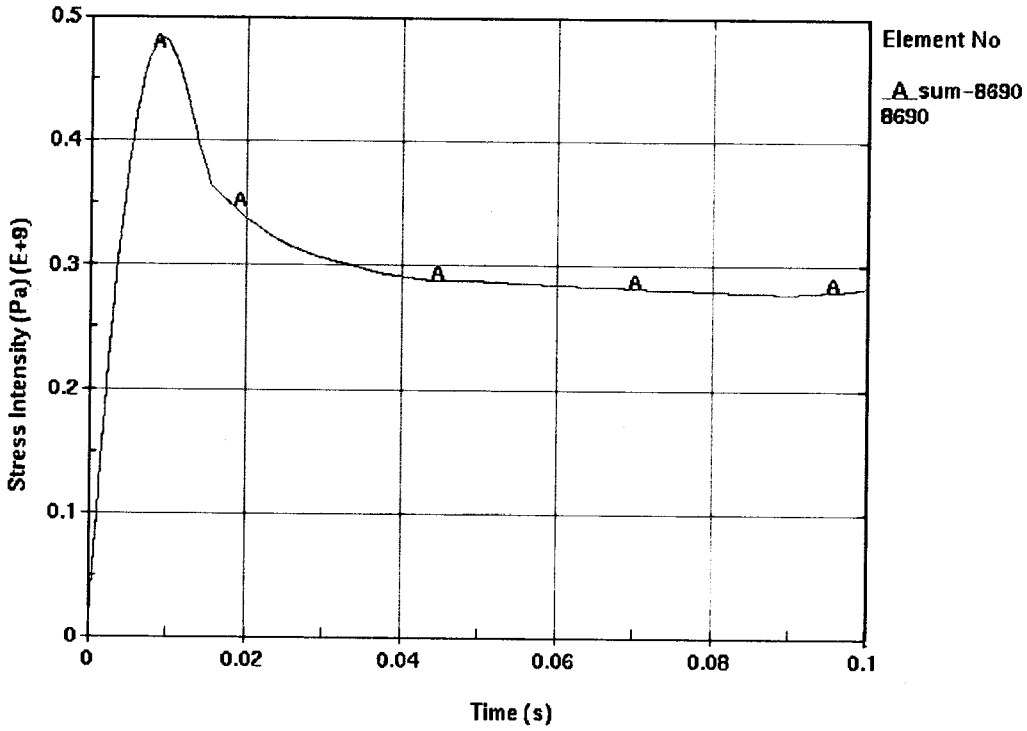

Figure II-11. Stress Intensity Plot for Element No. 8690 of Outer Shell Outer Surface (Case C)

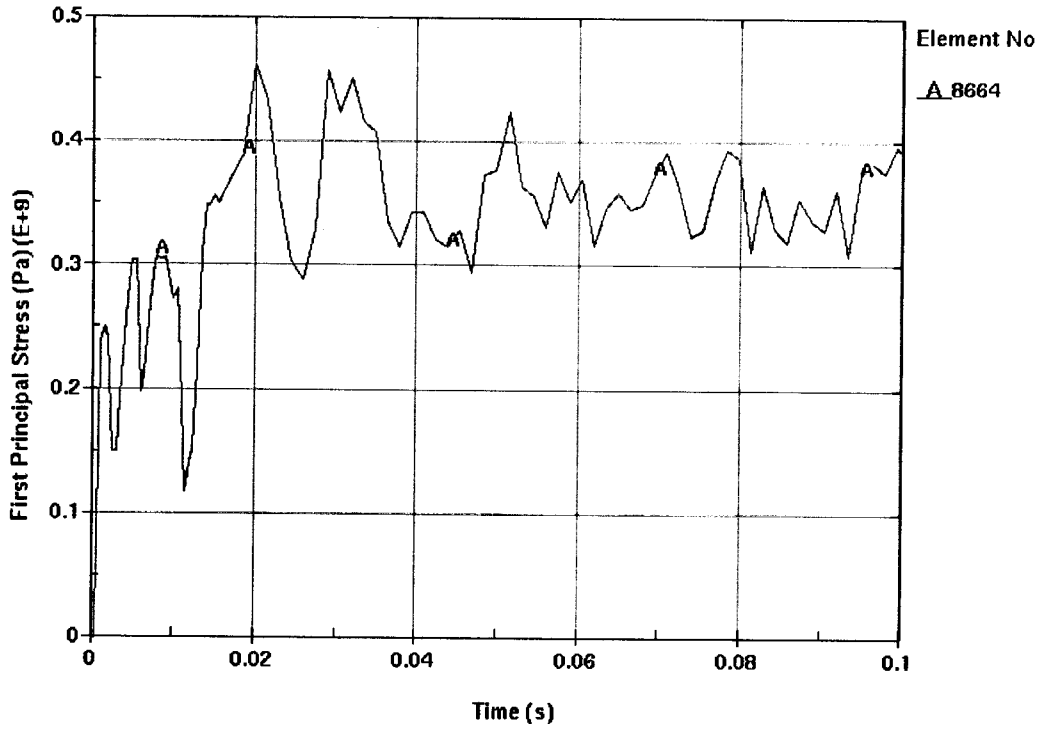

Figure II-12. First Principal Stress Plot for Element No. 8664 of Outer Shell (Case C)

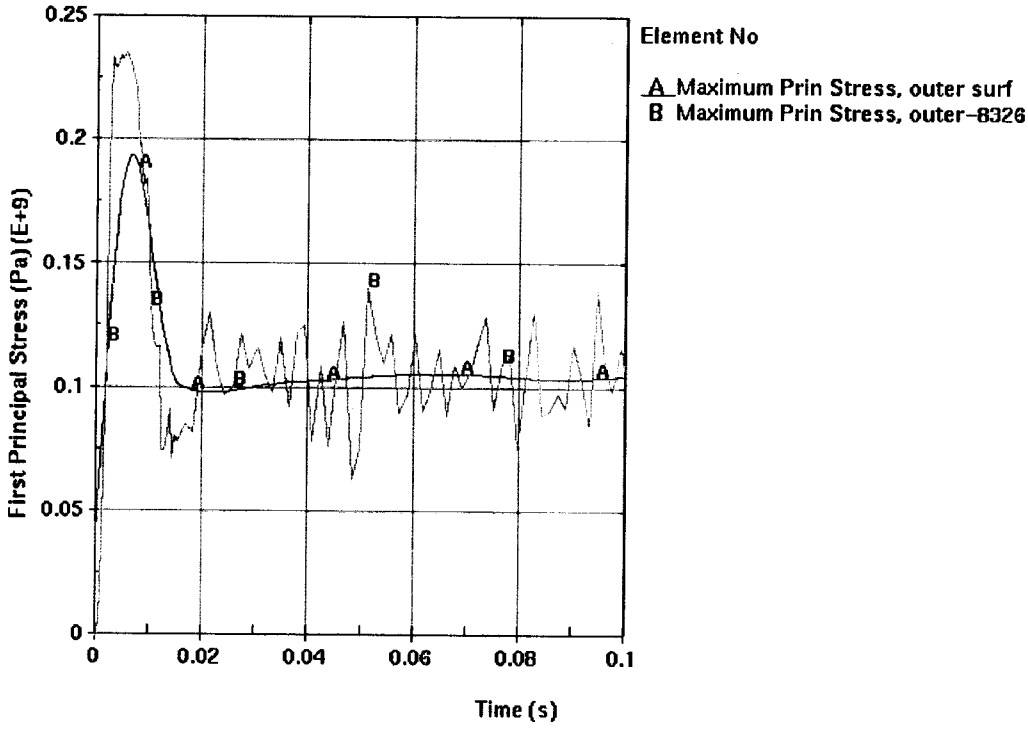

Figure II-13. Raw and Filtered First Principal Stress Plot Plot for Element No. 8326 of Outer Shell Outer Surface (Case C)

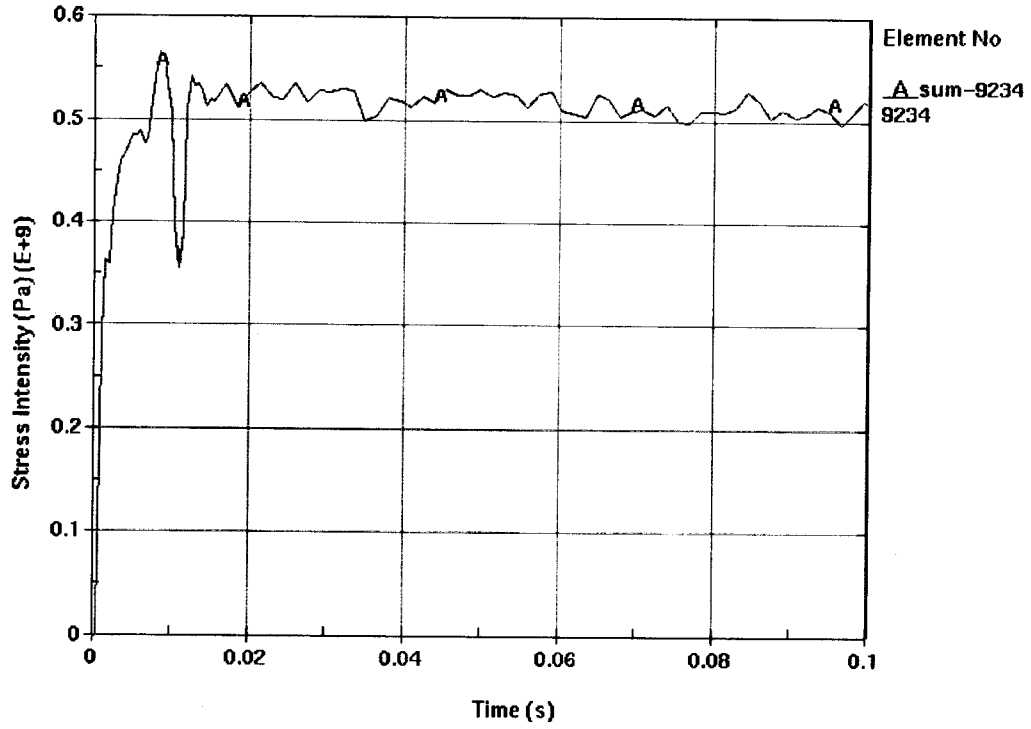

Figure II-14 Stress Intensity Plot for Element No. 9234 of Outer Shell with Refined Mesh (Case A)

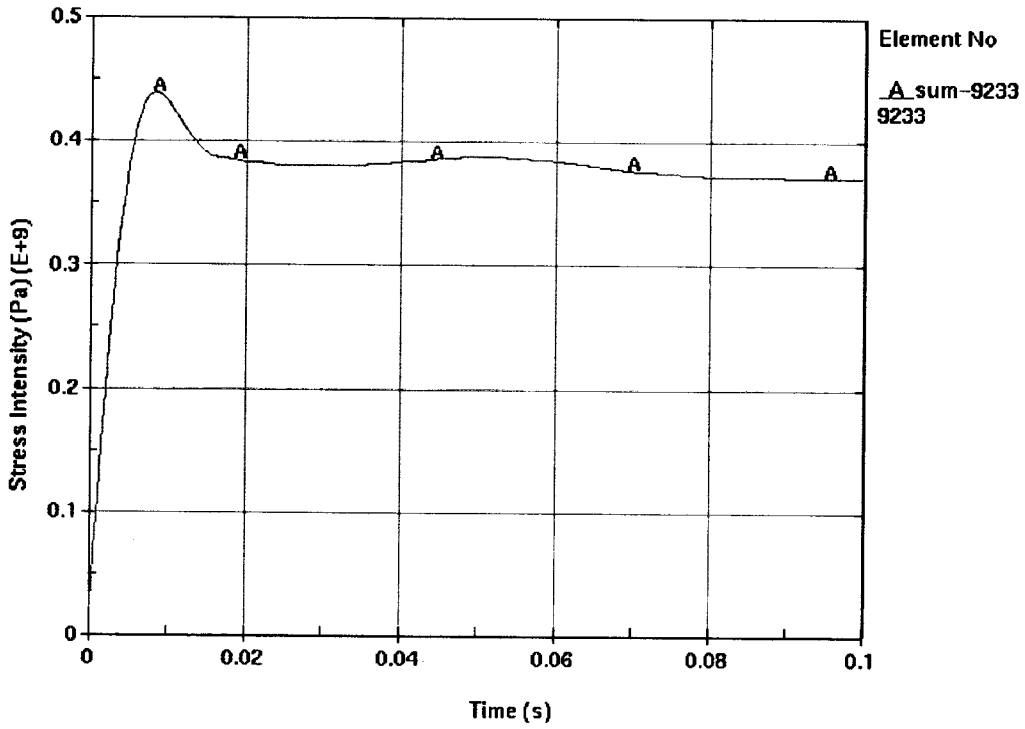

Figure II-15 Stress Intensity Plot for Element No. 9233 of Outer Shell Outer Surface with Refined Mesh (Case A)

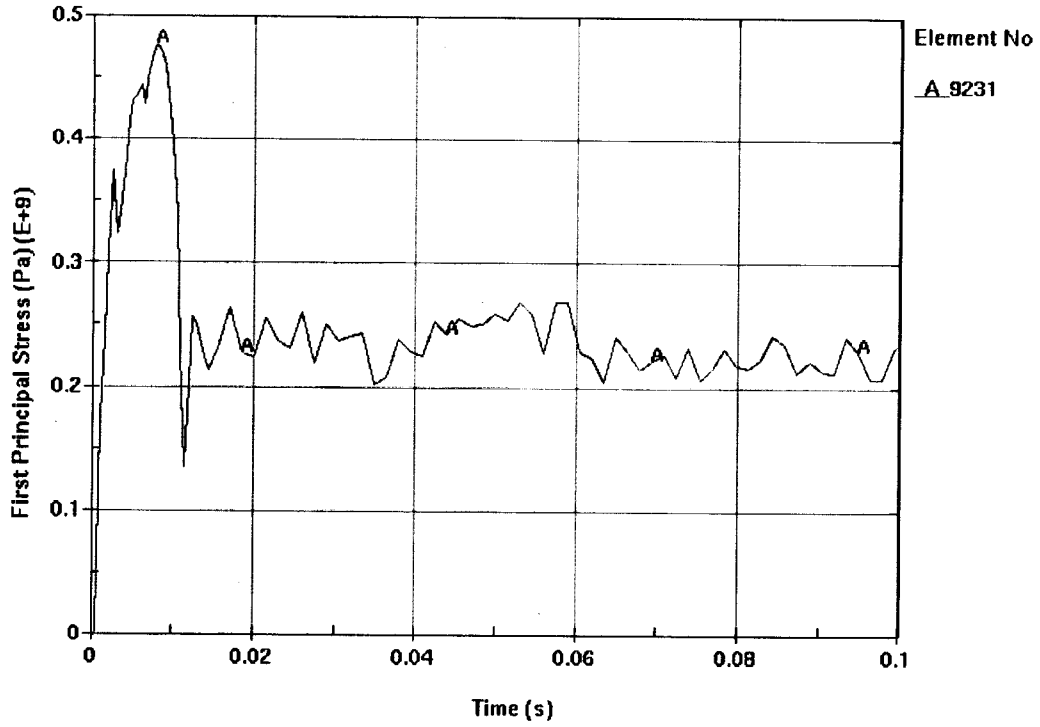

Figure II-16 First Principal Stress Plot for Element No. 9231 of Outer Shell with Refined Mesh (Case A)

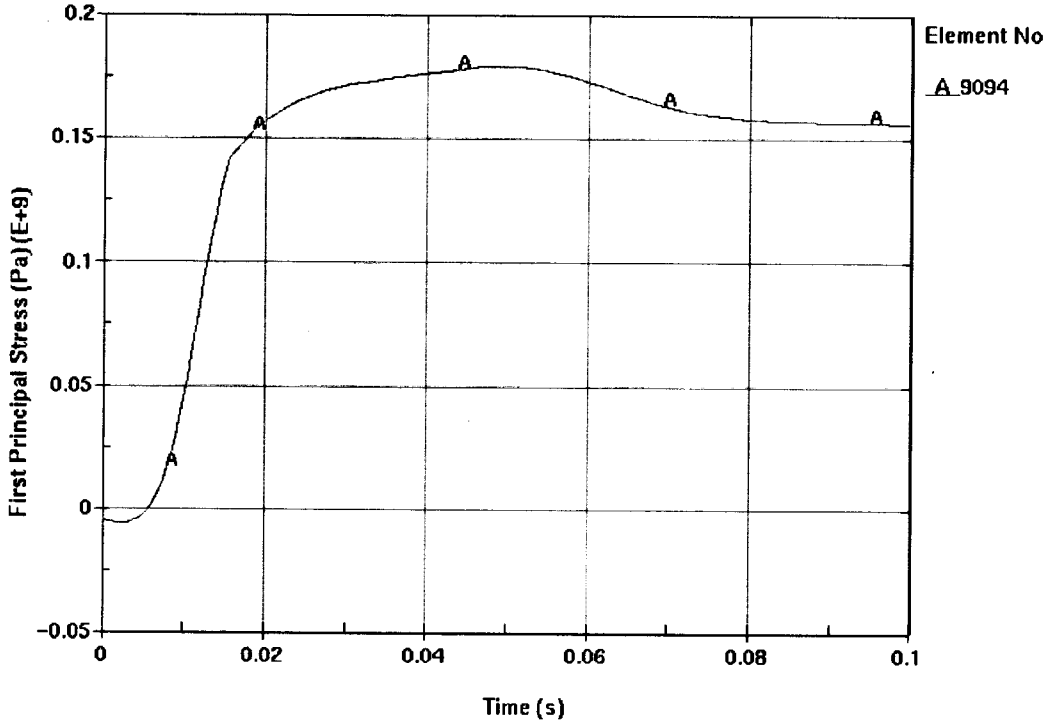

Figure II-17 First Principal Stress Plot for Element No. 9094 of Outer Shell Outer Surface with Refined Mesh (Case A)

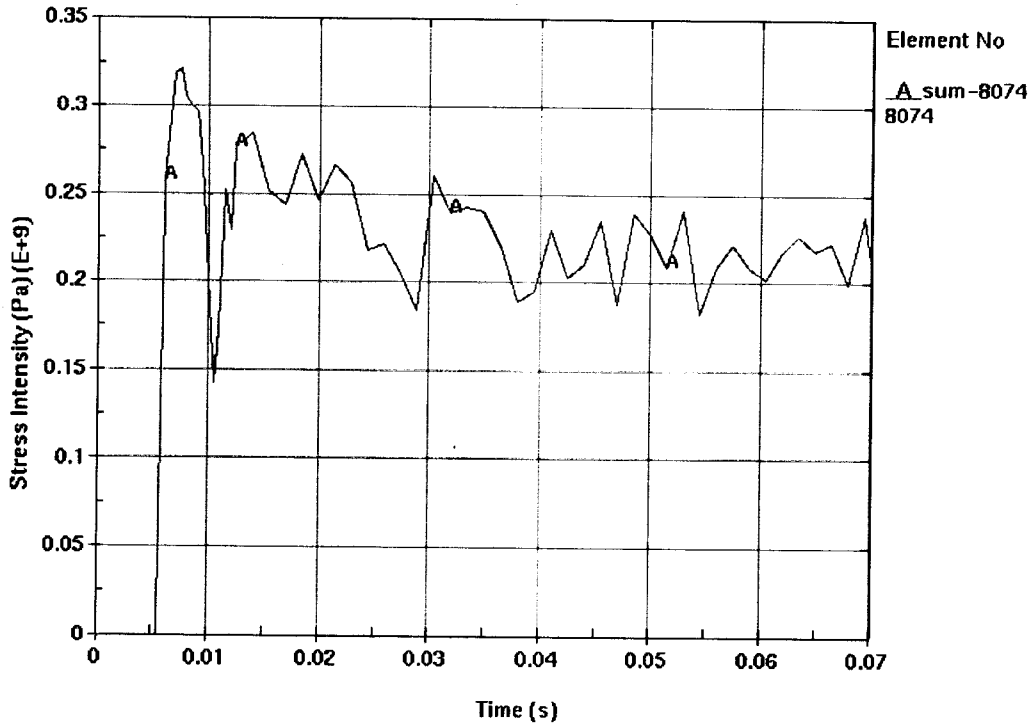

Figure II-18. Stress Intensity in Outer Shell (Element No. 8074) during Horizontal 1-MT Rock Fall

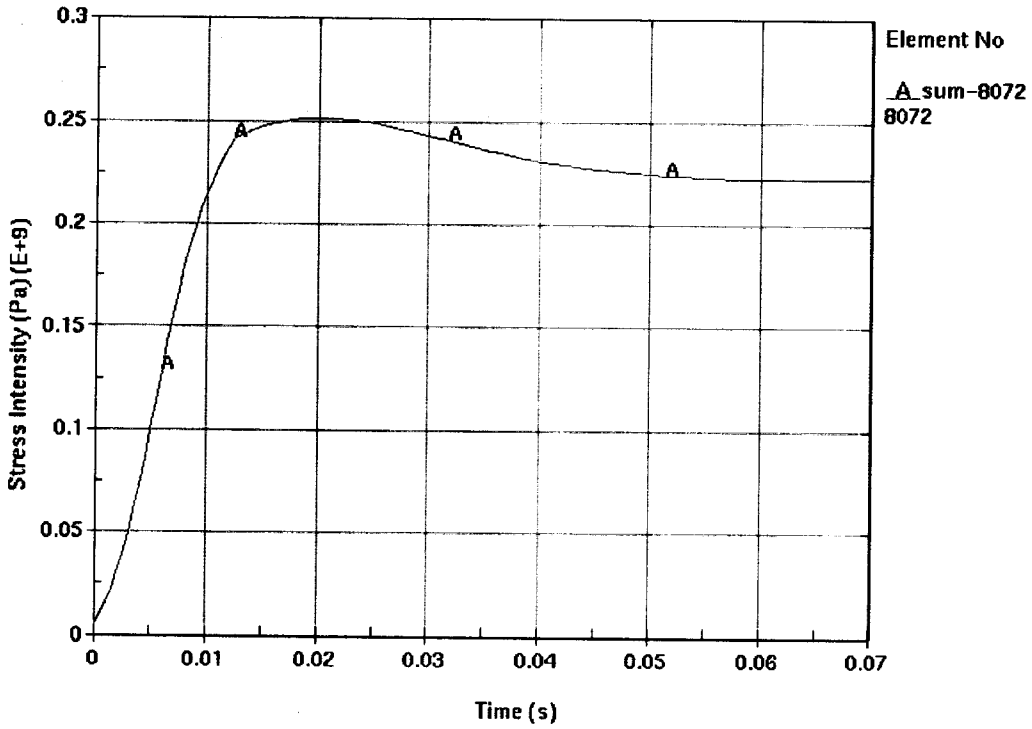

Figure II-19. Stress Intensity in Outer Shell Outer Surface (Element No. 8072) during Horizontal 1-MT Rock Fall

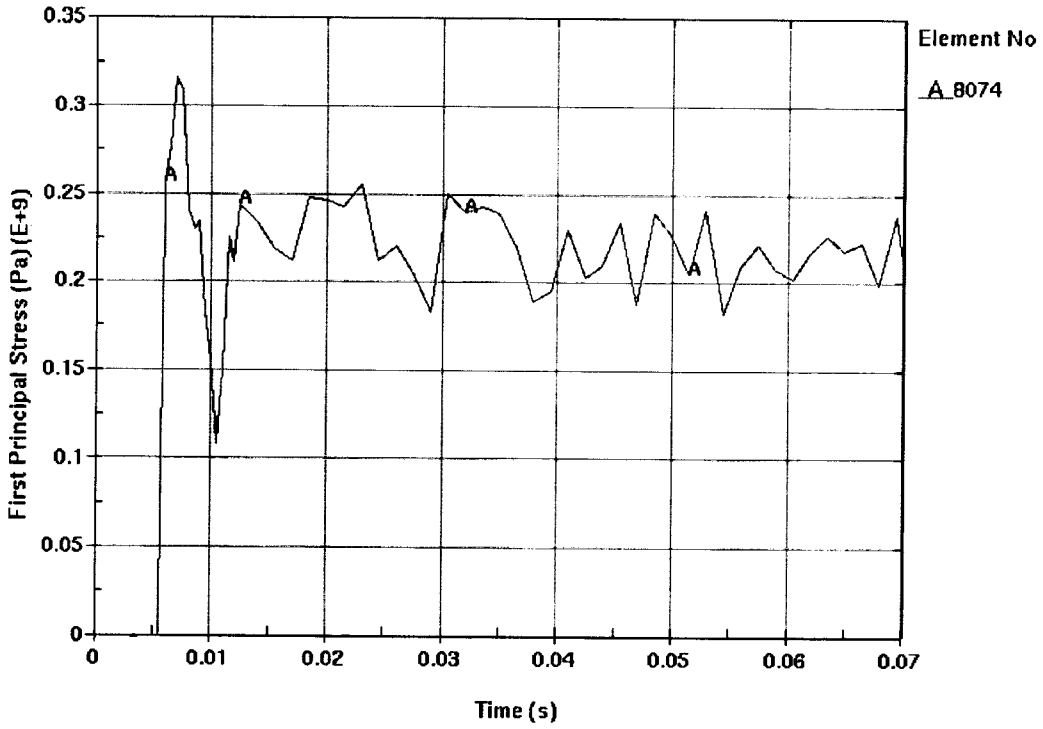

Figure II-20. First Principal Stress in Outer Shell (Element No. 8074) during Horizontal 1-MT Rock Fall

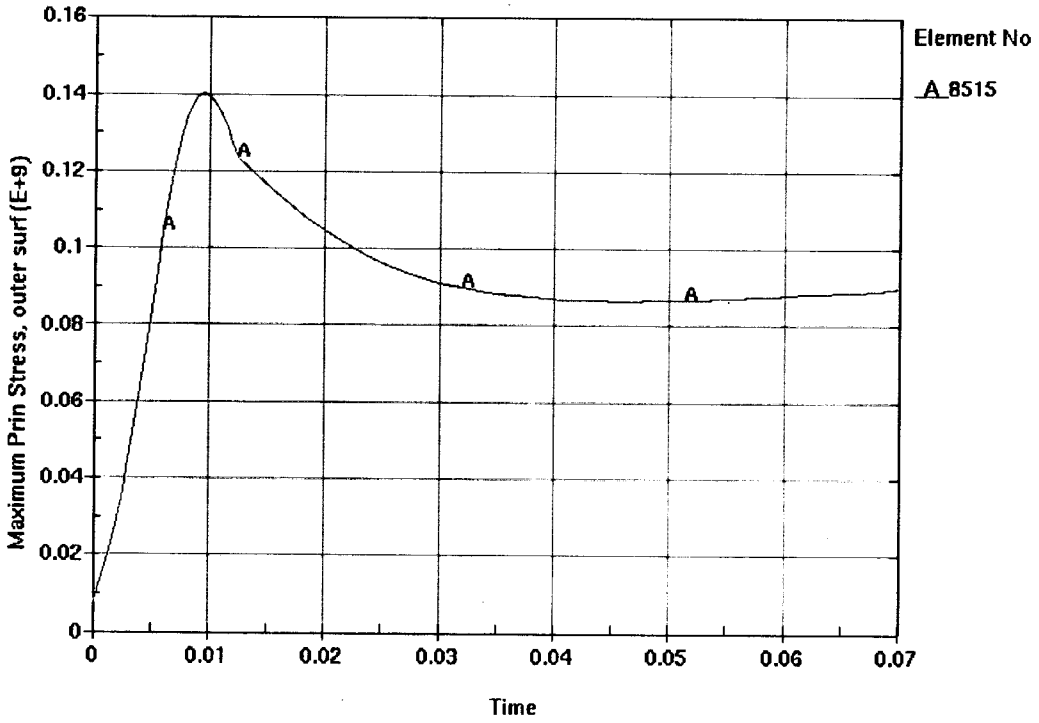

Figure II-21. First Principal Stress in Outer Shell Outer Surface (Element No. 8515) during Horizontal 1-MT Rock Fall

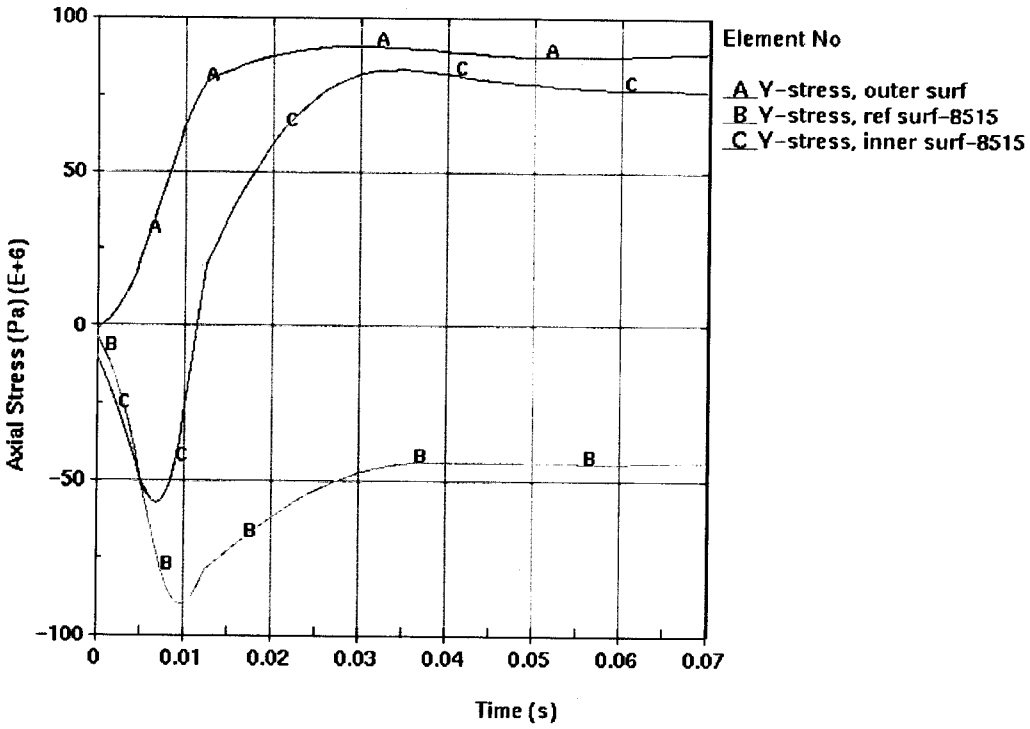

Figure II-22. Axial Stress Across Outer Shell Thickness (Element No. 8515) during Horizontal 1-MT Rock Fall

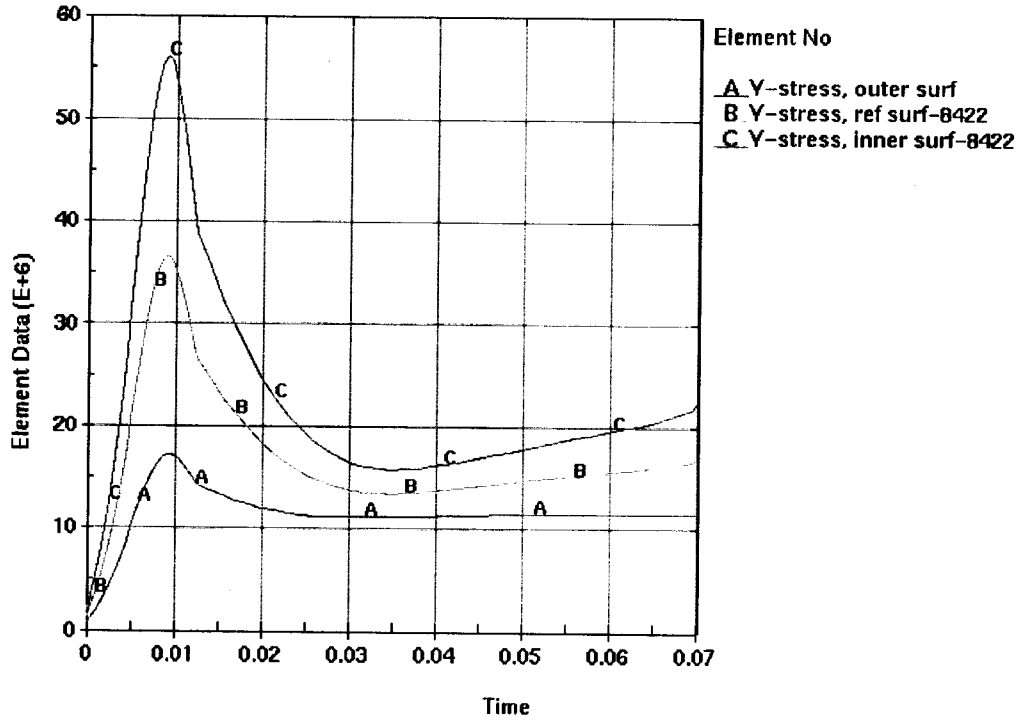

Figure II-23. Axial Stress Across Outer Shell Thickness (Element No. 8422) during Horizontal 1-MT Rock Fall

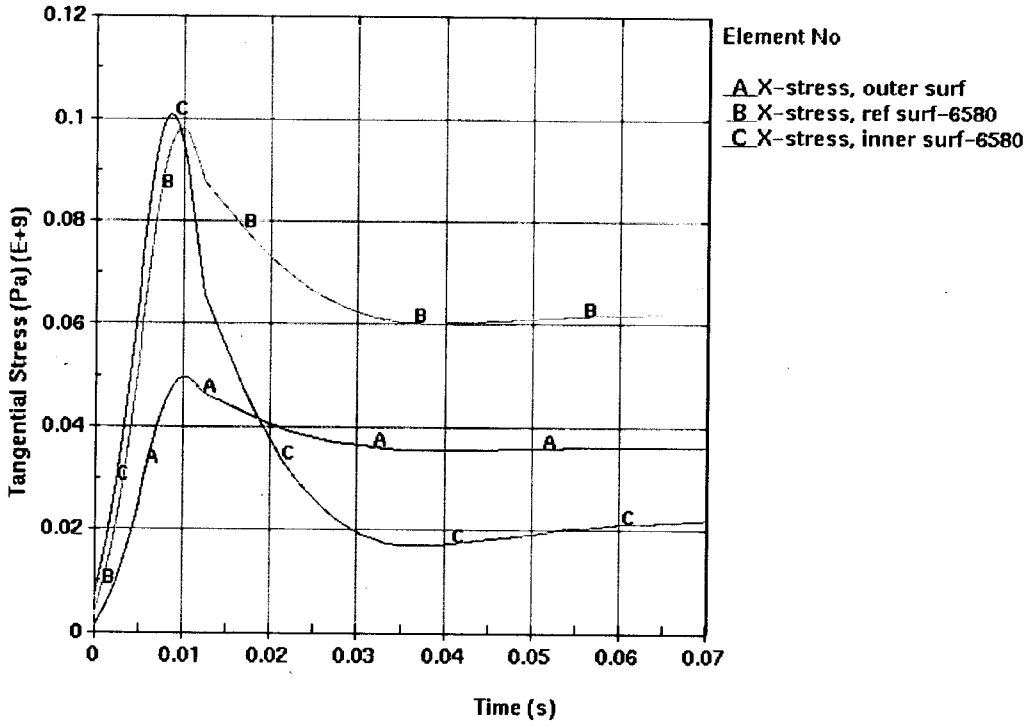

Figure II-24. Tangential Stress Across Outer Shell Thickness Thickness (Element No. 6580) during Horizontal 1-MT Rock Fall

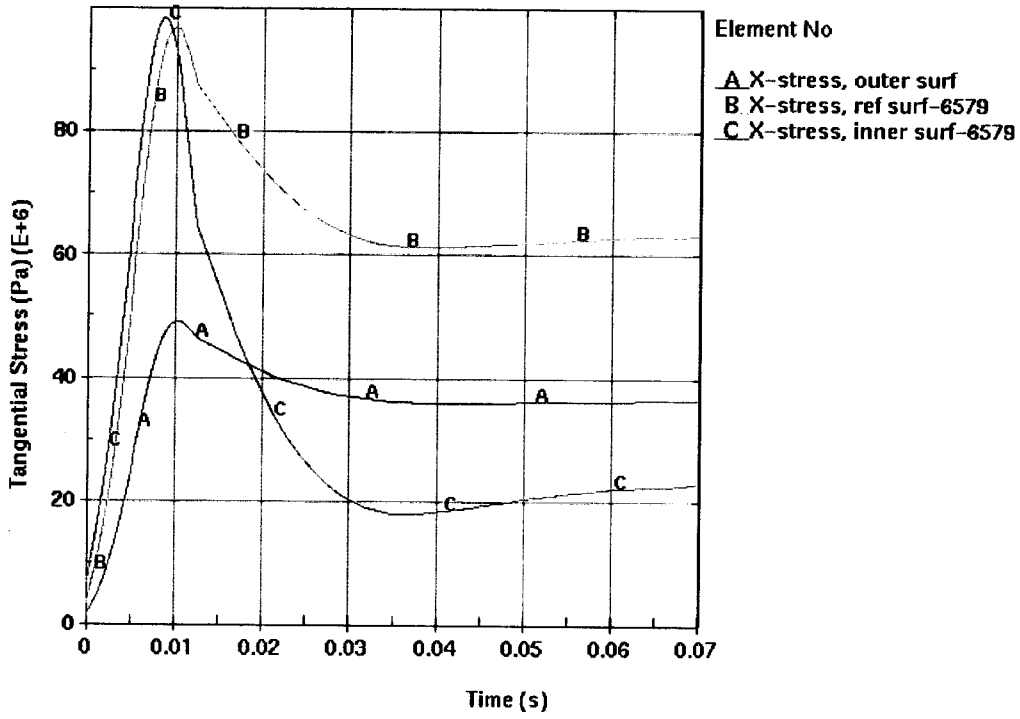

Figure II-25. Tangential Stress Across Outer Shell Thickness Thickness (Element No. 6579) during Horizontal 1-MT Rock Fall

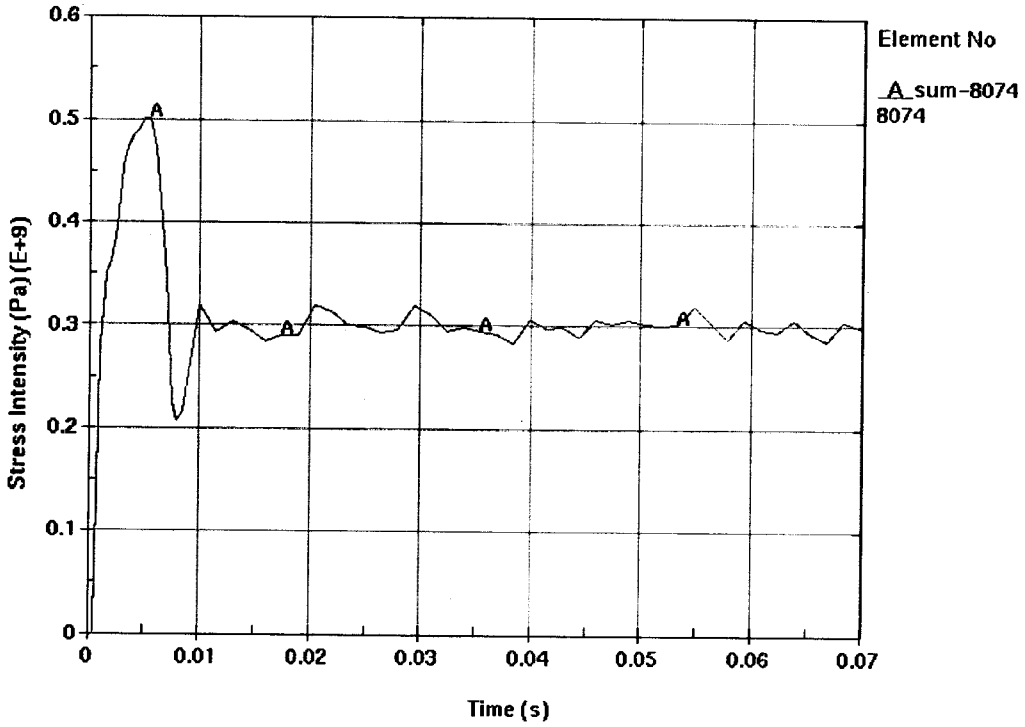

Figure II-26. Stress Intensity in Outer Shell (Element No. 8074) during 57-degrees 1-MT Rock Fall

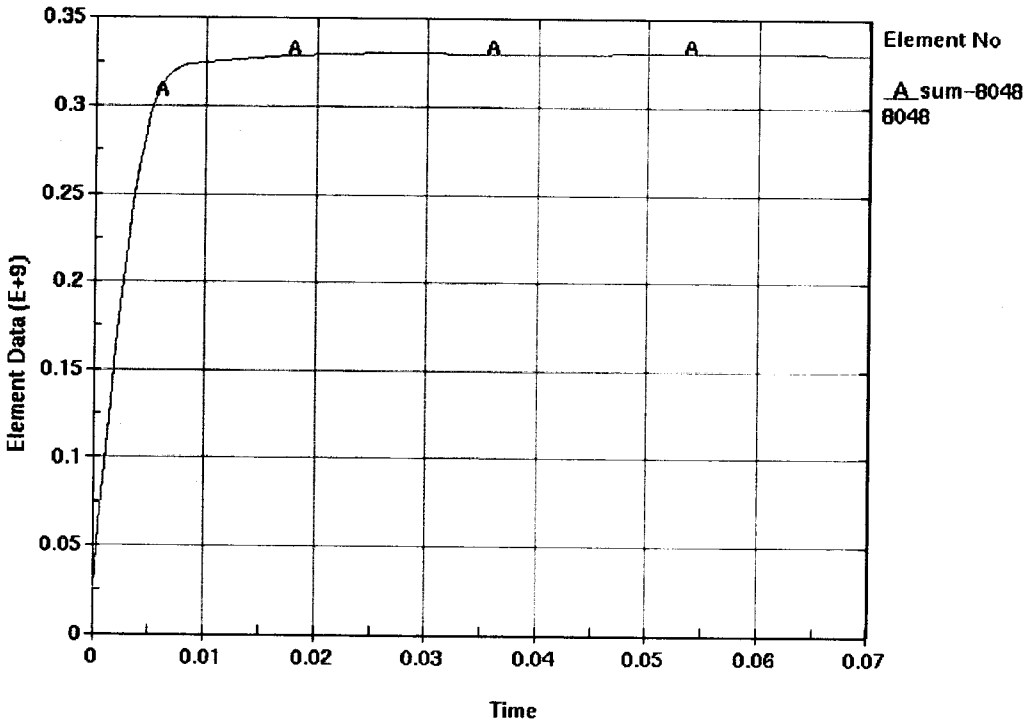

Figure II-27. Stress Intensity in Outer Shell Outer Surface (Element No. 8048) during 57-degrees 1-MT Rock Fall

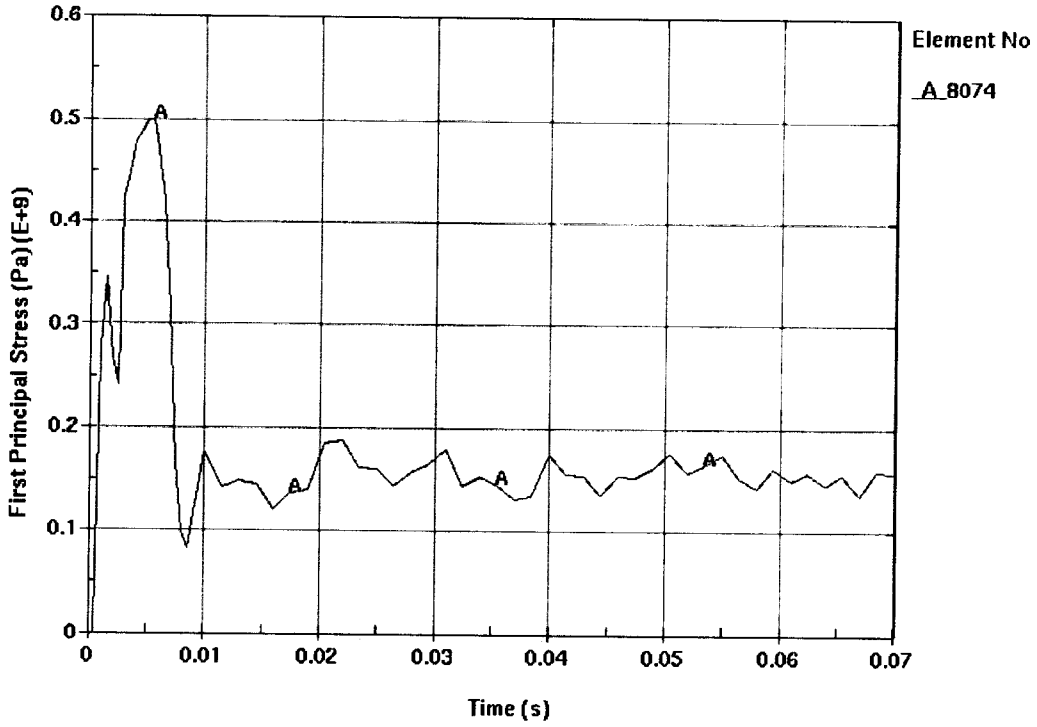

Figure II-28. First Principal Stress in Outer Shell (Element No. 8074) during 57-degrees 1-MT Rock Fall

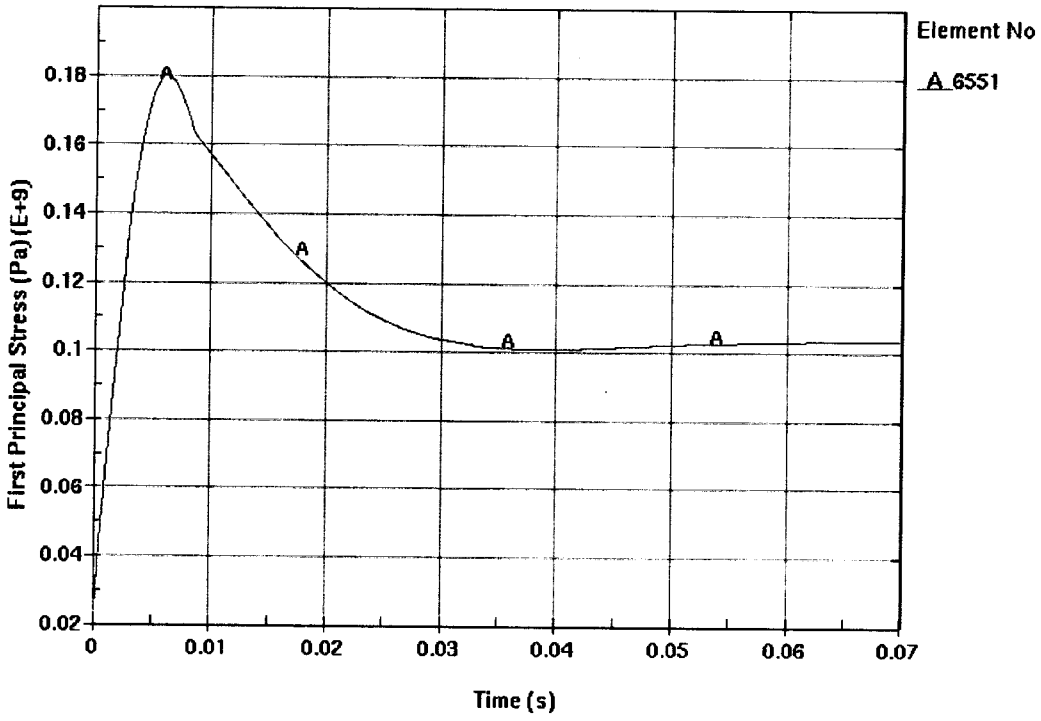

Figure II-29. First Principal Stress in Outer Shell Outer Surface (Element No. 6551) during 57-degrees 1-MT Rock Fall

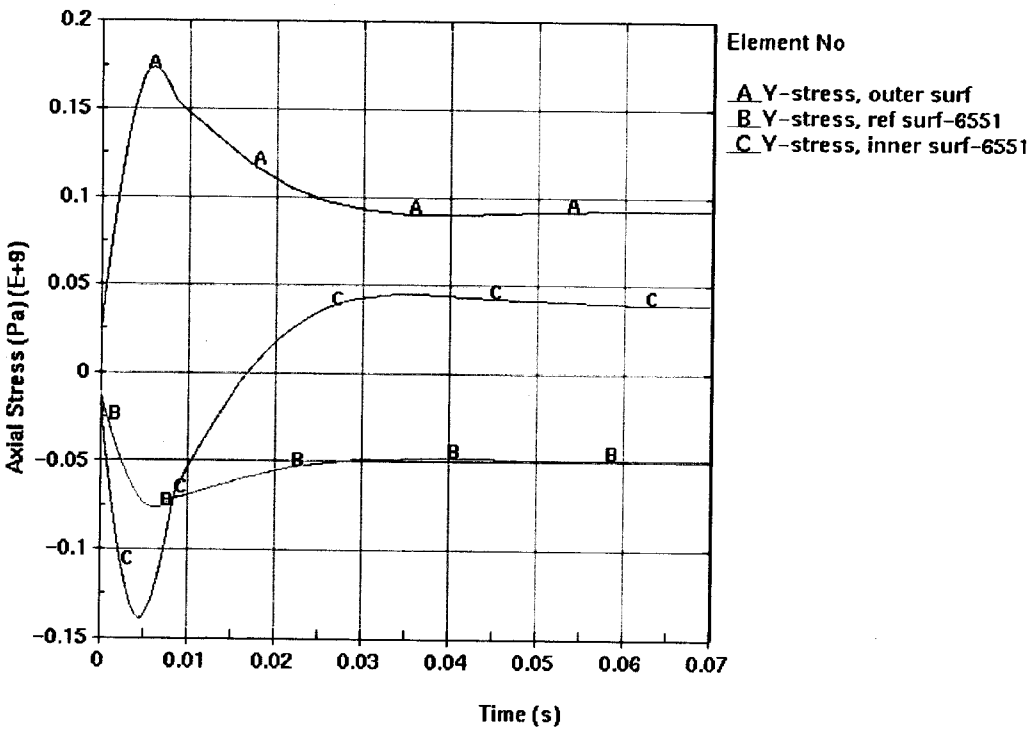

Figure II-30. Axial Stress Across Outer Shell Thickness (Element No. 6551) during 57-degrees 1-MT Rock Fall

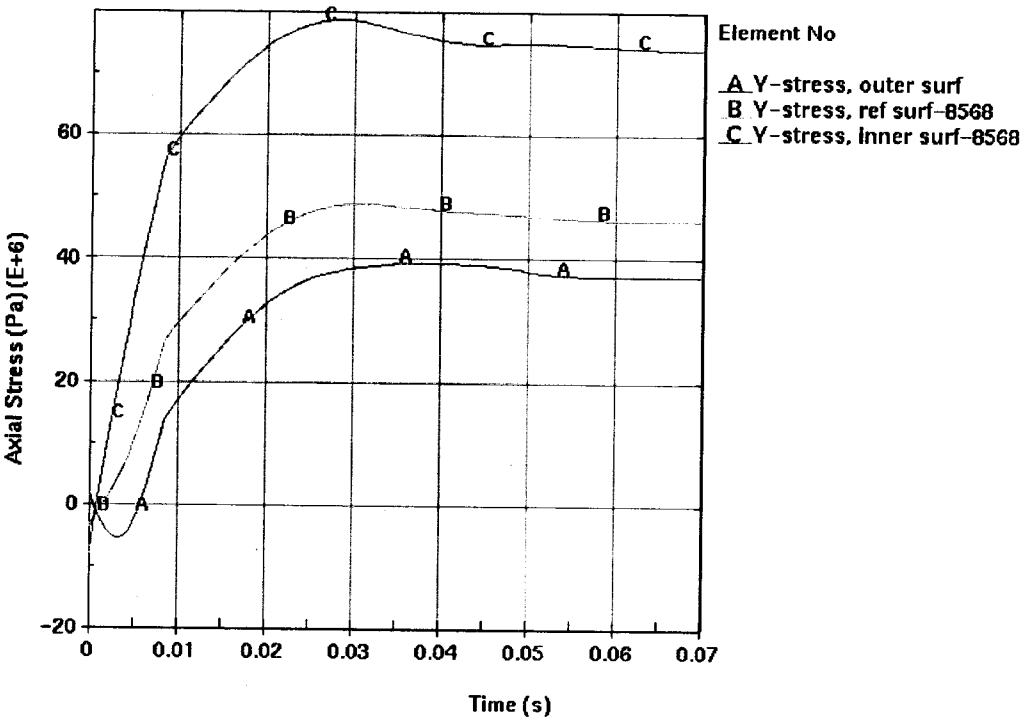

Figure II-31. Axial Stress Across Outer Shell Thickness (Element No. 8568) during 57-degrees 1-MT Rock Fall

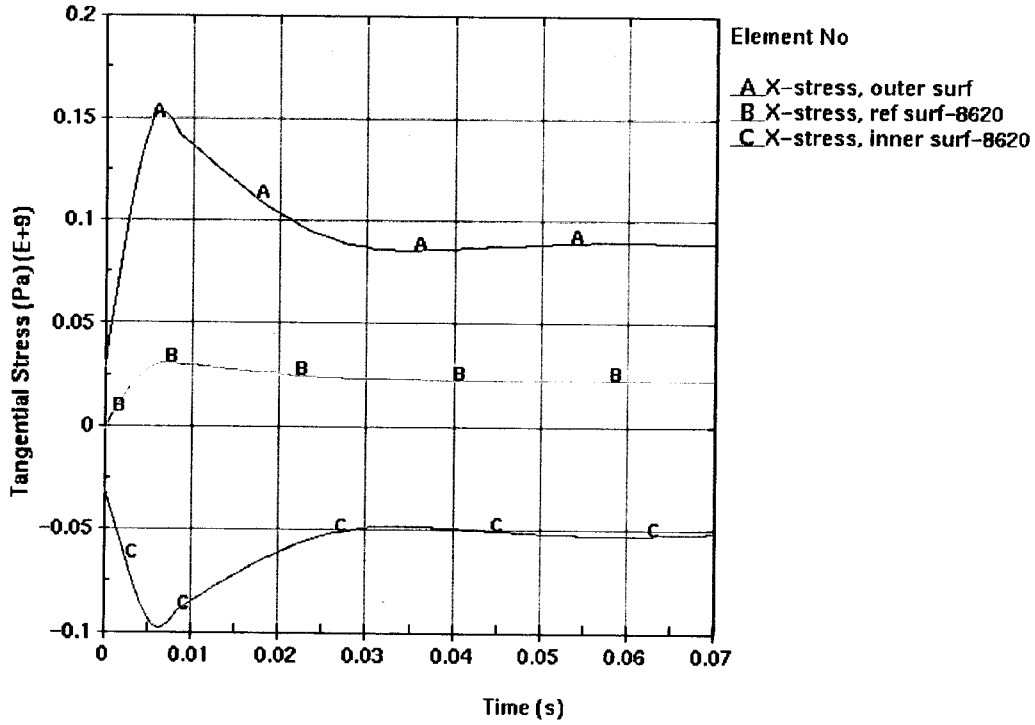

Figure II-32. Tangential Stress Across Outer Shell Thickness (Element No. 8620) during 57-degrees 1-MT Rock Fall

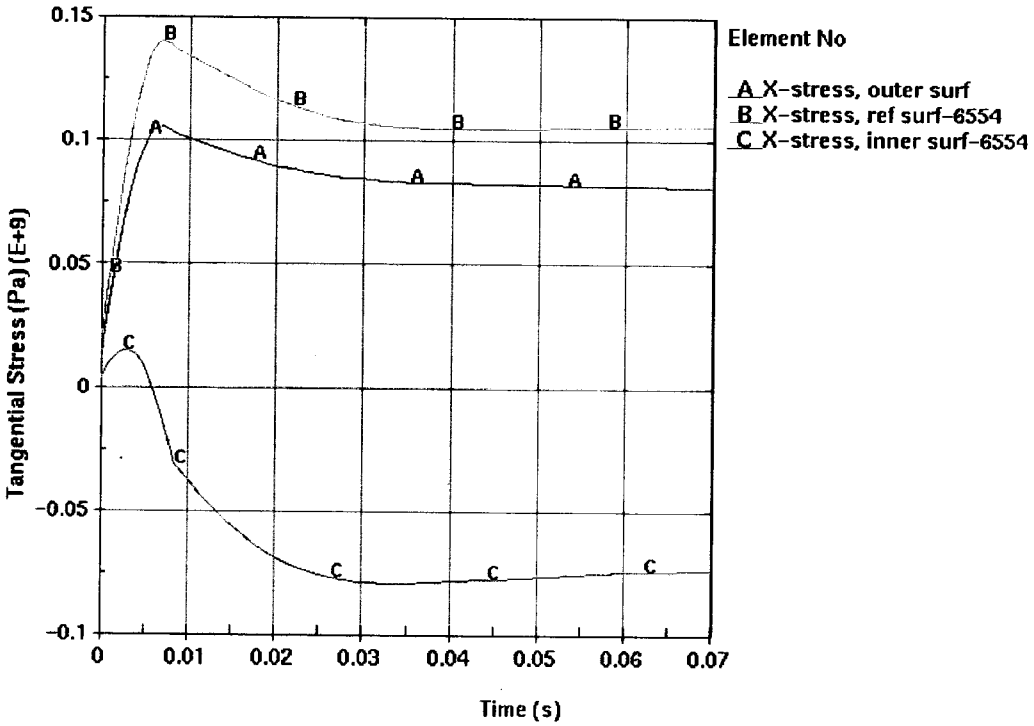

Figure II-33. Tangential Stress Across Outer Shell Thickness (Element No. 6554) during 57-degrees 1-MT Rock Fall

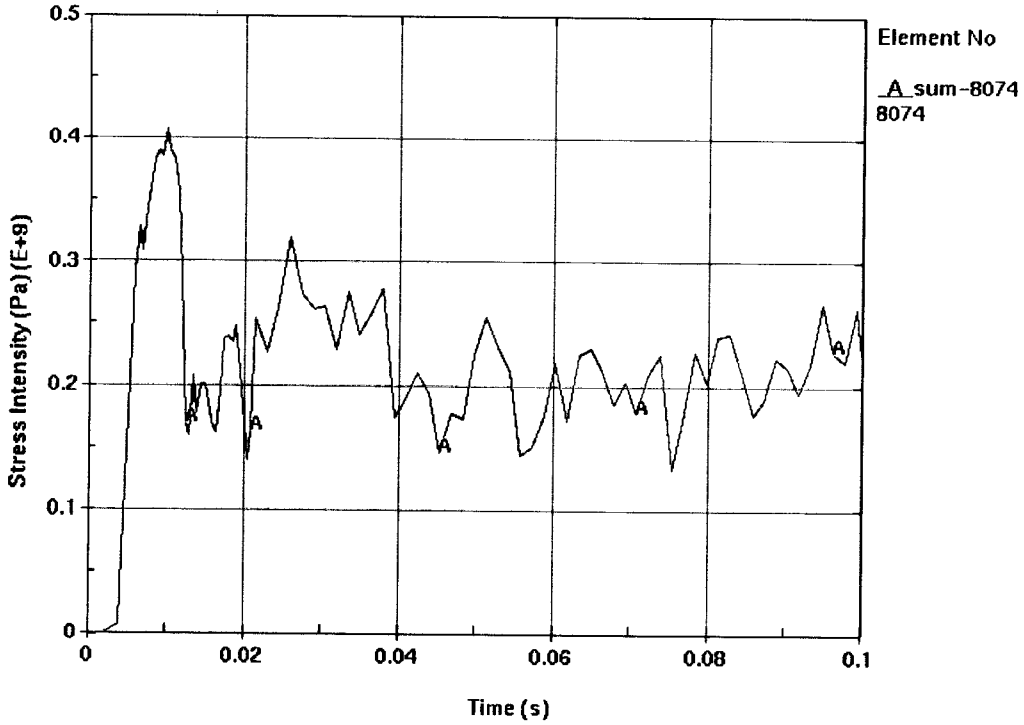

Figure II-34. Stress Intensity in Outer Shell (Element No. 8074) during Horizontal 6-MT Rock Fall

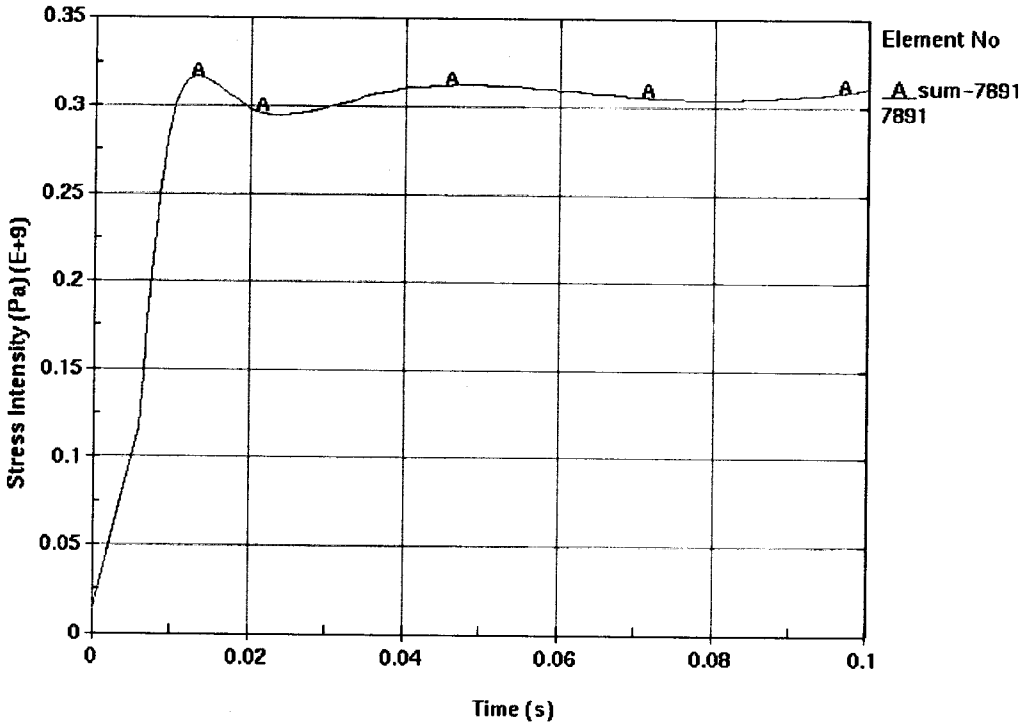

Figure II-35. Stress Intensity in Outer Shell Outer Surface (Element No. 7891) Horizontal 6-MT Rock Fall

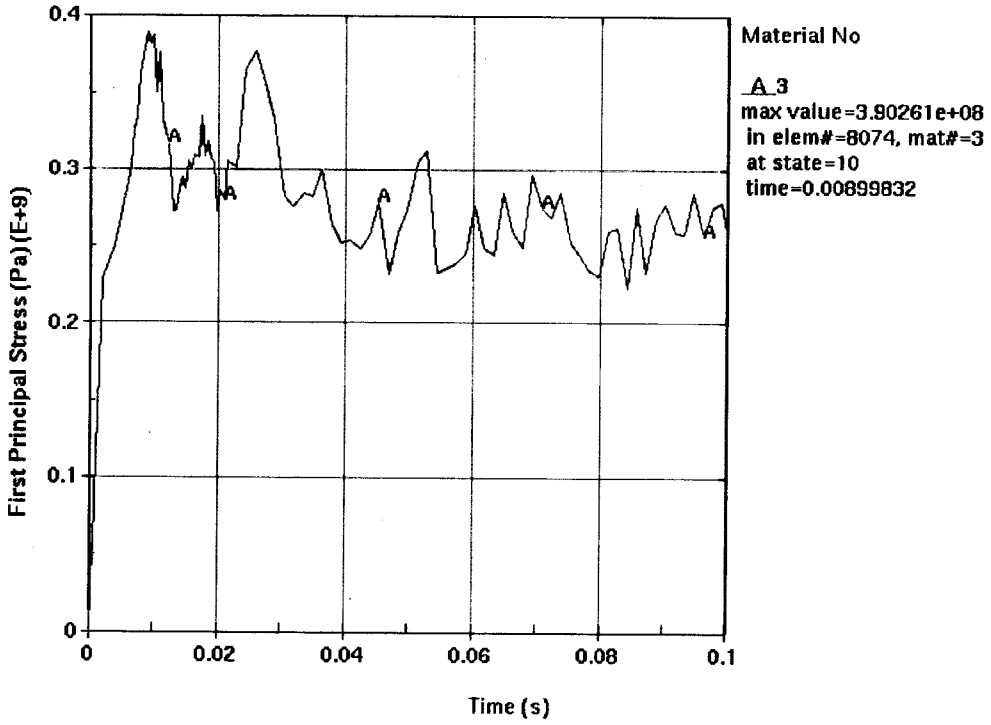

Figure II-36. First Principal Stress in Outer Shell (Element No. 8074) during Horizontal 6-MT Rock Fall

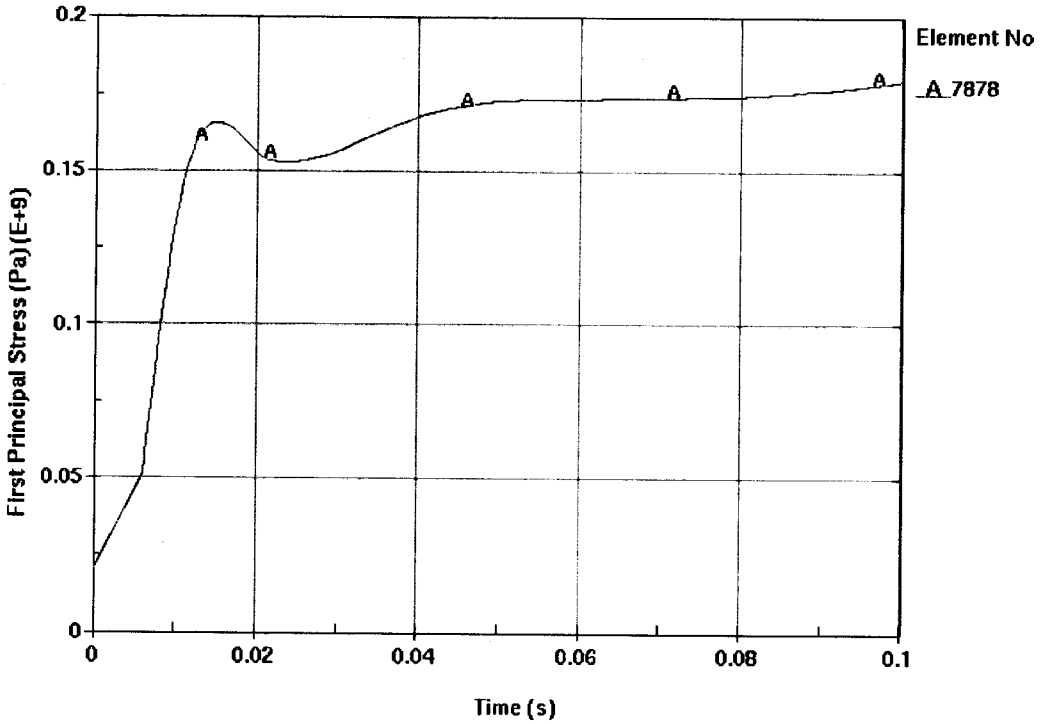

Figure II-37. First Principal Stress in Outer Shell Outer Surface (Element No. 7878) during Horizontal 6-MT Rock Fall

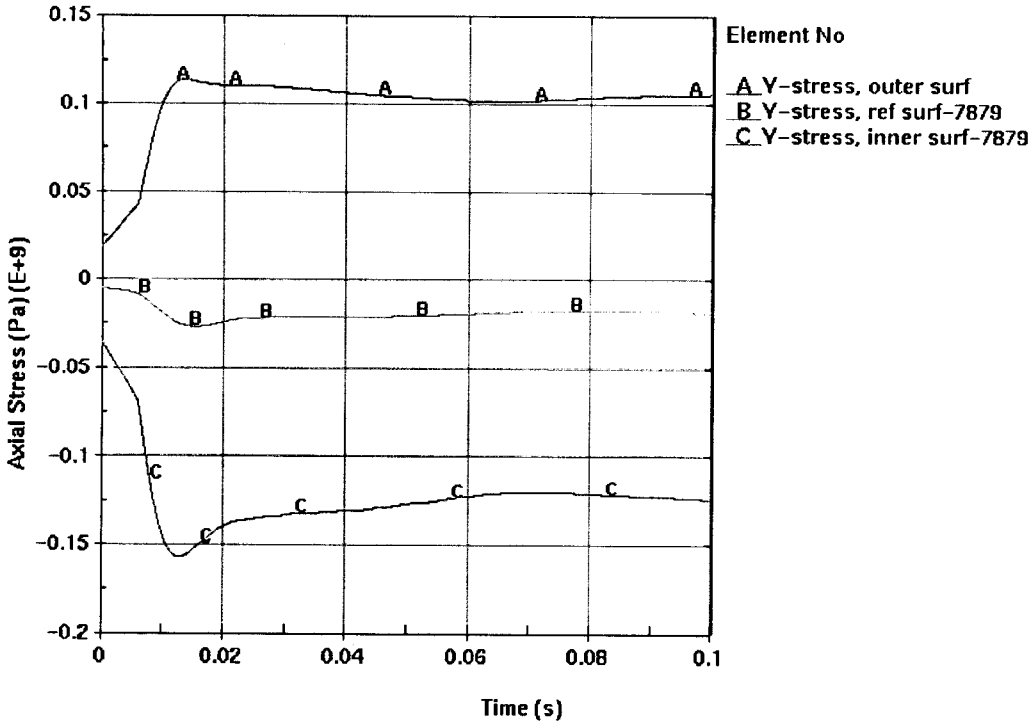

Figure II-38. Axial Stress Across Outer Shell Thickness (Element No. 7879) during Horizontal 6-MT Rock Fall

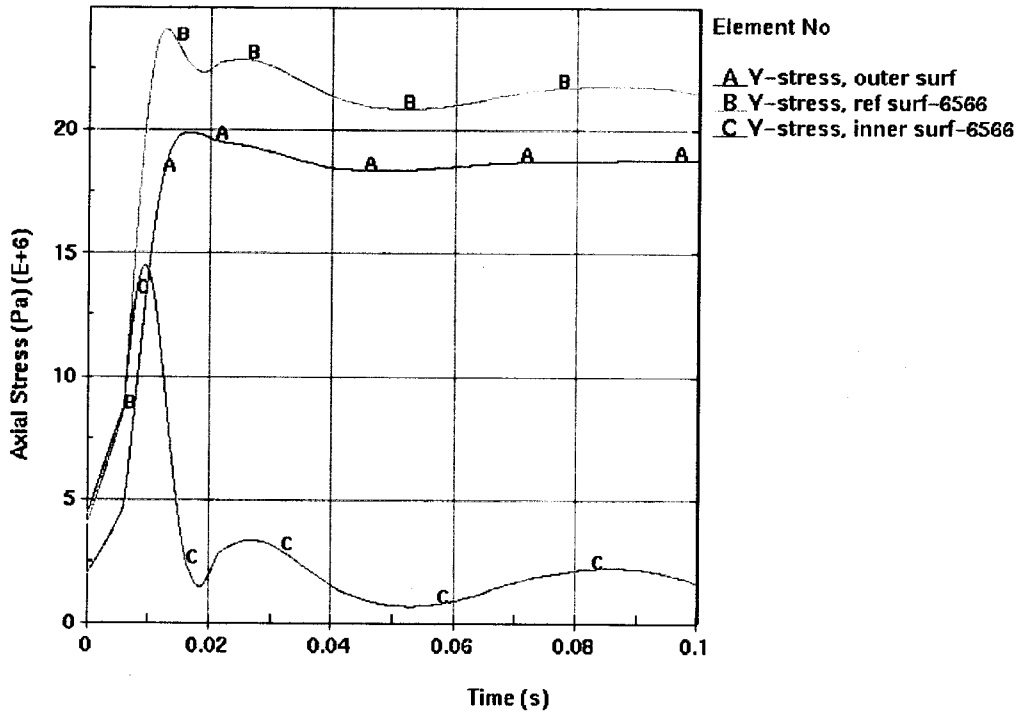

Figure II-39. Axial Stress Across Outer Shell Thickness (Element No. 6566) during Horizontal 6-MT Rock Fall

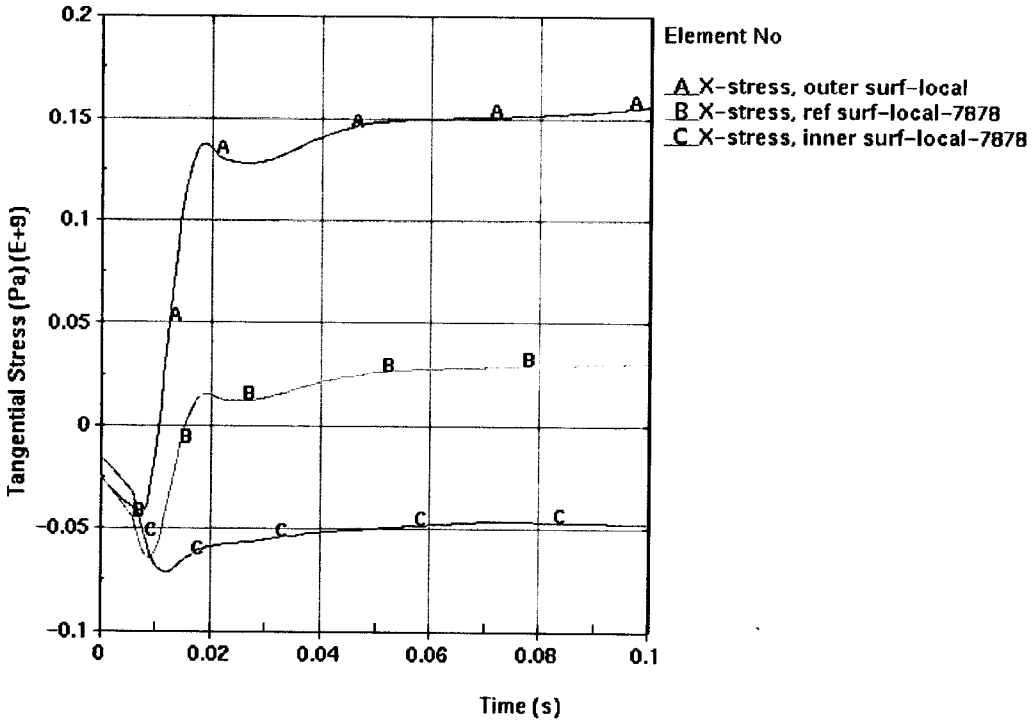

Figure II-40. Tangential Stress Across Outer Shell Thickness (Element No. 7878) during Horizontal 6-MT Rock Fall

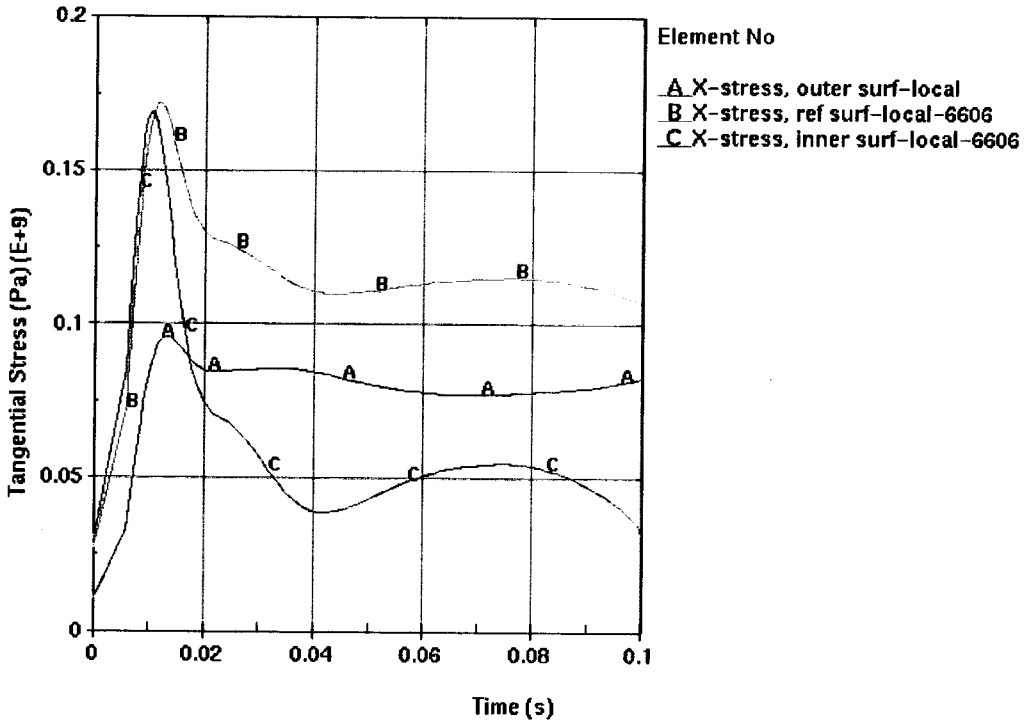

Figure II-41. Tangential Stress Across Outer Shell Thickness (Element No. 6606) during Horizontal 6-MT Rock Fall

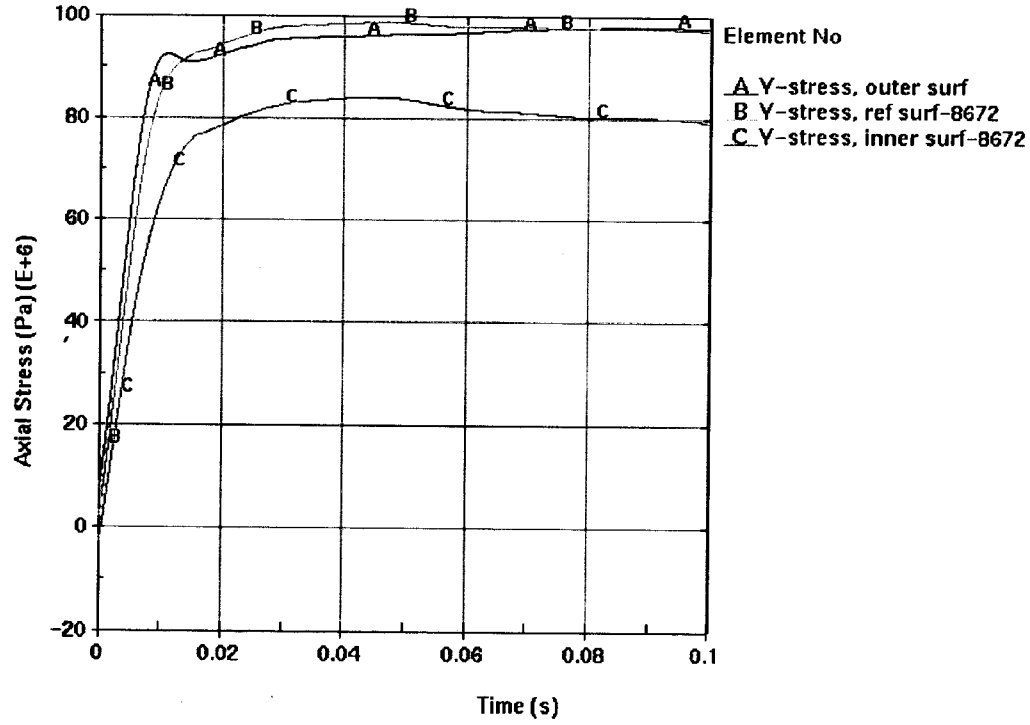

Figure II-42. Axial Stress Across Outer Shell Thickness (Element No. 8672) during 25-degrees 6-MT Rock Fall

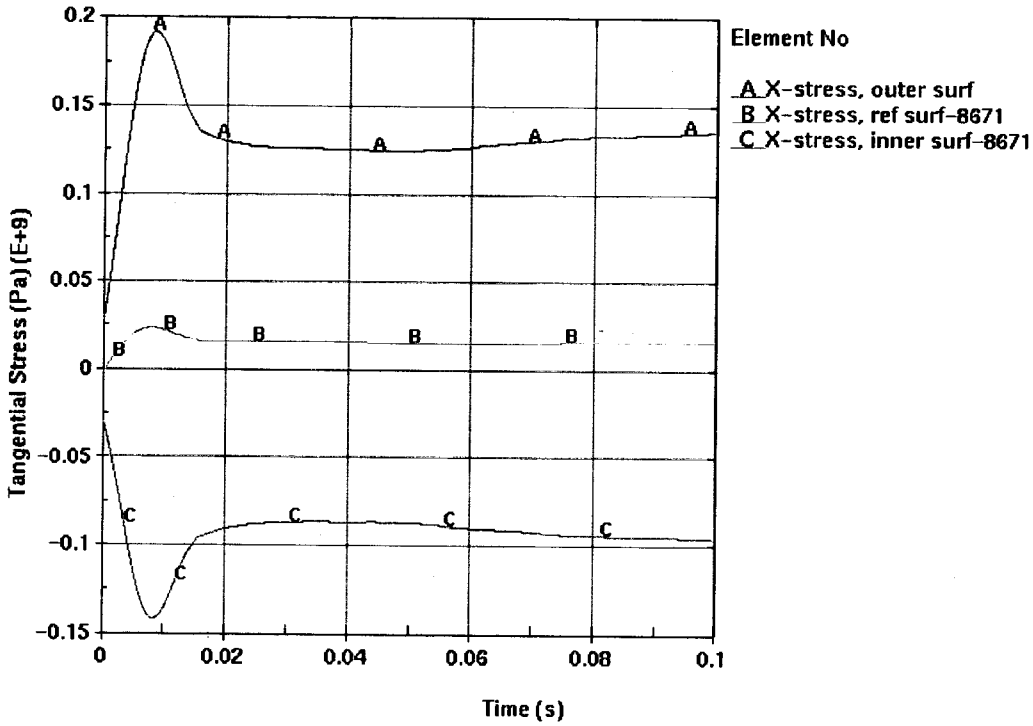

Figure II-43. Tangential Stress Across Outer Shell Thickness (Element No. 8671) during 25-degrees 6-MT Rock Fall

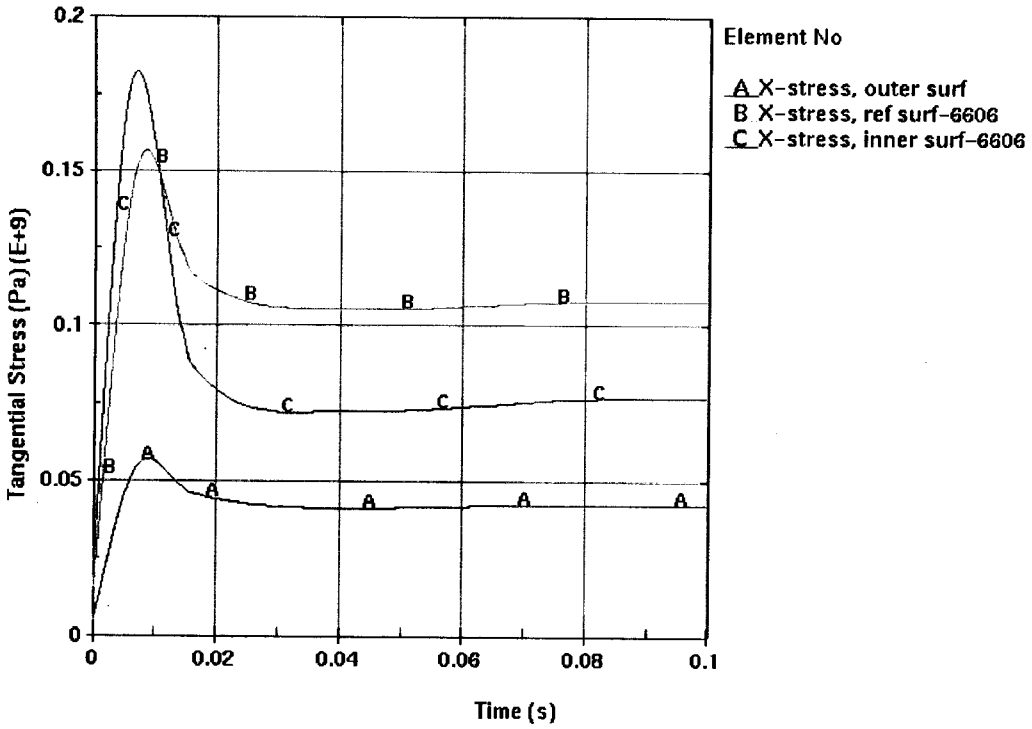

Figure II-44. Tangential Stress Across Outer Shell Thickness (Element No. 6606) during 25-degrees 6-MT Rock Fall

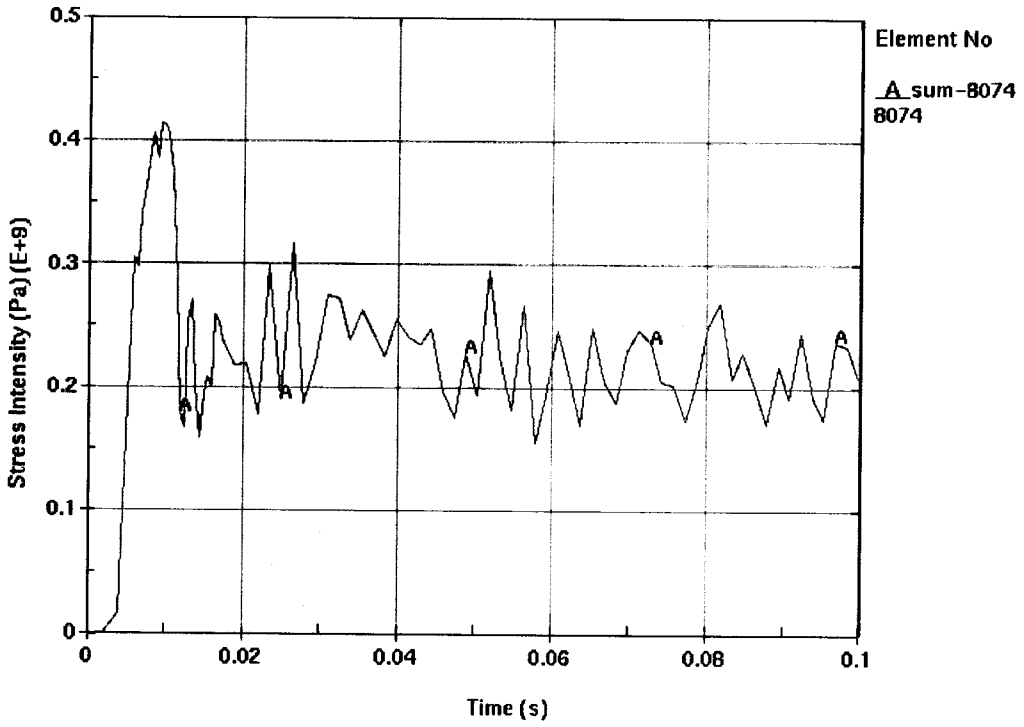

Figure II-45. Stress Intensity in Outer Shell (Element No. 8074) during Horizontal 10-MT Rock Fall

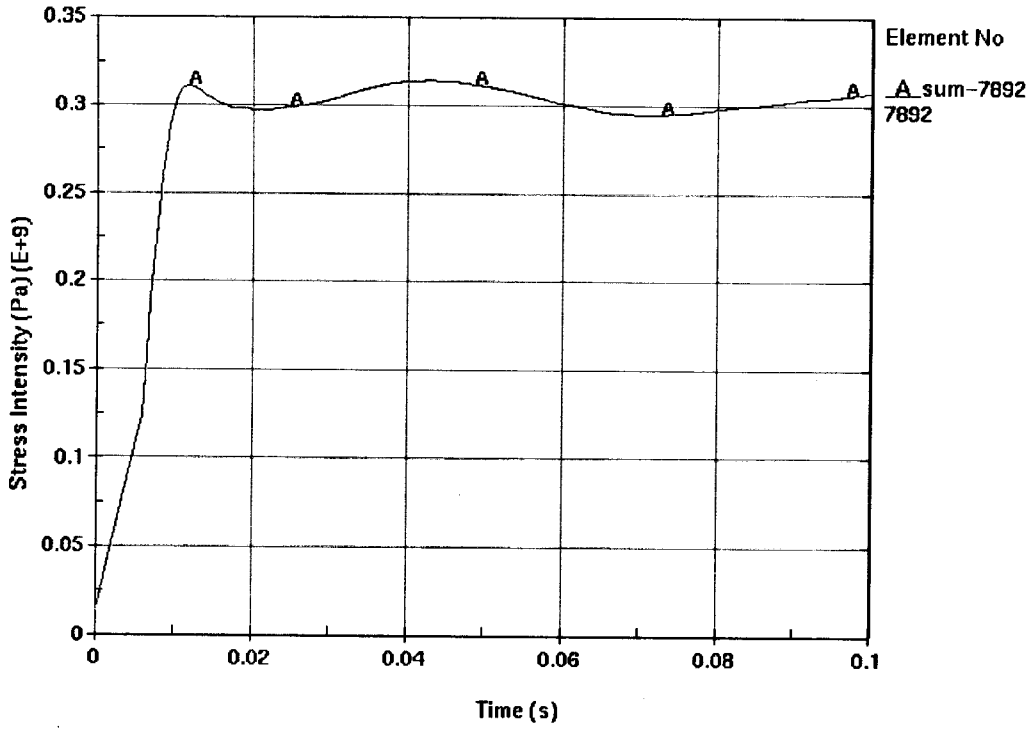

Figure II-46. Stress Intensity in Outer Shell Outer Surface (Element No. 7892) during Horizontal 10-MT Rock Fall

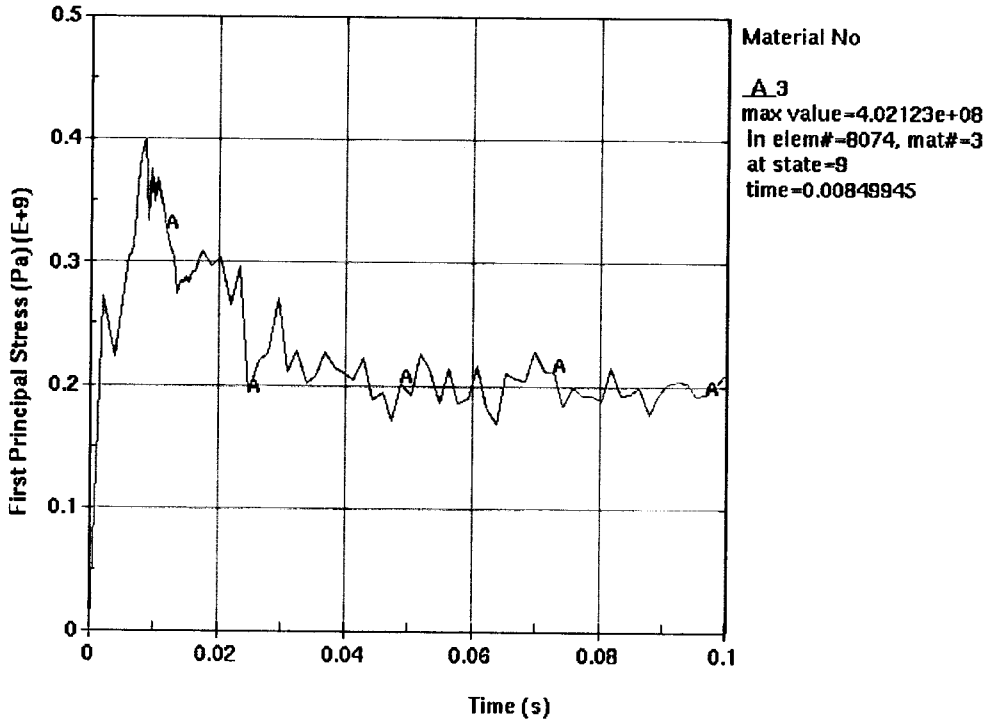

Figure II-47. First Principal Stress in Outer Shell (Element No. 8074) during Horizontal 10-MT Rock Fall

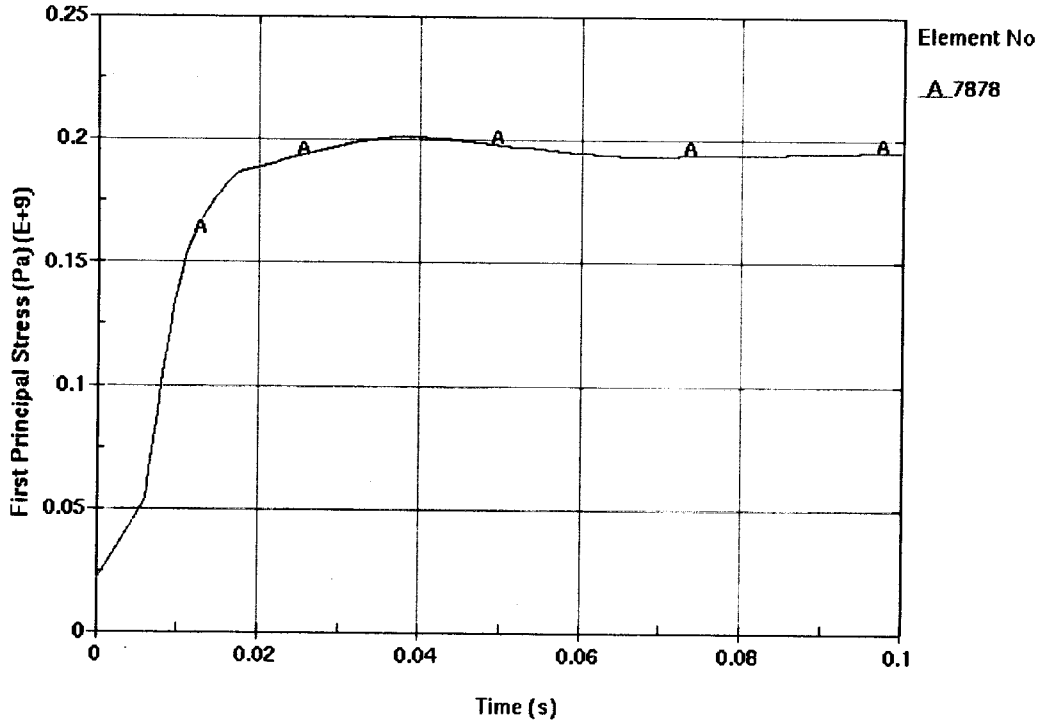

Figure II-48. First Principal Stress in Outer Shell Outer Surface (Element No. 7878) during Horizontal 10-MT Rock Fall

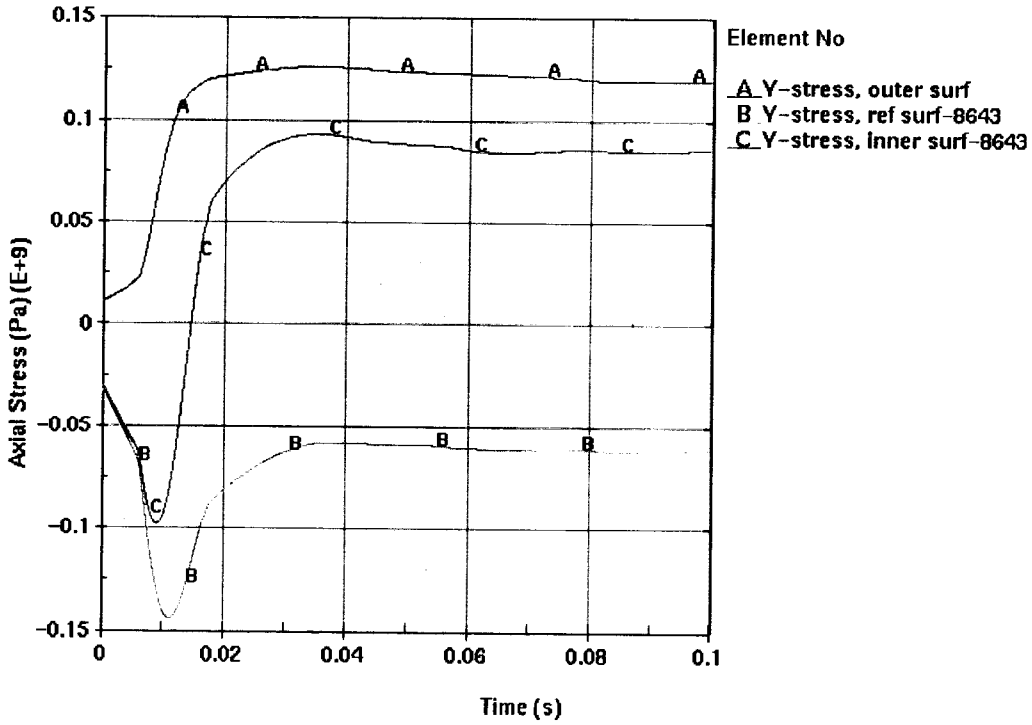

Figure II-49. Axial Stress Across Outer Shell Thickness (Element No. 8643) during Horizontal 10-MT Rock Fall

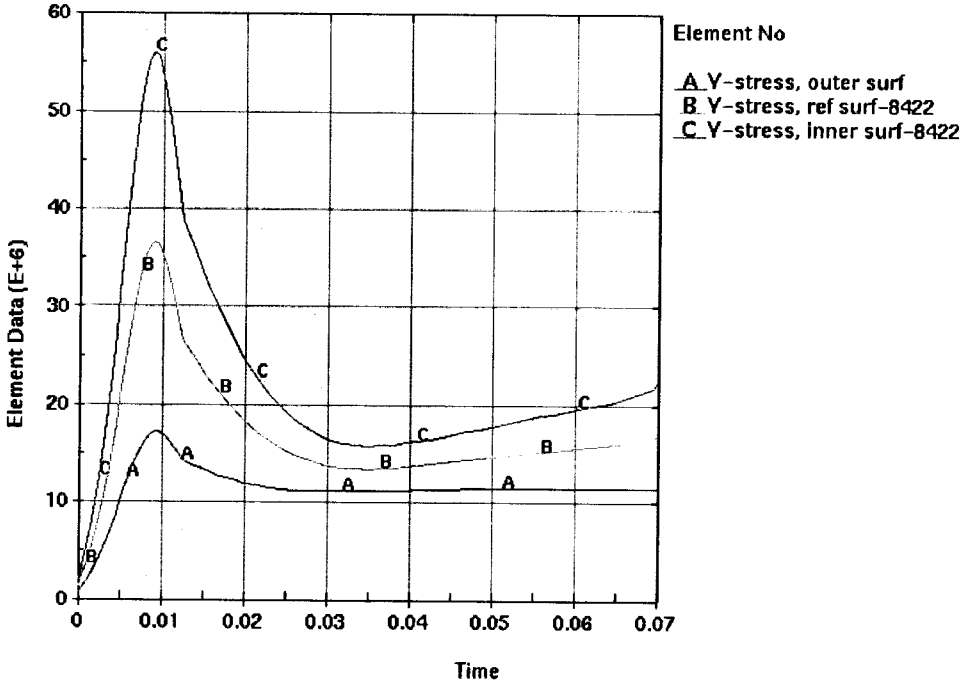

Figure II-50. Axial Stress Across Outer Shell Thickness (Element No. 8422) during Horizontal 10-MT Rock Fall

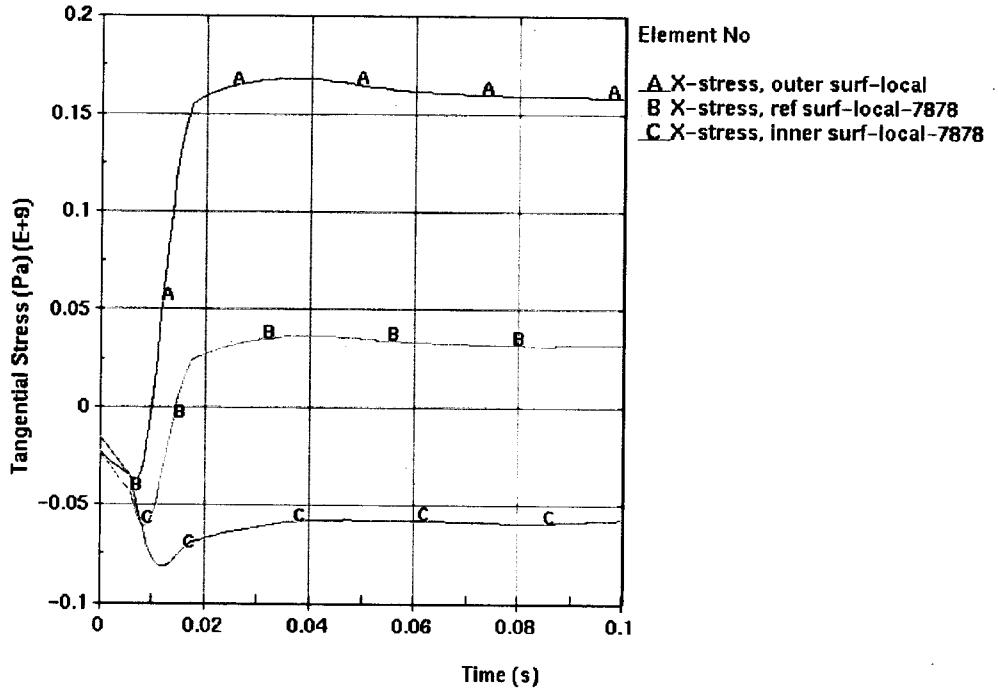

Figure II-51. Tangential Stress Across Outer Shell Thickness Thickness (Element No. 7878) during Horizontal 10-MT Rock Fall

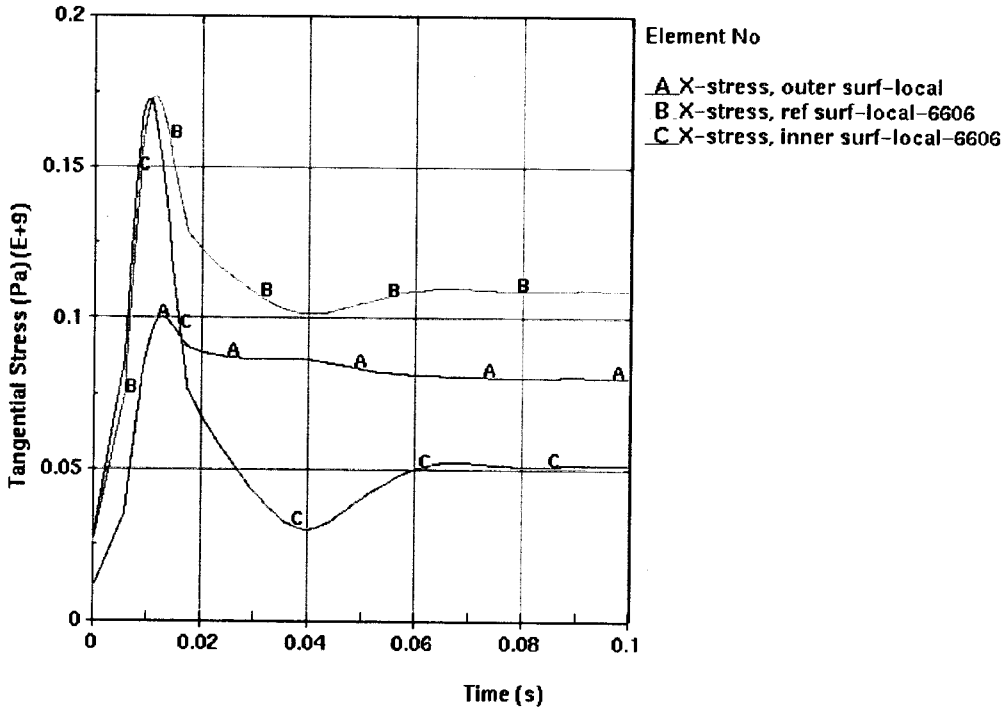

Figure II-52. Tangential Stress Across Outer Shell Thickness Thickness (Element No. 6606) during Horizontal 10-MT Rock Fall

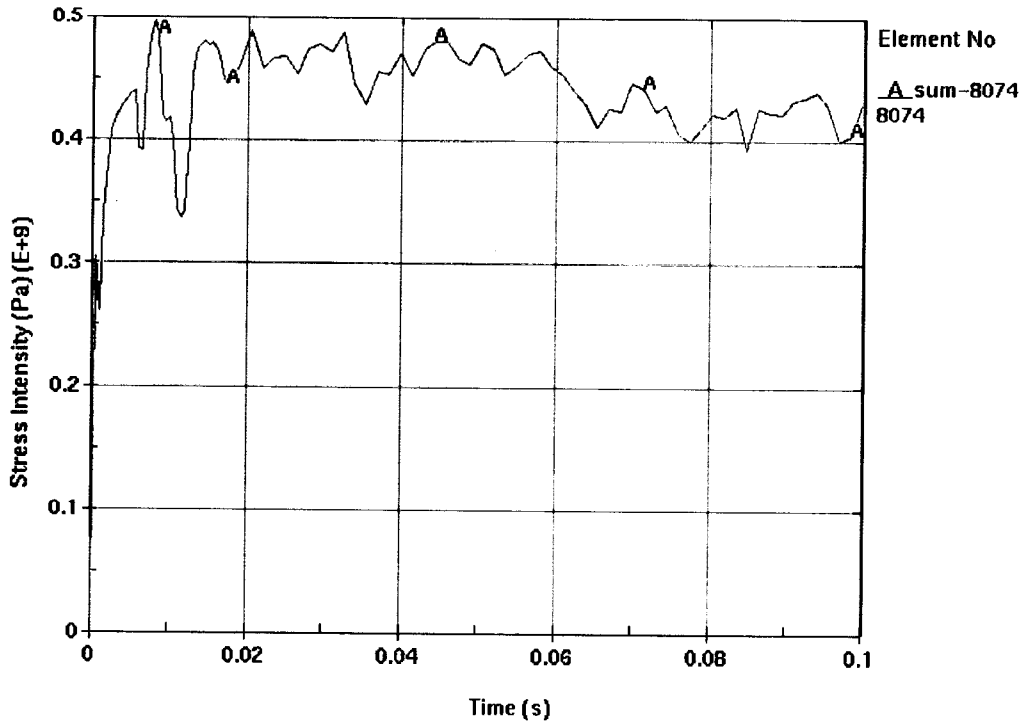

Figure II-53. Stress Intensity in Outer Shell (Element No. 8074) during 16-degrees 10-MT Rock Fall

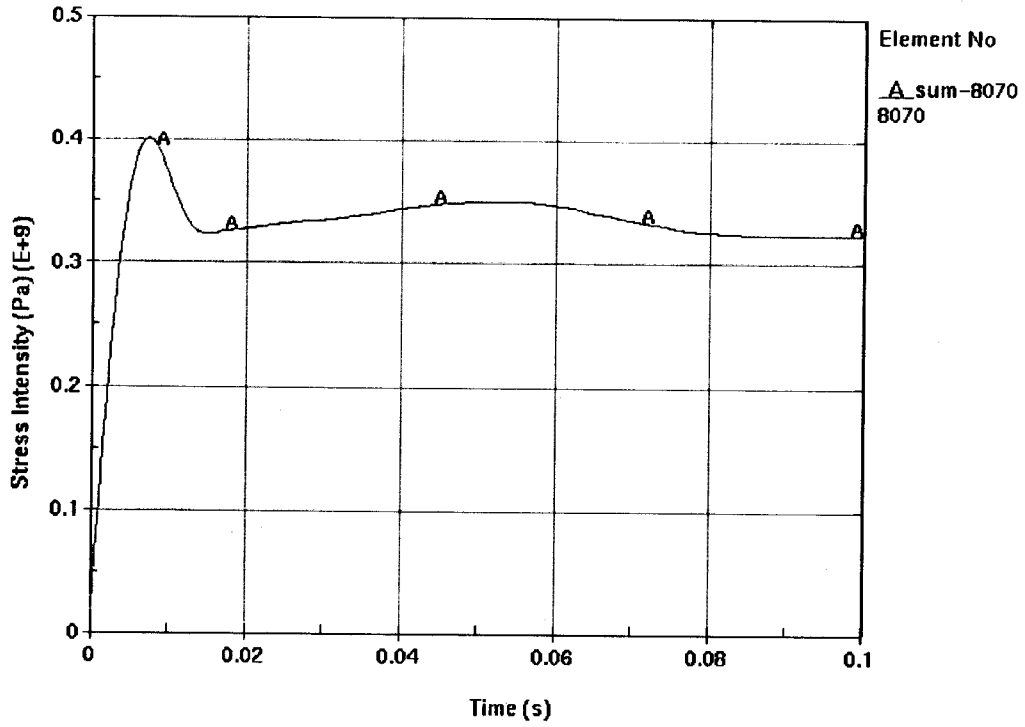

Figure II-54. Stress Intensity in Outer Shell Outer Surface (Element No. 8070) during 16-degrees 10-MT Rock Fall

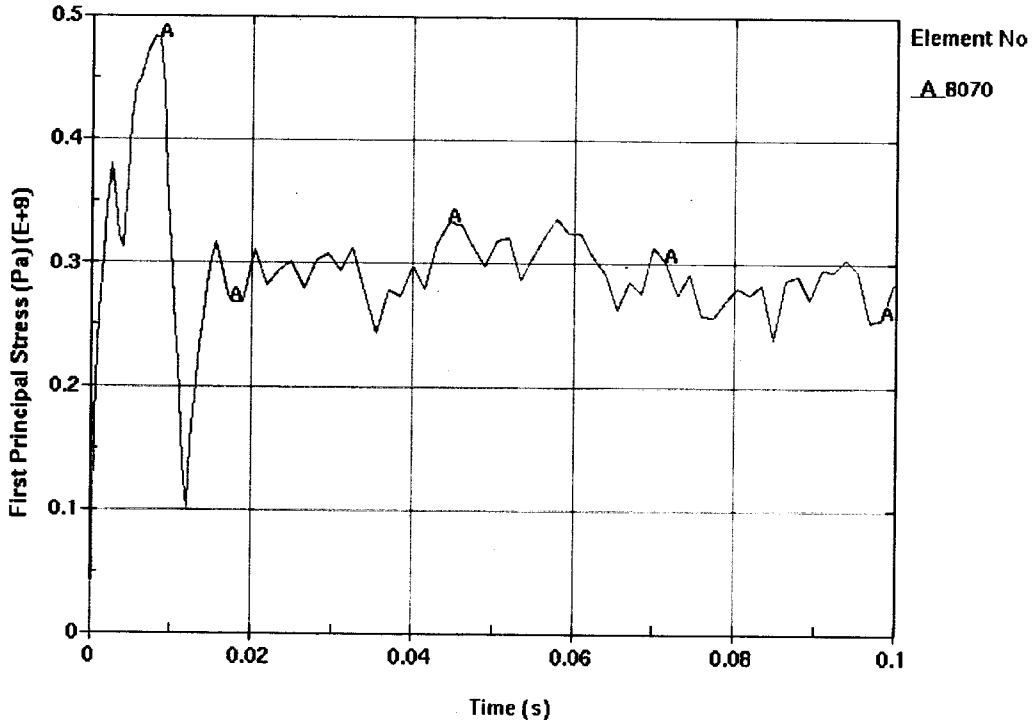

Figure II-55. First Principal Stress in Outer Shell (Element No. 8070) during 16-degrees 10-MT Rock Fall

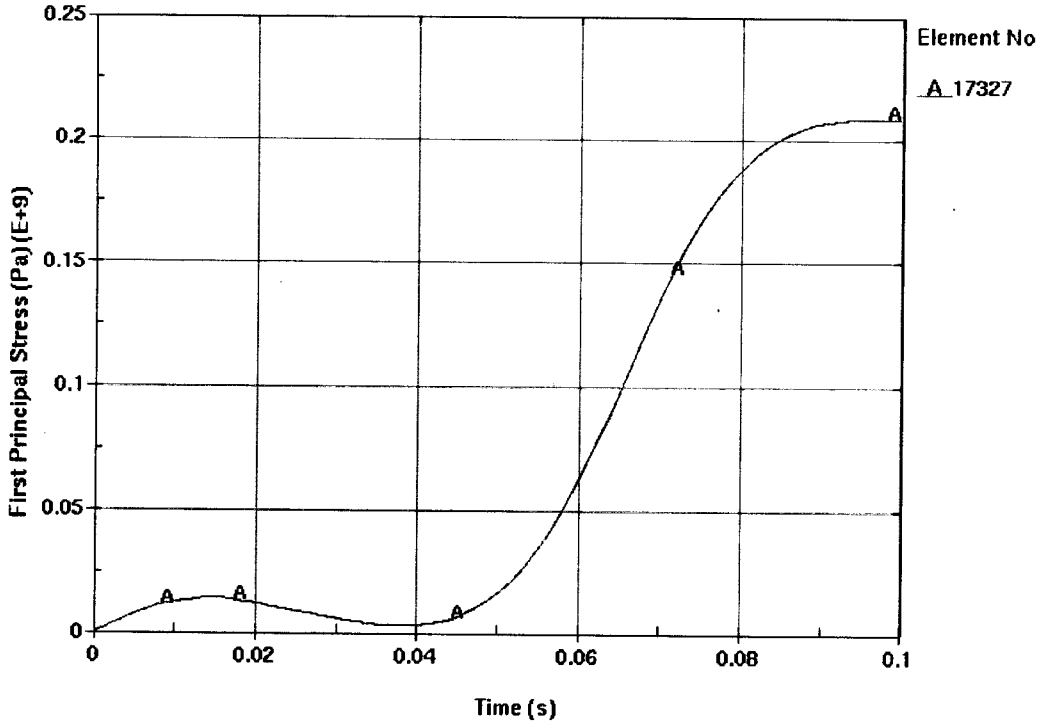

Figure II-56. First Principal Stress in Outer Shell Outer Surface (Element No. 17327) during 16-degrees 10-MT Rock Fall

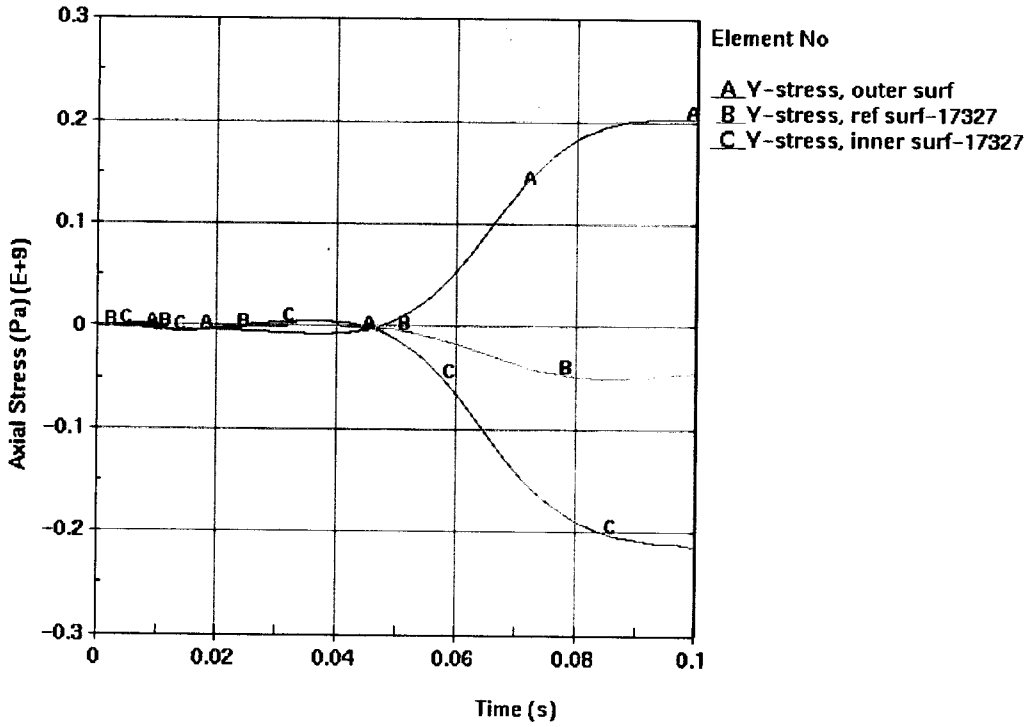

Figure II-57. Axial Stress Across Outer Shell Thickness (Element No. 17327) during 16-degrees 10-MT Rock Fall

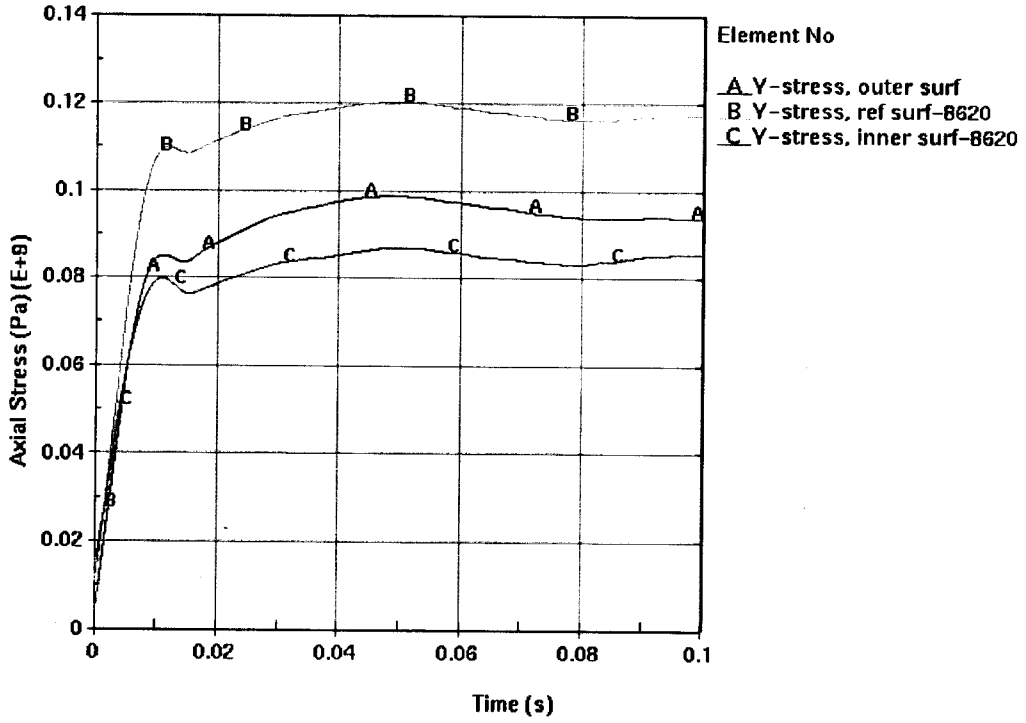

Figure II-58. Axial Stress Across Outer Shell Thickness (Element No. 8620) during 16-degrees 10-MT Rock Fall

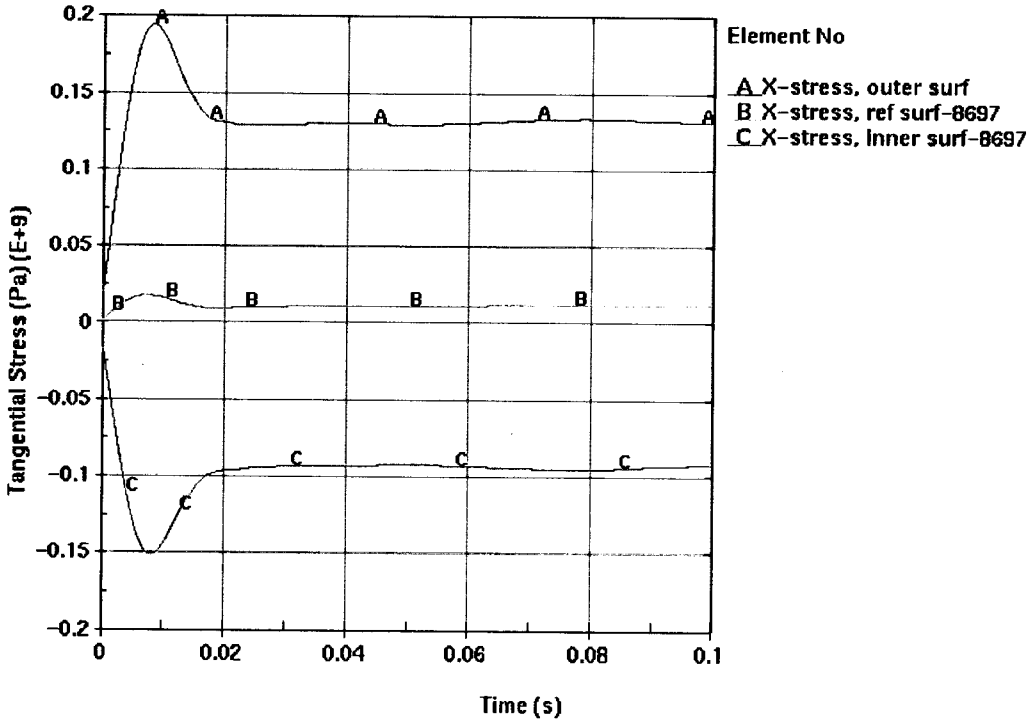

Figure II-59. Tangential Stress Across Outer Shell Thickness (Element No. 8697) during 16-degrees 10-MT Rock Fall

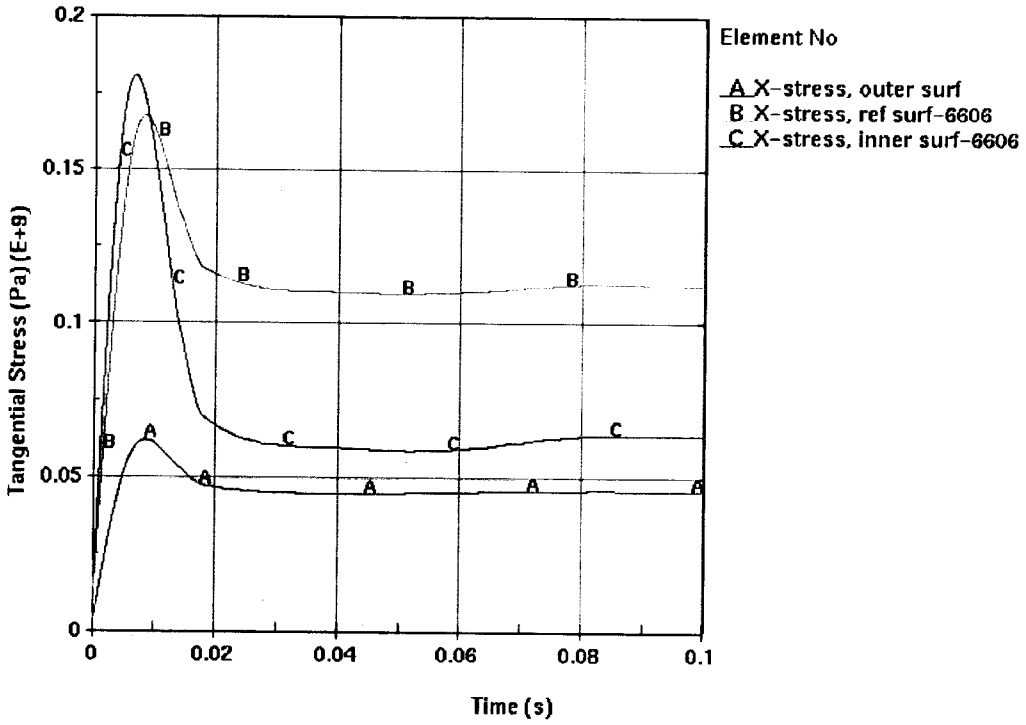

Figure II-60. Tangential Stress Across Outer Shell Thickness (Element No. 6606) during 16-degrees 10-MT Rock Fall

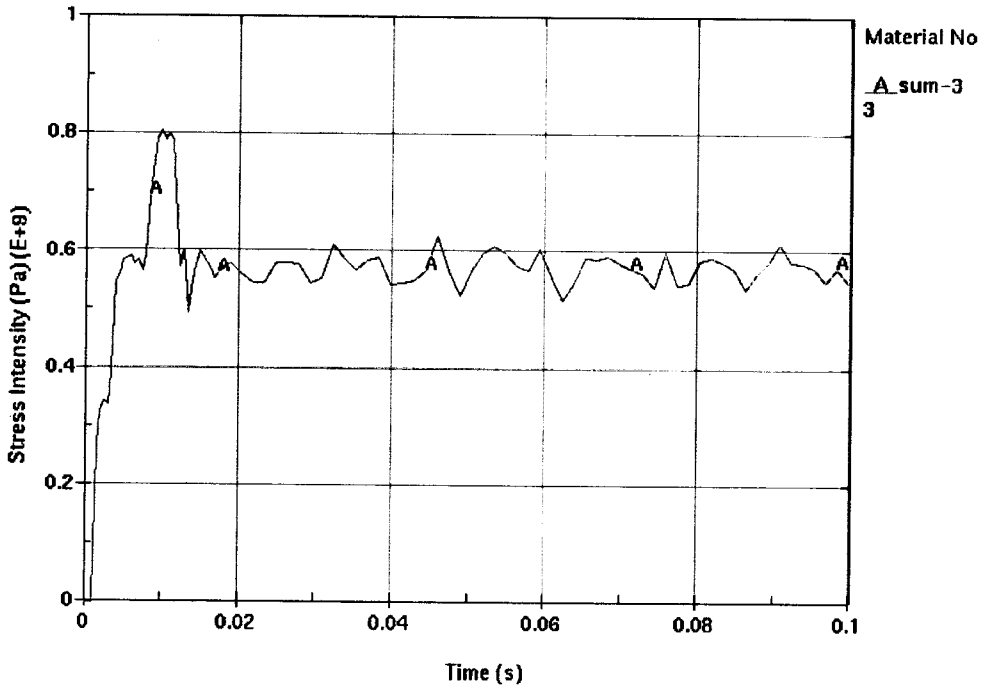

Figure II-61. Stress Intensity in Corroded Outer Shell (Element No. 8074) during 25-degrees 6-MT Rock Fall

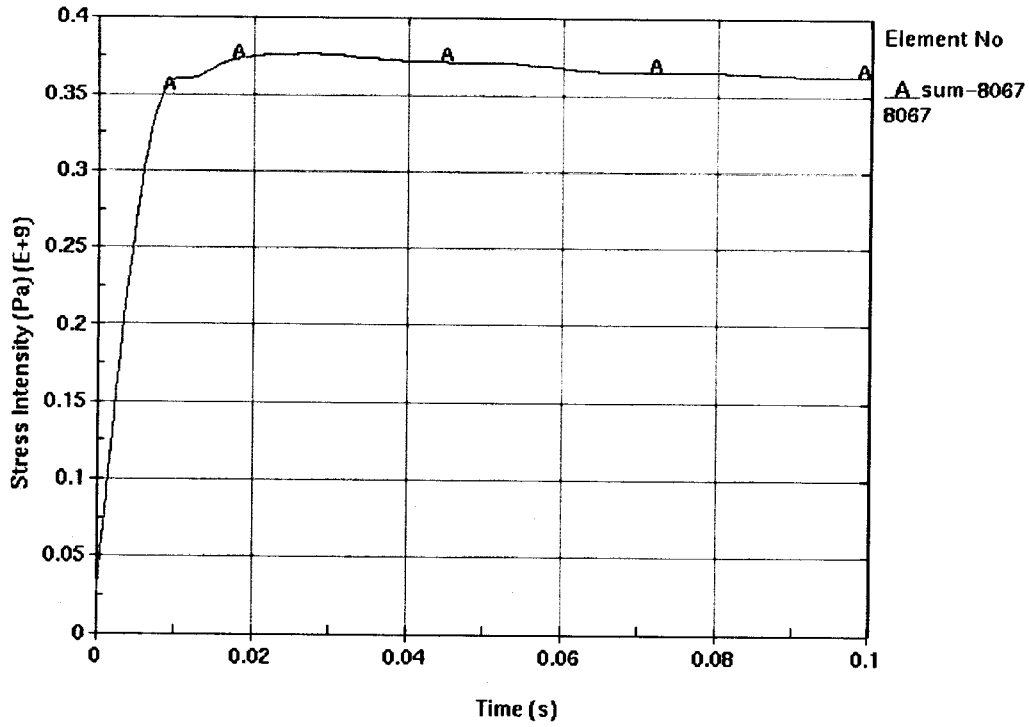

Figure II-62. Stress Intensity in Corroded Outer Shell (Element No. 8067) during 25-degrees 6-MT Rock Fall

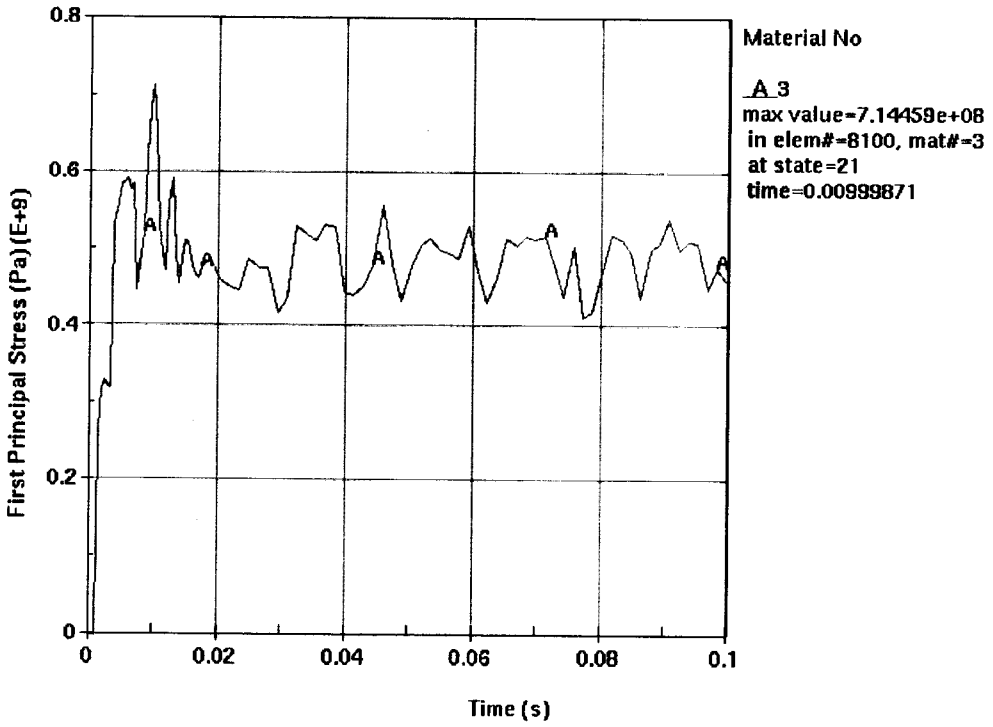

Figure II-63. First Principal Stress in Corroded Outer Shell (Element No. 8100) during 25-degrees 6-MT Rock Fall

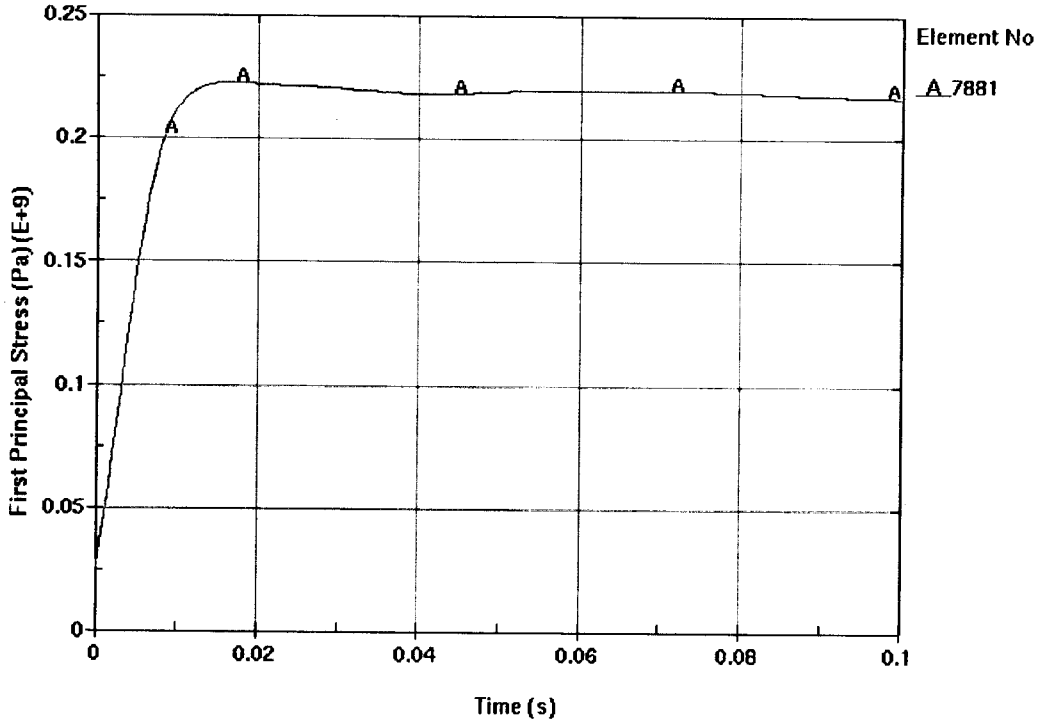

Figure II-64. First Principal Stress in Corroded Outer Shell (Element No. 7881) during 25-degrees 6-MT Rock Fall

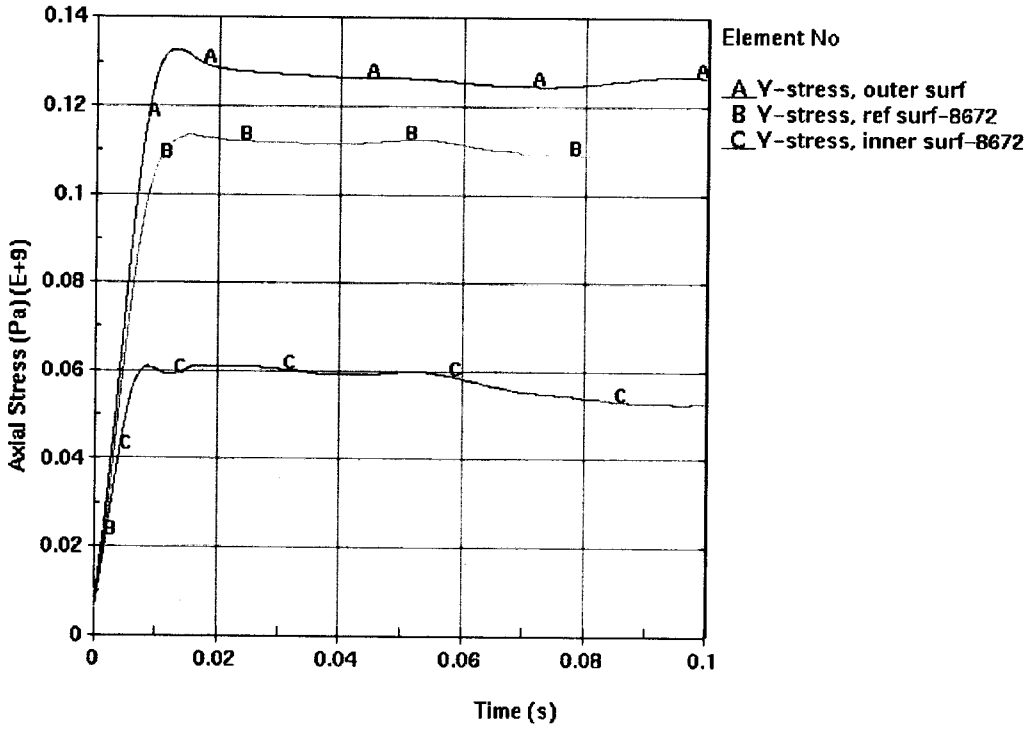

Figure II-65. Axial Stress Across Corroded Outer Shell Thickness (Element No. 8672) during 25-degrees 6-MT Rock Fall

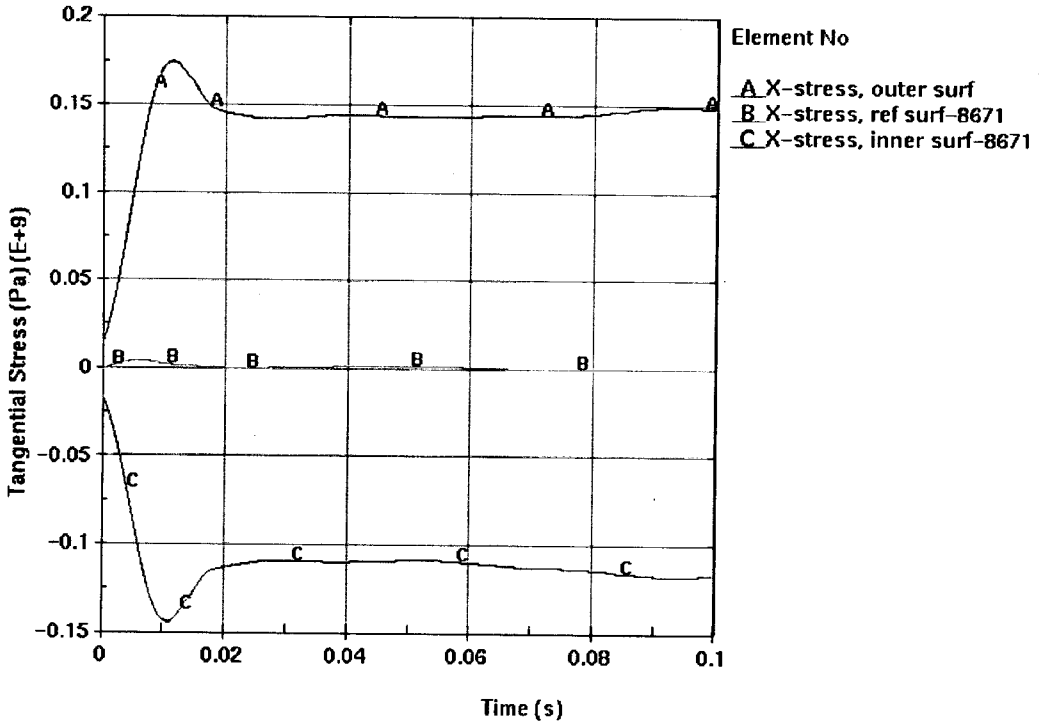

Figure II-66. Tangential Stress Across Corroded Outer Shell Thickness (Element No. 8671) during 25-degrees 6-MT Rock Fall

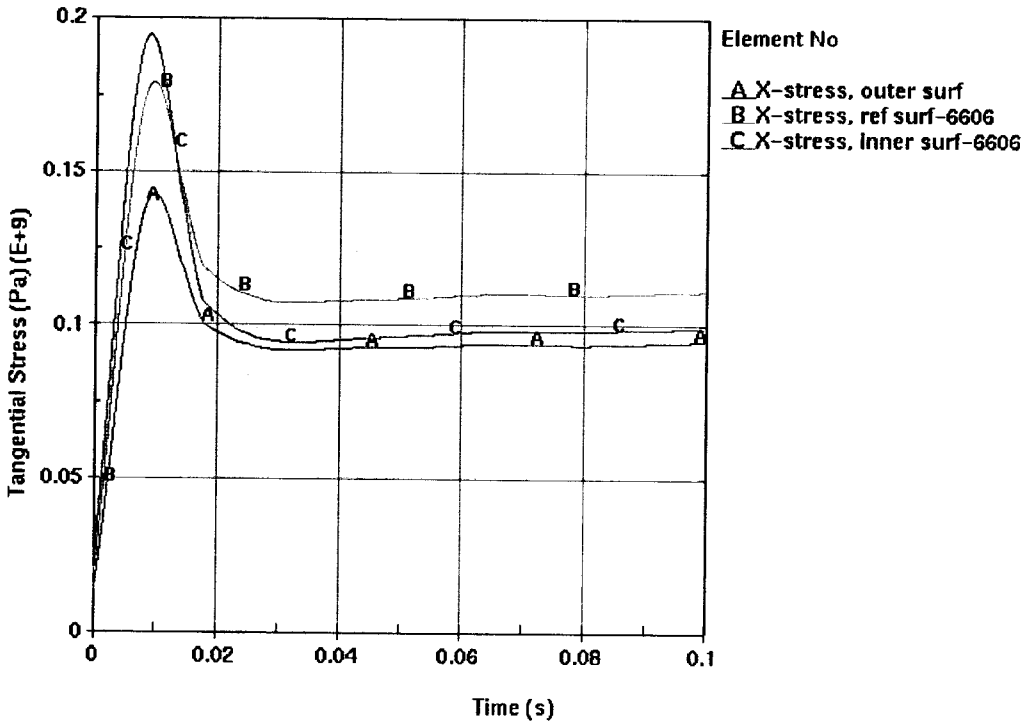

Figure II-67. Tangential Stress Across Corroded Outer Shell Thickness (Element No. 6606) during 25-degrees 6-MT Rock Fall

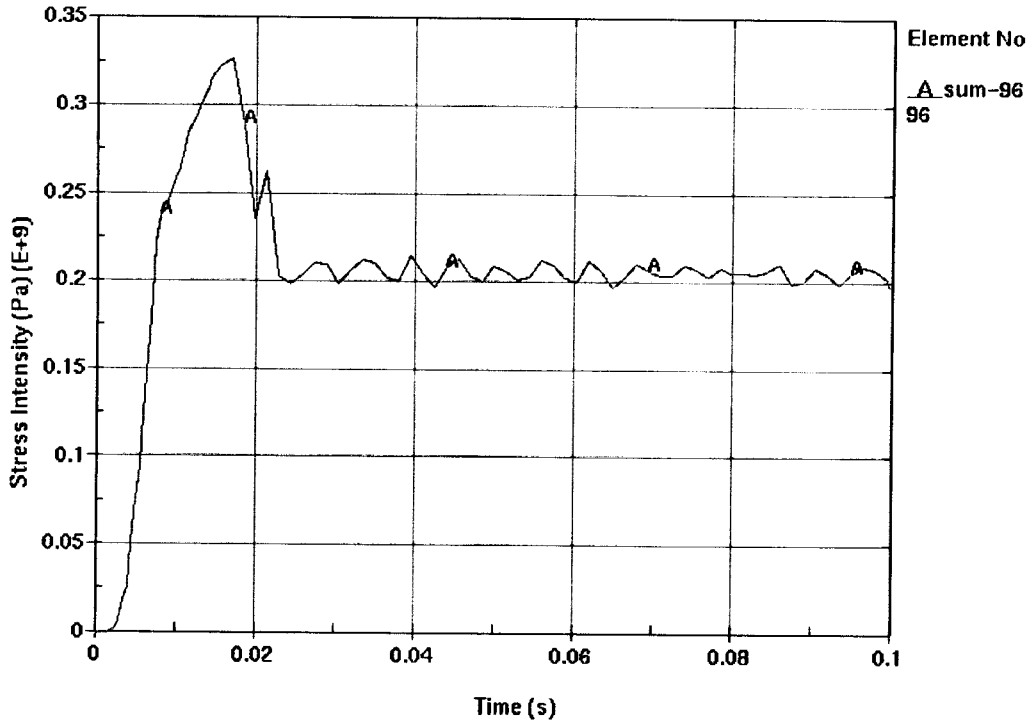

Figure II-68. Stress Intensity in Intact Emplacement Pallet (Element No. 96) during 25-degrees 6-MT Rock Fall

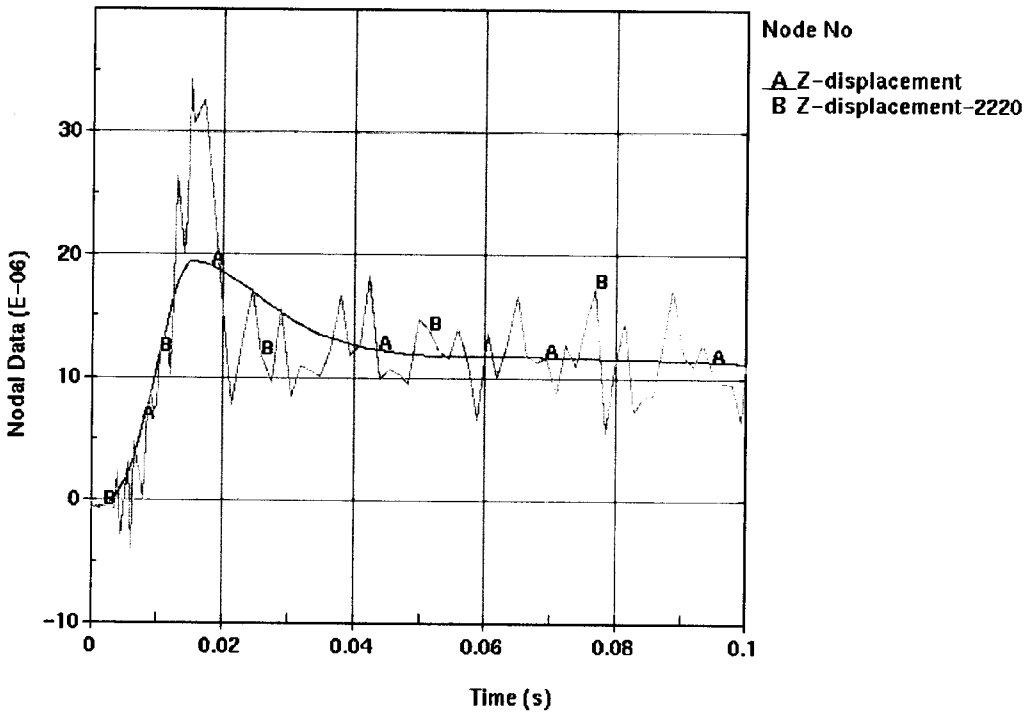

Figure II-69. Raw and Filtered Vertical Displacement of Lifting Surface of Intact Emplacement Pallet (Node No. 2220, Plate #9) during 25-degrees 6-MT Rock Fall

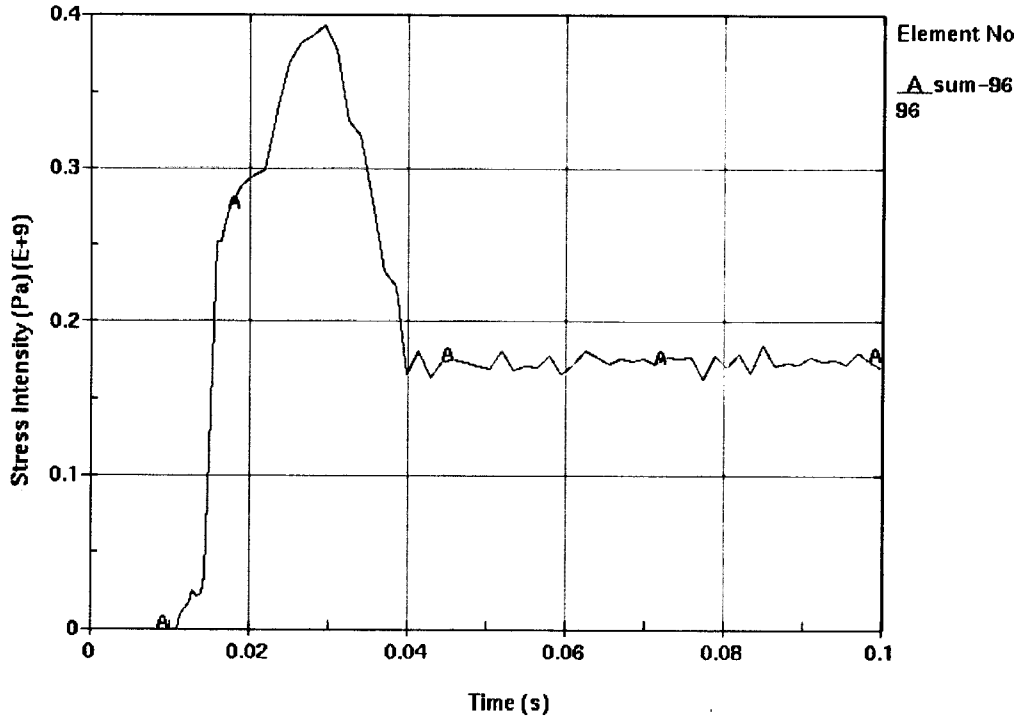

Figure II-70. Stress Intensity in Corroded Emplacement Pallet (Element No. 96) during 25-degrees 6-MT Rock Fall

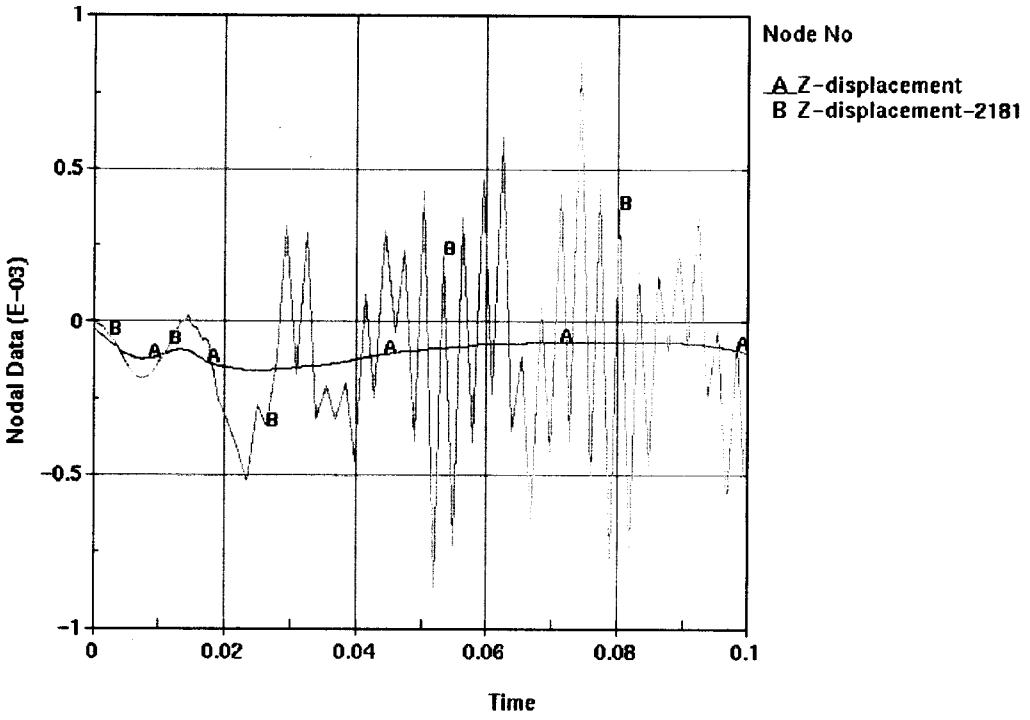

Figure II-71. Raw and Filtered Vertical Displacement of Lifting Surface of Corroded Emplacement Pallet (Node No. 2181, Plate #9) during 25-degrees 6-MT Rock Fall

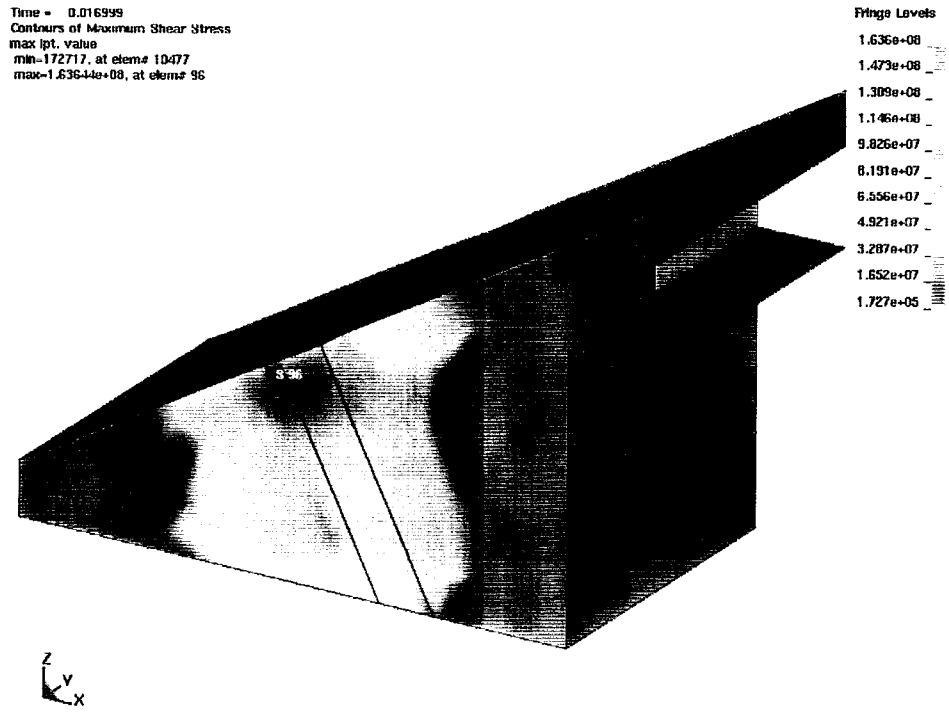

Figure II-72. Maximum Shear Stress Plot in Alloy 22 Components of Intact Emplacement Pallet during 25-degrees 6-MT Rock Fall

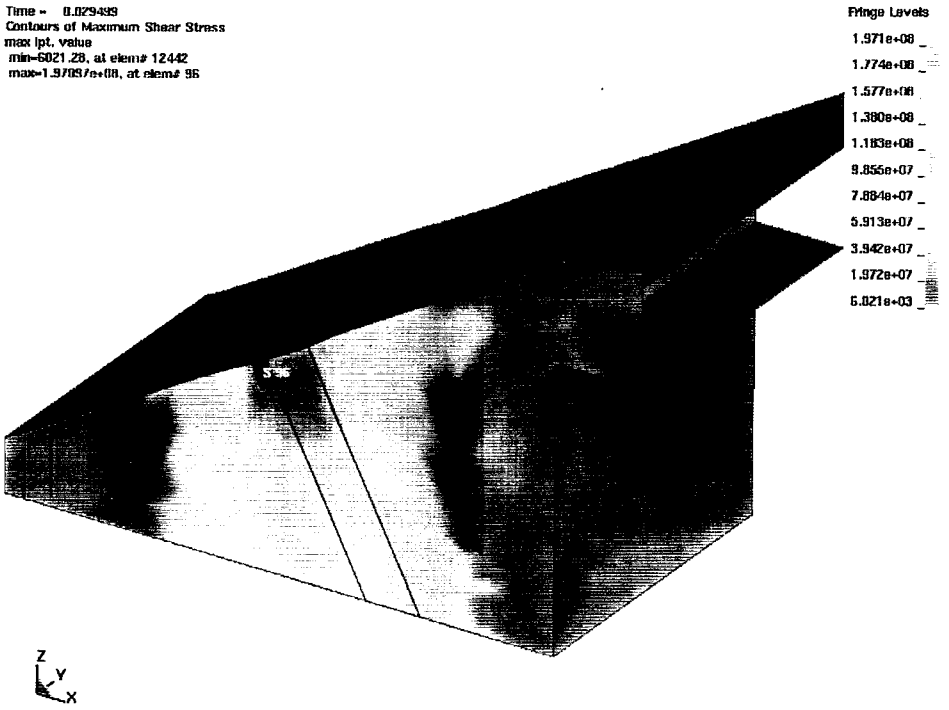

Figure II-73. Maximum Shear Stress Plot in Alloy 22 Components of Corroded Emplacement Pallet during 25-degrees 6-MT Rock Fall

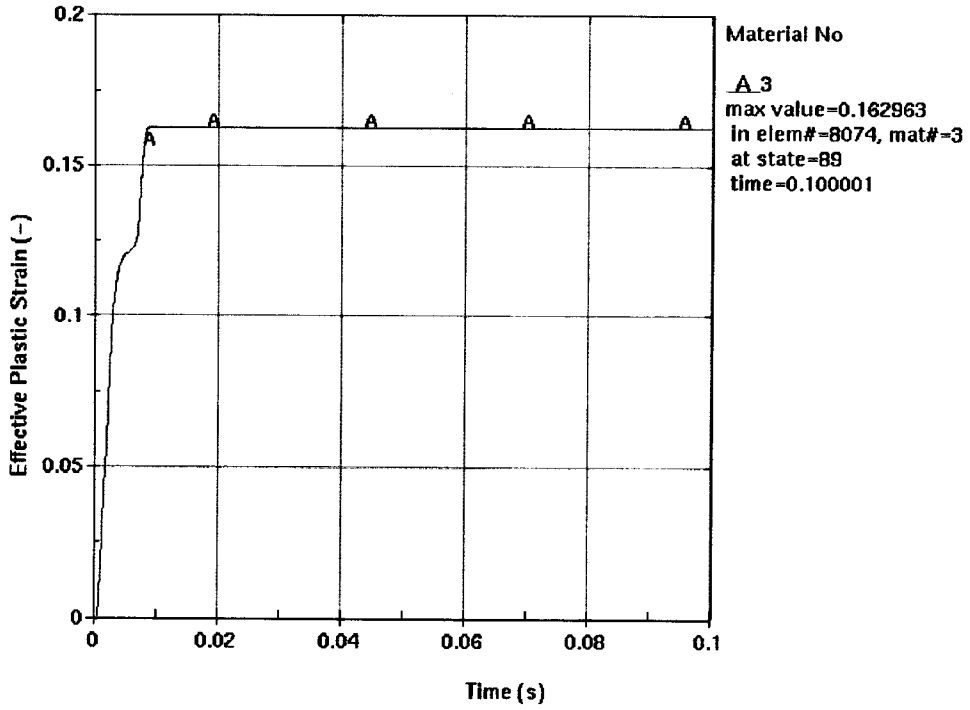

Figure II-74. Effective Plastic Strain in Outer Shell (Element No. 8074) during 25-degrees 6-MT Rock Fall

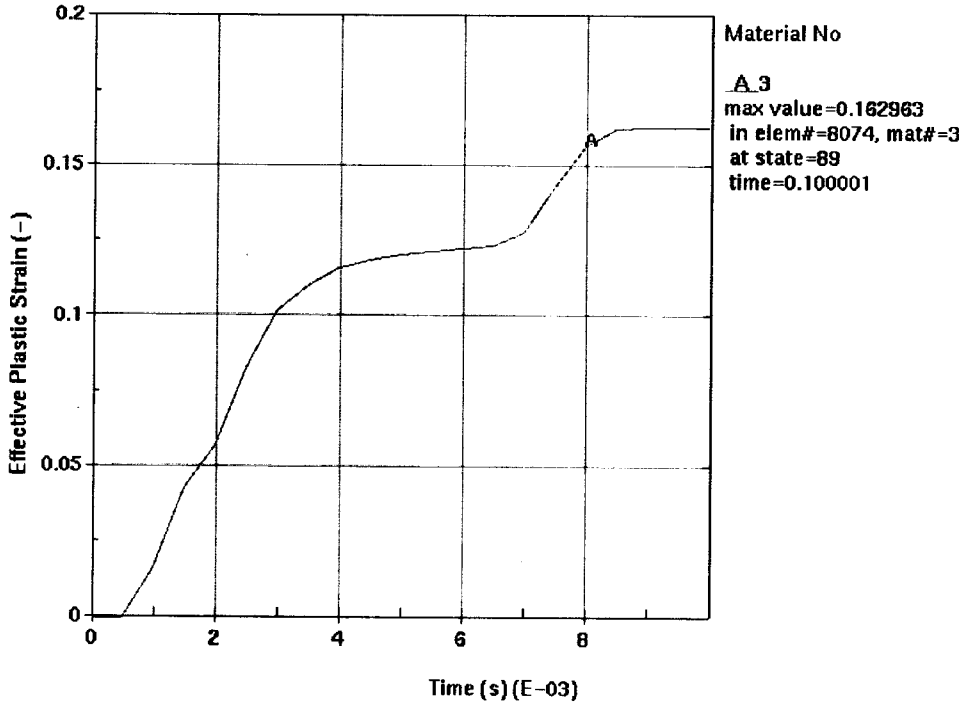

Figure II-75. Effective Plastic Strain in Outer Shell (Element No. 8074) during 25-degrees 6-MT Rock Fall (Detail)

8. ATTACHMENTS

Attachment I (16 pages): Design sketches (*Naval SNF Long Waste Package Configuration for Site Recommendation* [SK-0194 REV 01], two sheets [this attachment uses Reference 27]; *Naval SNF Long Waste Package Weld Configuration* [SK-0195 REV 00], one sheet; *Emplacement Pallet Long* [SK-0232 REV 00], thirteen sheets)

Attachment II (38 pages): Figures obtained from LS-DYNA V950

Attachments III (Compact Disc): ANSYS V5.4 and LS-DYNA V950 electronic files

Table 9. Attachment III: File Directories, Names, Dates, Times, and Sizes

Directory	Name	Date	Time	Size
1_mt/0-degrees	d3hsp	07/20/01	10:08 a.m.	6,959 KB
	r1mt.k	07/20/01	10:08 a.m.	8 KB
	r1mte2.inc	07/20/01	10:08 a.m.	111 KB
	r1mtn2.inc	07/20/01	10:08 a.m.	97 KB
	r1mts2.inc	07/20/01	10:08 a.m.	18 KB
	r1mts22.inc	07/20/01	10:08 a.m.	2 KB
	rmte1.inc	07/20/01	10:08 a.m.	1,032 KB
	rmtn1.inc	07/20/01	10:08 a.m.	1,158 KB
	rmts1.inc	07/20/01	10:08 a.m.	9 KB
	rmts12.inc	07/20/01	10:08 a.m.	10 KB
	rmts13.inc	07/20/01	10:08 a.m.	1 KB
	rock.inp	07/20/01	10:08 a.m.	7 KB
	rock.out	07/20/01	10:08 a.m.	92 KB
	wpp1.inp	07/20/01	10:08 a.m.	22 KB
	wpp1.out	07/20/01	10:08 a.m.	190 KB
1_mt/57-degrees	d3hsp	07/20/01	03:14 p.m.	7,396 KB
	r1mt.k	07/20/01	10:09 a.m.	8 KB
	r1mte2.inc	07/20/01	10:09 a.m.	234 KB
	r1mtn2.inc	07/20/01	10:09 a.m.	195 KB
	r1mts2.inc	07/20/01	10:09 a.m.	35 KB
	r1mts22.inc	07/20/01	10:09 a.m.	3 KB
	rmte1.inc	07/20/01	10:09 a.m.	1,032 KB
	rmtn1.inc	07/20/01	10:09 a.m.	1,158 KB
	rmts1.inc	07/20/01	10:09 a.m.	9 KB
	rmts12.inc	07/20/01	10:09 a.m.	10 KB
	rmts13.inc	07/20/01	10:09 a.m.	1 KB
	rock.inp	07/20/01	10:09 a.m.	7 KB
	rock.out	07/20/01	10:09 a.m.	150 KB
	wpp1.inp	07/20/01	10:09 a.m.	22 KB
	wpp1.out	07/20/01	10:09 a.m.	190 KB

10_mt/0-degrees	d3hsp	07/20/01	10:07 a.m.	10,296 KB
	r10mt.k	07/20/01	10:06 a.m.	8 KB
	r10mte2.inc	07/20/01	10:06 a.m.	1,082 KB
	r10mtn2.inc	07/20/01	10:06 a.m.	845 KB
	r10mts2.inc	07/20/01	10:06 a.m.	150 KB
	r10mts22.inc	07/20/01	10:06 a.m.	8 KB
	rmte1.inc	07/20/01	10:06 a.m.	1,032 KB
	rmtn1.inc	07/20/01	10:06 a.m.	1,158 KB
	rmts1.inc	07/20/01	10:06 a.m.	9 KB
	rmts12.inc	07/20/01	10:06 a.m.	10 KB
	rmts13.inc	07/20/01	10:06 a.m.	1 KB
	rock.inp	07/20/01	10:06 a.m.	7 KB
	rock.out	07/20/01	10:06 a.m.	475 KB
	wpp1.inp	07/20/01	10:06 a.m.	22 KB
	wpp1.out	07/20/01	10:06 a.m.	190 KB
10_mt/16-degrees	d3hsp	07/23/01	08:14 a.m.	10,299 KB
	r10mt.k	07/23/01	08:14 a.m.	8 KB
	r10mte2.inc	07/23/01	08:14 a.m.	1,082 KB
	r10mtn2.inc	07/23/01	08:14 a.m.	845 KB
	r10mts2.inc	07/23/01	08:14 a.m.	150 KB
	r10mts22.inc	07/23/01	08:14 a.m.	8 KB
	rmte1.inc	07/23/01	08:14 a.m.	1,032 KB
	rmtn1.inc	07/23/01	08:14 a.m.	1,158 KB
	rmts1.inc	07/23/01	08:14 a.m.	9 KB
	rmts12.inc	07/23/01	08:14 a.m.	10 KB
	rmts13.inc	07/23/01	08:14 a.m.	1 KB
	rock.inp	07/23/01	08:14 a.m.	7 KB
	rock.out	07/23/01	08:14 a.m.	475 KB
	wpp1.inp	07/23/01	08:14 a.m.	22 KB
	wpp1.out	07/23/01	08:14 a.m.	190 KB
6_mt/0-degrees	d3hsp	07/23/01	08:13 a.m.	7,687 KB
	r6mt.k	07/23/01	08:13 a.m.	8 KB
	r6mte2.inc	07/23/01	08:13 a.m.	321 KB
	r6mtn2.inc	07/23/01	08:13 a.m.	264 KB
	r6mts2.inc	07/23/01	08:13 a.m.	47 KB
	r6mts22.inc	07/23/01	08:13 a.m.	4 KB
	rmte1.inc	07/23/01	08:13 a.m.	1,032 KB
	rmtn1.inc	07/23/01	08:13 a.m.	1,158 KB
	rmts1.inc	07/23/01	08:13 a.m.	9 KB
	rmts12.inc	07/23/01	08:13 a.m.	10 KB
	rmts13.inc	07/23/01	08:13 a.m.	1 KB
	rock.inp	07/23/01	08:13 a.m.	7 KB
	rock.out	07/23/01	08:13 a.m.	99 KB
	wpp1.inp	07/23/01	08:13 a.m.	22 KB
	wpp1.out	07/23/01	08:13 a.m.	190 KB

6_mt/25-degrees/Case_A/Intact	d3hsp	07/20/01	10:03 a.m.	7,687 KB
	r6mt.k	07/20/01	10:03 a.m.	8 KB
	r6mte2.inc	07/20/01	10:03 a.m.	321 KB
	r6mtn2.inc	07/20/01	10:03 a.m.	264 KB
	r6mts2.inc	07/20/01	10:03 a.m.	47 KB
	r6mts22.inc	07/20/01	10:03 a.m.	4 KB
	rmte1.inc	07/20/01	10:03 a.m.	1,032 KB
	rmtn1.inc	07/20/01	10:03 a.m.	1,158 KB
	rmts1.inc	07/20/01	10:03 a.m.	9 KB
	rmts12.inc	07/20/01	10:03 a.m.	10 KB
	rmts13.inc	07/20/01	10:03 a.m.	1 KB
	rock.inp	07/20/01	10:03 a.m.	7 KB
	rock.out	07/20/01	10:03 a.m.	99 KB
	wpp1.inp	07/20/01	10:03 a.m.	22 KB
	wpp1.out	07/20/01	10:03 a.m.	190 KB
6_mt/25-degrees/Case_A/Corroded	d3hsp	07/23/01	01:21 p.m.	7,074 KB
	r6mt.k	07/23/01	01:21 p.m.	8 KB
	r6mte2.inc	07/23/01	01:21 p.m.	321 KB
	r6mtn2.inc	07/23/01	01:21 p.m.	264 KB
	r6mts2.inc	07/23/01	01:21 p.m.	47 KB
	r6mts22.inc	07/23/01	01:21 p.m.	4 KB
	rmte1.inc	07/23/01	01:21 p.m.	900 KB
	rmtn1.inc	07/23/01	01:21 p.m.	1,158 KB
	rmts1.inc	07/23/01	01:21 p.m.	9 KB
	rmts12.inc	07/23/01	01:21 p.m.	10 KB
	rmts13.inc	07/23/01	01:21 p.m.	1 KB
	rock.inp	07/23/01	01:21 p.m.	7 KB
	rock.out	07/23/01	01:21 p.m.	99 KB
	wpp1.inp	07/23/01	01:20 p.m.	22 KB
	wpp1.out	07/23/01	01:20 p.m.	190 KB
6_mt/25-degrees/Case_B	d3hsp	07/23/01	03:14 p.m.	7,696 KB
	r6mt.k	07/20/01	10:08 a.m.	8 KB
	r6mte2.inc	07/20/01	10:08 a.m.	321 KB
	r6mtn2.inc	07/20/01	10:08 a.m.	264 KB
	r6mts2.inc	07/20/01	10:08 a.m.	47 KB
	r6mts22.inc	07/20/01	10:08 a.m.	4 KB
	rmte1.inc	07/20/01	10:08 a.m.	1,013 KB
	rmtn1.inc	07/20/01	10:08 a.m.	1,136 KB
	rmts1.inc	07/20/01	10:08 a.m.	9 KB
	rmts12.inc	07/20/01	10:08 a.m.	10 KB
	rmts13.inc	07/20/01	10:08 a.m.	1 KB
	rock.inp	07/20/01	10:08 a.m.	7 KB
	rock.out	07/20/01	10:08 a.m.	99 KB
	wpp1.inp	07/20/01	10:08 a.m.	22 KB
	wpp1.out	07/20/01	10:08 a.m.	184 KB

6_mt/25-degrees/Case_C	d3hsp	07/23/01	10:05 p.m.	7,562 KB
	r6mt.k	07/20/01	10:05 a.m.	8 KB
	r6mte2.inc	07/20/01	10:05 a.m.	321 KB
	r6mtn2.inc	07/20/01	10:05 a.m.	264 KB
	r6mts2.inc	07/20/01	10:05 a.m.	47 KB
	r6mts22.inc	07/20/01	10:05 a.m.	4 KB
	rmte1.inc	07/20/01	10:05 a.m.	1,010 KB
	rmtn1.inc	07/20/01	10:04 a.m.	1,133 KB
	rmts1.inc	07/20/01	10:04 a.m.	9 KB
	rmts12.inc	07/20/01	10:04 a.m.	10 KB
	rmts13.inc	07/20/01	10:04 a.m.	1 KB
	rock.inp	07/20/01	10:04 a.m.	7 KB
	rock.out	07/20/01	10:04 a.m.	99 KB
	wpp1.inp	07/20/01	10:04 a.m.	22 KB
	wpp1.out	07/20/01	10:04 a.m.	184 KB
6_mt/25-degrees/Case_A/Refined_Mesh	d3hsp	07/23/01	10:11 p.m.	8,745 KB
	r6mt.k	07/20/01	10:11 a.m.	8 KB
	r6mte2.inc	07/20/01	10:11 a.m.	321 KB
	r6mtn2.inc	07/20/01	10:11 a.m.	264 KB
	r6mts2.inc	07/20/01	10:11 a.m.	47 KB
	r6mts2.inc	07/20/01	10:11 a.m.	4 KB
	rmte1.inc	07/20/01	10:11 a.m.	1,213 KB
	rmtn1.inc	07/20/01	10:11 a.m.	1,367 KB
	rmts1.inc	07/20/01	10:11 a.m.	9 KB
	rmts12.inc	07/20/01	10:11 a.m.	10 KB
	rmts13.inc	07/20/01	10:11 a.m.	1 KB
	rock.inp	07/20/01	10:11 a.m.	7 KB
	rock.out	07/20/01	10:11 a.m.	99 KB
	wpp1.inp	07/20/01	10:11 a.m.	22 KB
	wpp1.out	07/20/01	10:11 a.m.	203 KB

NOTE: The file sizes may vary with operating system.

OFFICE OF CIVILIAN RADIOACTIVE WASTE MANAGEMENT
SPECIAL INSTRUCTION SHEET file list 8-15-01 nfc

1. QA: QA

MB 8/15/01

Complete Only Applicable Items

This is a placeholder page for records that cannot be scanned.

2. Record Date 08/09/2001	3. Accession Number ATT-TO MOL.20010815.0270
4. Author Name(s) SRETEN MASTILOVIC	5. Author Organization N/A

6. Title/Description
SYMMETRIC ROCK FALL ON WASTE PACKAGE

7. Document Number(s) CAL-EBS-ME-000009	8. Version Designator REV. 00
9. Document Type DATA	10. Medium CD-ROM

11. Access Control Code
PUB

12. Traceability Designator
DC #26239

13. Comments
THIS IS A SPECIAL PROCESS CD-ROM AS PART OF ATTACHMENT III
DC #26239

THIS DATA SUBMITTAL TO THE RECORDS PROCESSING CENTER IS FOR ARCHIVE PURPOSES ONLY, AND IS NOT AVAILABLE FOR ~~RE~~VIEWING OR REPRODUCTION AB 8/16/01

OFFICE OF CIVILIAN RADIOACTIVE WASTE MANAGEMENT
ELECTRONIC FILE CERTIFICATION

QA: N/A

1. DOCUMENT TITLE: Symmetric Rock Fall on Waste Package	
2. IDENTIFIER (e.g., DI OR PI): CAL-EBS-ME-0000009	3. REVISION DESIGNATOR: Rev. 00
ATTACHED SOFTWARE FILE INFORMATION	4. PDF FILE SUBMITTED: ☐ YES ☑ NO
5. FILE NAMES(S) WITH FILE EXTENSION(S) PROVIDED BY THE SOFTWARE: See Attached	
6. DATE LAST MODIFIED: See Attached	7. NATIVE APPLICATION: (i.e., EXCEL, WORD, CORELDRAW) See Attached
8. FILE SIZE IN KILOBYTES: See Attached	
9. FILE LINKAGE INSTRUCTIONS/INFORMATION: Standard	
10. PRINTER SPECIFICATION (I.E., HP4SI) INCLUDING POSTSCRIPT INFORMATION (i.e., PRINTER DRIVER) AND PRINTING PAGE SETUP: (i.e., LANDSCAPE, 11 X 17 PAPER) HP5MC (8 1/2 x 11 in) and HP5SI (8 1/2 x 11 in and 11 x 17 in)	
11. COMPUTING PLATFORM USED: (i.e., PC, SUN, WIN 95, NT, HP) PC# 16724	12. OPERATING SYSTEM AND VERSION: (i.e., WINDOWS UNIX, SOLARIS) Windows
13. ADDITIONAL HARDWARE/SOFTWARE REQUIREMENT USED TO CREATE FILE(S): None	14. ACCESS RESTRICTIONS: (COPYRIGHT OR LICENSE ISSUES) None

COMMENTS/SPECIAL INSTRUCTIONS

15. IS SOFTWARE AVAILABLE FROM SOFTWARE CONFIGURATION MANAGEMENT? ☑ YES ☐ NO
SOFTWARE MEDIA TRACKING NUMBER N/A .

***NOTE: The software product(s) to develop this document are Commercial-Off-The-Shelf (COTS) software products which require no Software Media Number (SMN). The COTS software products are under Software Configuration Management (SCM) control.

CERTIFICATION

16. DOCUMENT OWNER (Print and Sign): Sreten Mastilovic			17. DATE: 08/06/2001
18. ORGANIZATION: BSC	19. DEPARTMENT: WPD	20. LOCATION/MAIL STOP: MS423/1030N	21. PHONE: 295-5046
22. SUBMITTED BY (Print and Sign): Daynett D. Vosicky			23. DATE: 8-10-01

DC USE ONLY

24. DATE RECEIVED: 8/13/2001	25. DATE FILES TRANSFERRED: N/A	26. DC NO.: 26239
27. NAME (Print and Sign): N/A		28. DATE: 8/13/2001